Alma Mater Studiorum · University of Bologna

Department of Physics and Astronomy
Department of Biological, Geological and Environmental Sciences

Master Degree in Science of Climate

On the multi-scale nature of the UHI during heatwaves - Evidence from an experimental field campaign in the city of Bologna

Supervisor:
Prof.ssa Silvana Di Sabatino

Co-supervisors:
Prof. Francesco Barbano
Dott. Luigi Brogno

Submitted by:
Alessia Fideli

Academic Year 2024/2025

Abstract

As global temperatures rise and urban areas expand, the impacts of Urban Heat Islands (UHI) are becoming of even greater concern. In the Padan Plain, a densely populated area in the north of Italy, the warming rate is especially high. To quantify the magnitude of the UHI in one of its largest cities, an intensive 24-hour field campaign was conducted in Bologna under heatwave conditions; with the objective of exploring the multi-scale characteristics and processes associated with the UHI during a heatwave, focusing on the interplay between thermal forcing and local effects. To fulfill this type of evaluation, a central and a more peripheral zone with different morphological characteristics and vegetation distribution were probed via portable sensor devices, with the aim of mapping the air temperature at the pedestrian level, while thermal imaging of urban surfaces was acquired to assess the behaviour of the heat sources. The results were also related to a climatological review of the city of Bologna and the whole Emilia-Romagna region, particularly regarding temperature trends, UHI and heatwaves. The data gathered during the field campaign revealed an Urban Heat Island of almost 7 °C between the city centre and the outskirts, along with an intra-city scale UHI of 2 °C between the densely built central area and the greener urban neighbourhood. Considerations on the different scales of the UHI, on the convergence velocity, urban canopy cooling trends, and relation with planar and frontal area coefficients were presented. The climatological analysis also revealed how heatwave events that were once rare are becoming the new norm. In face of this and of the implications for the growing urban population, case studies and tailored mitigation strategies for cities are now of literally vital importance.

Contents

Introduction

More than half of the world's population now resides in cities, a figure projected to reach 60% by 2030 (UN, 2018), with an estimated 5 billion people living in urban areas. In cities, heat stress poses significant risks to public health and the environment, amplified by both the urban setting and anthropogenic activities. The coexistence of extreme heat conditions, brought about both by large-scale phenomena, such as heatwaves, and local phenomena like the Urban Heat Island (UHI) effect, render urban areas hot spots for climate change. The increasing trend of global temperatures will further exacerbate the impacts of these phenomena, potentially evolving into public health emergencies and socio-economic crises.

In July 2022, Italy recorded 18,000 excess deaths, that were largely attributed to the extreme heat events that took place in the densely populated Po Valley (Adil et al, 2025; ISTAT, 2022). Such events are not isolated outliers, as they are becoming the new norm: heatwaves, now more prolonged and more frequent, are taking a higher toll on cities, since their impacts are being intensified by the very way cities are designed. Bologna, the regional capital of Emilia-Romagna, is one of the places where heat builds up, due to its densely urbanized historical centre and limited green infrastructures and areas (Possega et al, 2022).

In light of this, and as a multiscale assessment of the UHI in one of the most populated cities of the plain appeared yet to be realised, a field campaign was designed to examine the UHI of Bologna at multiple scales, such as city, inter-neighbourhood and intra-neighbourhood scale. The study also allowed the investigation of multiple phenomena that were key topics of interest in the area, such as the spatial evolution of the UHI in the urban fabric, the interplay between thermal forcings and their effects, and the behaviour of the UHI during heatwaves. The overarching goal of the research is thus to explore the multi-scale characteristics and processes associated with the UHI during a heatwave period, focusing on the interplay between thermal forcing and local effects. The campaign was carried out by coupling hourly 360° infrared captures of the central surfaces and ground air temperature measurements in two different neighbourhoods for a 24-hour period. The recollected data was examined with the objective of investigating the thermal behaviour of urban surfaces, characterizing the theoretical circulation induced by the UHI and studying how the temperature changes with different types of terrain and morphological characteristics. The field campaign was further integrated with a climatological contextualization of the city in the region and in the municipality, along with an analysis on heatwaves.

The structure of this thesis is as follows: Chapter 1 presents a literature review that contextualizes the city’s climatic classification, historical data trends, and the definitions of UHI and heatwaves, along with providing insight on the dynamics, mitigation strategies and processes from city-level to street-level scales. The methodology, outlined in Chapter 2, explains the protocols used during the campaign, the reasoning behind the choices of the databases and the procedures utilized during the data analysis. The thesis combines conventional datasets from weather stations and reanalysis records with the realized field campaign involving mobile sensors and thermal imagery. Chapter 3 presents the results regarding the UHI of the city of Bologna, under the clear sky and heatwave conditions that were present during the measuring campaign. The role of urban surface materials and building density in shaping the inter-neighbourhood thermal differences was investigated using GIS-derived indexes and thermal imagery analysis. The characteristics of recent heatwaves, using percentile-based indices are also detailed. The climatology, trends, UHI and dynamics of the city of Bologna are further analysed and compared at the regional and municipality scale. In the end, the conclusions are drawn and further prospects of this thesis work are suggested.

Chapter 1

1 Literature Review

This chapter schematizes the climatology of the city of Bologna and its relationship with the valley it's located in, then it transitions into the description of the Urban Heat Island, its definition, its dynamics and consequences, supplying research papers and data. After, heatwave events are defined and related to the UHI, and their consequences and projected trends are stated.

1.1 Climatology

The thesis focuses on the city of Bologna and its micro-climatic characteristics.

In general, Bologna and most of the Emilia-Romagna region have a climate that is defined as Cfa in the Köppen-Geiger classification (Kottek et al., 2006), i.e. Humid Subtropical Climate, as the coldest month has an average above 0°C and there are at least four months with temperatures above 10°C. Furthermore, there are no significant precipitation differences between seasons. The region is characterized by significant yearly fluctuations in air temperatures, as shown in graph 1:

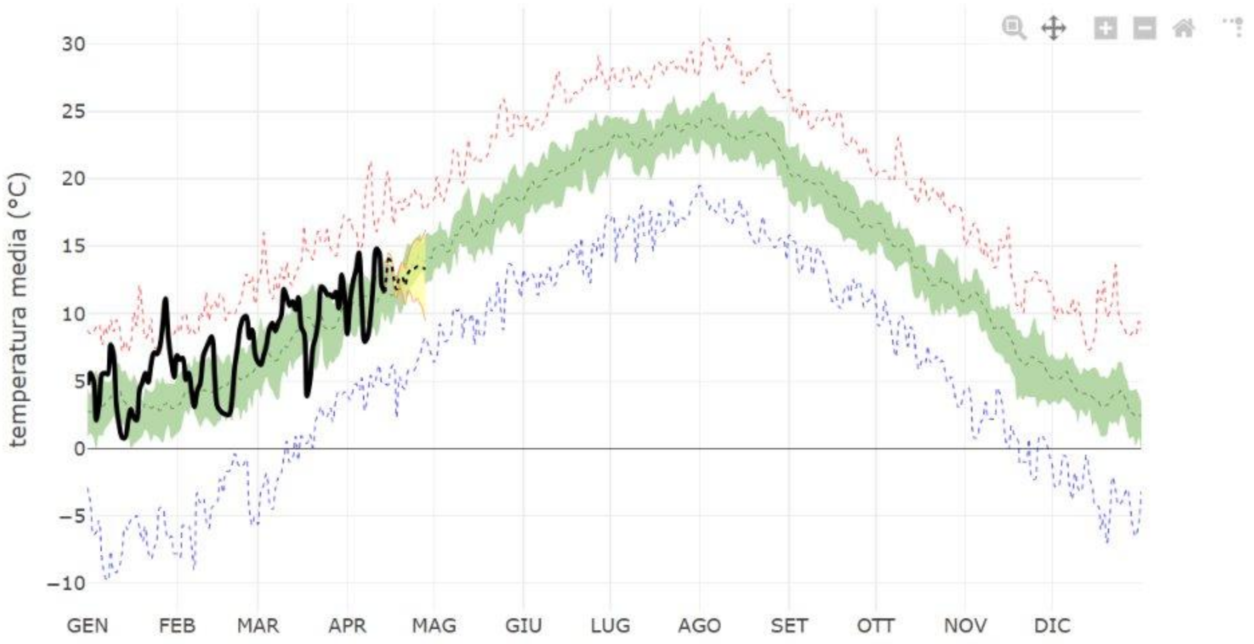

Figure 1 Climatology – ARPAE Emilia-Romagna '61-current. In blue, minimum temperature; in red, maximum temperature; in green, average temperature; in black, 2025 average.

1.1.1 Urban Heat Island

Moving to smaller scales, there are dissimilarities between various areas of the region: for example, cities and rural areas exhibit temperature differences. These discrepancies will likely evolve with climate change and strengthen the gradient between urban and country districts.

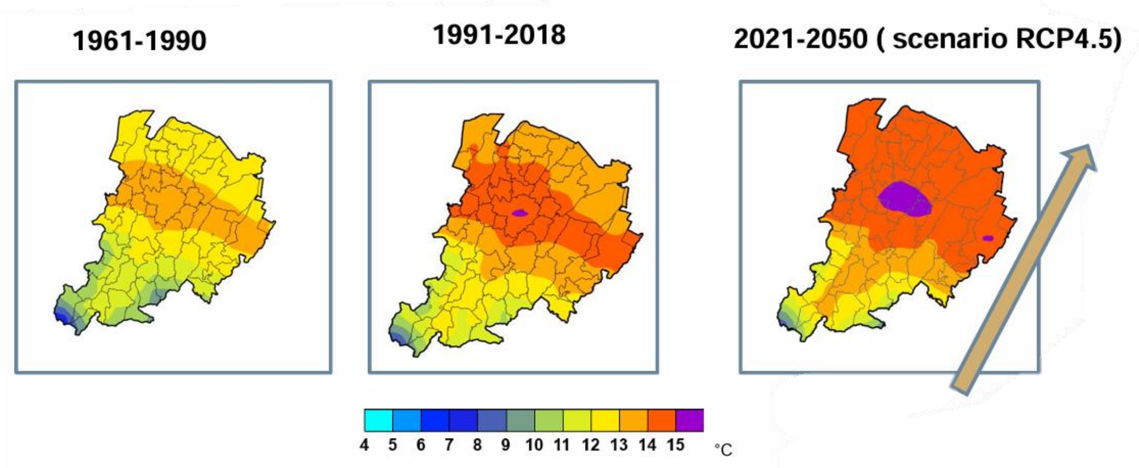

Figure 2 Average temperature evolution in the municipality of Bologna and projection under RCP 4.5. (Comune di Bologna, ARPAE)

Under the RCP 4.5 scenario, the city of Bologna has a projected increase of annual average temperatures of 1.7°C, an increase of 2.8°C for the summer maxima and an increase of 1.3°C for winter minima, according to ARPAE, when comparing the 1961-1990 period to the 2021-2050 period. The number of tropical nights is estimated to rise by an additional 17 from the 'current' 25.

Table 1 schematizes the data for Bologna and for the nearby 'pianura est' and 'collina est' areas (ARPAE, Proiezioni climatiche 2021-2050).

Table 1

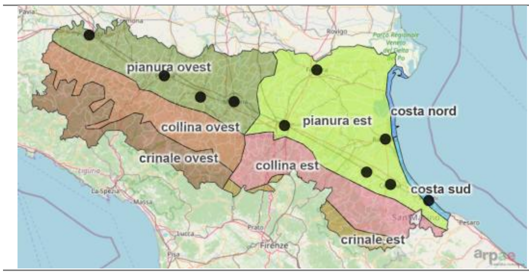	**Pianura Est**		**Bologna**		**Collina Est**	
	1961-1990	2021-2050	1961-1990	2021-2050	1961-1990	2021-2050
Mean of Average T [°C]	12.9	14.5	13.9	15.6	11.7	13.4
Mean of Max Summer T [°C]	28.2	31.0	29.0	31.8	25.5	28.8
Mean of Min Winter T [°C]	-0.3	1.3	0.7	2.0	0.0	1.4
Max Summer Heatwave Duration [days]	3	7	2	6	2	8
Summer Tropical Nights [number]	8	18	25	42	3	8

It can be noted how urban Bologna is hotter that the surrounding areas and has a significantly higher number of summer tropical nights. The maximum summer heatwave duration may seem lower, but the ARPAE definition of heatwave is ‘days with maximum temperatures above the 90th percentile of the local temperature climatology for the day, computed for the 1961-1990 period’: because the city’s temperature is higher, the comparison isn’t direct with the rural areas. Instead, the definition of tropical nights is absolute, as any night with values always above 20°C is considered to be one, making the comparison immediate.

Bologna is located in the Padan Plain (or Po Valley), which is surrounded by the Apennines and Alps mountains. The plain is also catalogued as Cfa in the Köppen-Geiger classification (humid subtropical climate) and is quite homogeneous, so the differences between temperatures can be explained by a specific effect.

The difference between Bologna and the countryside is, in fact, caused by the Urban Heat Island effect, defined as a local phenomenon characterized by heightened temperatures in the nocturnal period in densely built areas when compared to the rural surroundings. This anomaly can be explained by multiple factors, such as metropolitan land use, anthropogenic heat production from domestic or commercial buildings, traffic and generic energy consumption.

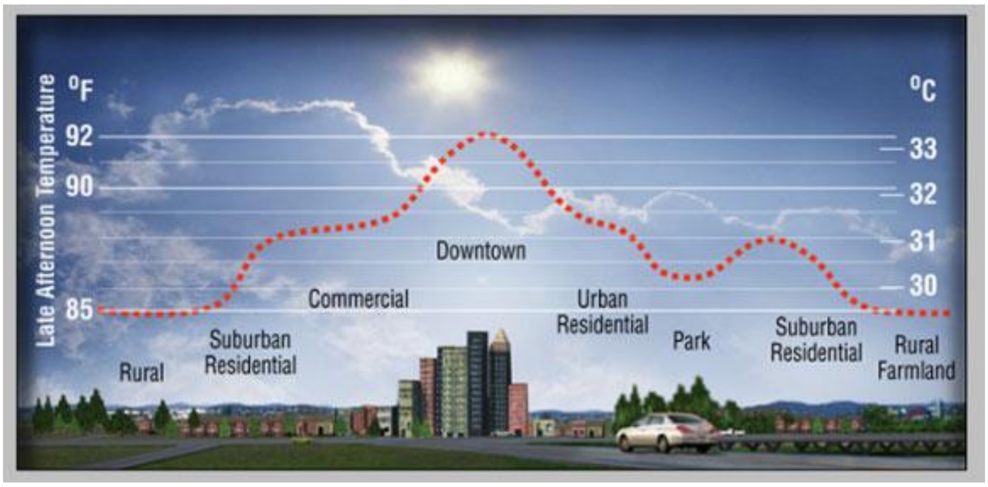

Figure 3 Schematization of the Urban Heat Island. (Heat Island Group, Lawrence Berkeley National Laboratory)

During the day, the opposite effect (warmer rural areas) can be exacerbated by the shade provided by tall buildings or, in arid climate, by urban irrigation and dry surroundings (no latent heat).

The magnitude of the UHI is defined as the difference between the urban and rural temperature, even though there isn’t a univocal protocol for doing so: some studies divide the urban area in subsections, while others do not. Additionally, morphological and topographical inhomogeneities can cause microscale thermal gradients and flows (for example, induced by a building shade or a park). Also, the UHI interacts with meso-scale flows: cities, because of their UHI effect, can be parametrized as localized heat sources that lead to meso-scale and smaller-scale flows; they can even trigger downstream thunderstorm formation by interacting with the synoptic flow (the UHI-induced updraft must be strong enough for this to occur).

Urbanized areas affect the lower part of the atmosphere and generate the Urban Boundary Layer (UBL). The UBL is of complex handling and is thus usually divided into dynamical layers (Figure 4, Fernando et al, 2010):

-Mixed Layer: entrainment and turbulent kinetic energy production are dominant;

-Constant Flux Layer or Inertial Sublayer: horizontally homogeneous;

-Roughness Sublayer: interface between turbulent kinetic energy production and dissipation, balancing layer;

-Urban Canopy Layer: it goes from the ground to the top of the buildings, here turbulent kinetic energy is prevalent.

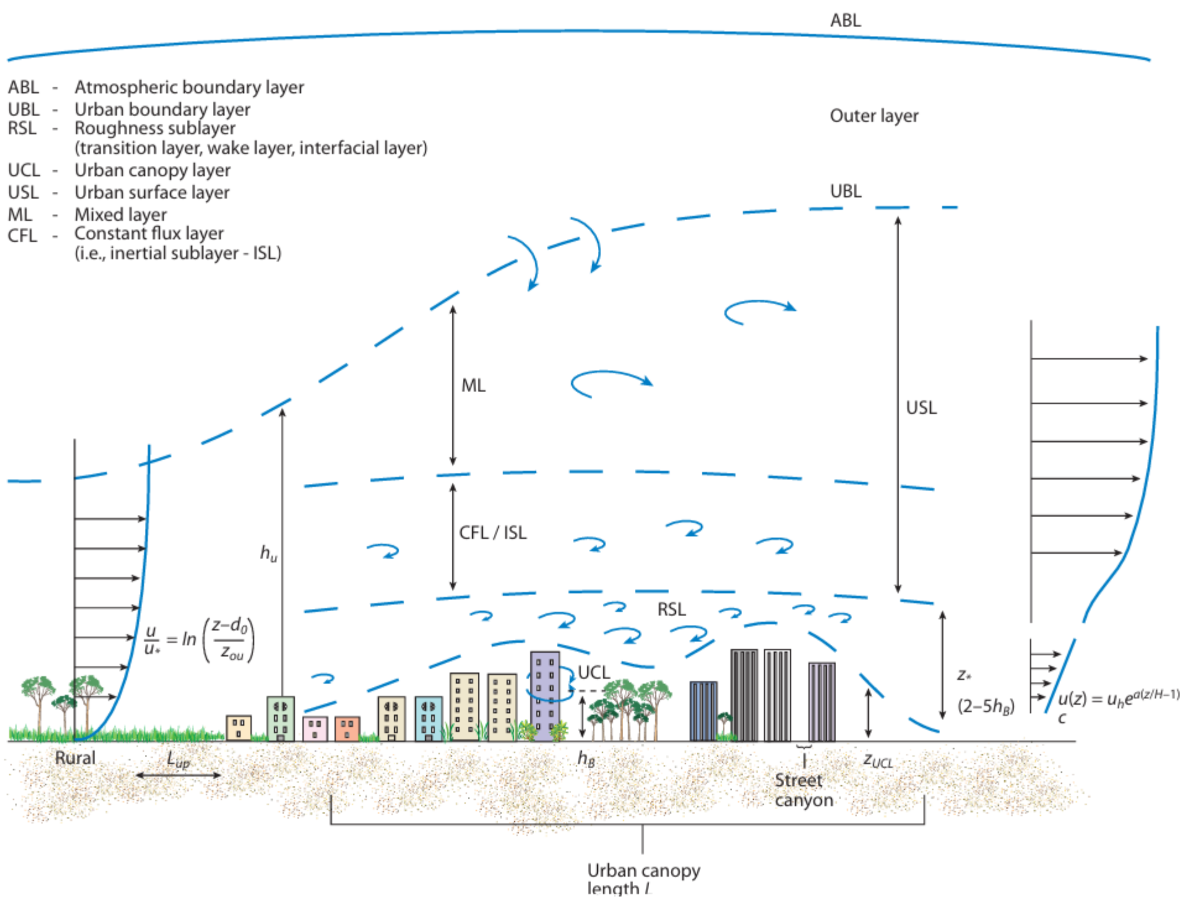

Figure 4 Schematization of the lower atmosphere over urban environment. (Fernando et al, 2010)

The treatment of momentum is also complex for the urban canopy. DuPont et al, 2004 proposes a drag-force approach for the momentum balance:

$$\frac{\partial(\rho U_i)}{\partial x} = R_{ui} + F_{ui}^{bui} + \sum_j D_{ui}^j$$

Where $j \in \{buildings, vega, vegn\}$ (respectively buildings, vegetation over paved surfaces, vegetation over bare soil), $j \in (x, y)$, U_i is the horizontal velocity, R_{ui} is a general forcing term, F_{ui}^{bui} are the momentum sources due to horizontal building surfaces and $D_{ui}^{j}$are momentum sources due to pressure and viscous drag by trees and vertical building surfaces.

Furthermore, the horizontal temperature gradient generated by the UHI induces the formation of updraft plumes, that can reach above the thermal inversion height, thus spreading at an equilibrium height. In turn, this creates a balancing convergence flow at the ground, i.e. a convergent wind field from the rural areas to the city. The ground-level convergence velocity can be defined as:

$$U_r = C\sqrt{g\alpha \Delta T_{u-r} L}$$

where C = 0.08 (Colomer et al.,1999), g is the gravitational acceleration, α is the thermal expansion coefficient, ΔT is the difference between the urban and rural temperature and L is the distance or scale length. The equation was elaborated by Colomer et al, 1999, that assimilated a heated disk in a stably stratified fluid to the bulk effect of the urbanized area.

Oke, 1973 derived a relationship between UHI ΔT, regional windspeed u and population P under cloudless skies:

$$\log \Delta T_{u-r} = 0.27 \log P - 0.56 \log u - 0.61$$

The standard error is of 1.6 °C.

For calm and clear conditions, the UHI reaches the maximum value and the relationship involves only the population P. For European cities:

$$\Delta T_{u-r(max)} = 2.01 \log P - 4.06$$

The standard error is of 0.9 °C.

An analysis conducted by Albini et al, 2025 reviewed remote sensing datasets for all the Italian regional capitals for the 2013-2023 period with the aim of measuring the Surface Urban Heat Index, that is, the ΔT between the urbanized and rural areas. They report that, in Bologna, artificial abiotic surfaces in the city centre cover 98.5% of the area and that the summer UHI is of 4.3°C (Real Estate Market Observatory approach). Additionally, they state that, 'for every 10 % increase in tree cover differences between outer and central belts, SUHI intensity increases by about 1.0 °C' for plain cities (p<0.001). Di Sabatino et al, 2020 conducted a field campaign in Bologna and results showed that trees and urban canopies with different morphologies can mitigate the UHI by 40%.

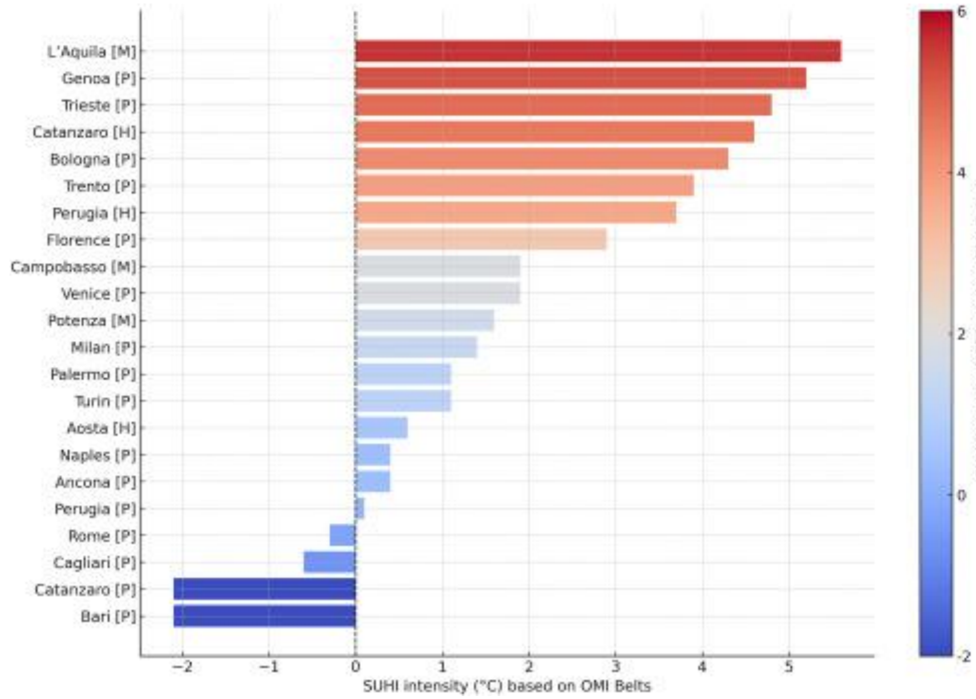

Figure 5 UHI index for italian regional capitals. Bologna is at n. 5. In coastal cities, like Bari, the effects can be negative (colder city centre). Albini et al, 2025

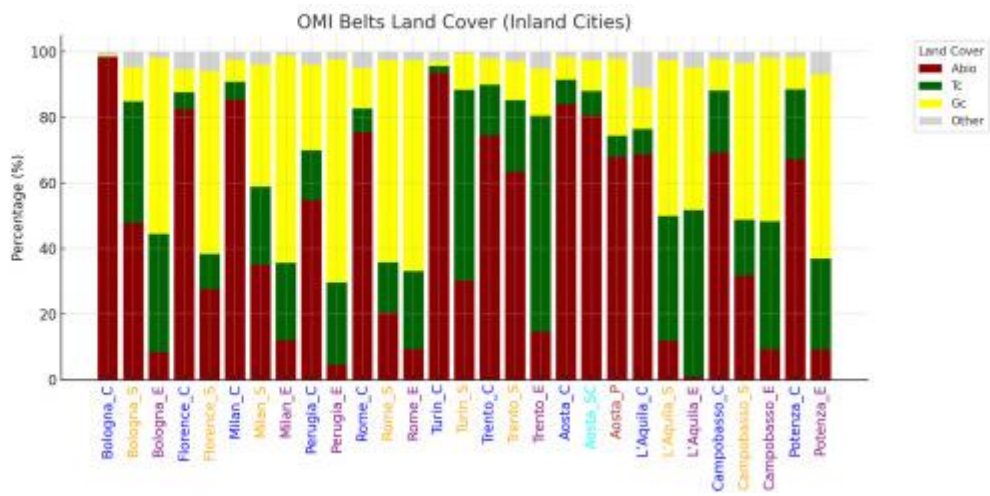

Figure 6 Land cover percentages for inland cities. C=central, S=suburban, E=extra urban. Albini et al, 2025

In fact, the developed terrain in cities usually presents a larger ratio of impervious ground that causes reduced evapotranspiration and other effects that alter the energy budget of the surface, along with a large amount of materials with a high thermal capacity.

The surface energy balance at the ground/on a surface can be formulated as (Ulpiani, 2021; Dickinson, 1986):

$$(1-\alpha)I_{\downarrow} + I_{Lw\downarrow} - \varepsilon\sigma T_s^4 - H_s - H_l - H_g = 0$$

Where α is the albedo of the surface, $I_{\downarrow}$is the downward shortwave radiation flux from the Sun, $I_{Lw\downarrow}$ is the downward longwave radiation flux from the atmosphere, ε is the surface emissivity, σ is the Stafan-Boltzmann constant, T_s is the surface temperature, $H_s$is the sensible heat flux from the surface, H_l is the latent heat flux from the surface and H_g is the ground heat flux. Overall, the components represent absorbed incoming solar radiation, incoming atmospheric longwave radiation, outgoing blackbody radiation and outgoing sensible, latent and ground heat fluxes. From this equation, the mechanisms that control the UHI are clear: low albedo surfaces capture more energy, thus heating the city's fabric, while highly emissive materials emit thermal radiation more effectively and cool down faster. Also, evapotranspiration generates a cooling outgoing heat flux, damping the UHI. The equation holds true for all surfaces; so, roofs, façades or streets emit radiation according to the surface energy balance, given their albedo, emissivity and positioning relative to other surfaces (that undergo the same processes of emission and absorption). Consequently, in a more densely urbanized area, the radiation gets reflected and re-absorbed many times from the urban canopy before being carried away by airflow.

Land use change is connected to local albedo modifications: streets covered by asphalt have low albedos, which lowers the amount of reflected light during the day and traps significant heat, that is then radiated at night, thus warming the city. The same process holds true for other low albedo structures, such as dark roofs or plots of land. (Liu et al, 2024)

Bodies of water can also alter UHI. Zhou et al, 2018 simulated the impact that a decrease in lake area in Wuhan (one third of the lake area or 130.5 km^2) had on the UHI, finding an increase of the Heat Island both during the day and during the night. During the night, lakes and open spaces can favour ventilation and heat dissipation while, during the day, water acts as a cold source. Also, the research revealed an increase in the night-time wind needed to balance the UHI, but dense urbanization obviously acts as an obstacle to the effectiveness of ventilation.

The IPCC reports urban greening, wetland and upstream forest ecosystem restoration (which can also synergistically assist in decreasing flooding) as UHI mitigation strategies. Nature Based Solutions (NBS) like green infrastructure, reflective or retro-reflective materials, introduction of vegetated areas and mindful urban planning are deemed as effective, though explicit evaluation for each case is desirable (Hayes et al., 2022).

Overall, UHI-reducing tactics can be classified as TSG (trees, shrubs and grass), HAM (high albedo materials) and UIWB (urban inland water bodies) and their effectiveness should be assessed by studies on the specific site. For example, O' Malley et al. compared the effects of these three strategies in the borough of West Kensington in London, finding vegetation to be the most beneficial.

Urban greenery can mitigate UHIs via absorption of shortwave radiation for photosynthesis, evapotranspiration (phase transitions from water to vapor at the leaf interface generate latent heat cooling) and shade and pervious surface provision, as pervious materials have lower heat absorption and re-emission (Qiu et. al, 2013). In fact, it is advisable to explore the right measures for the best outcome in each case at hand, considering the natural and anthropogenic topography, the microclimate and other factors (O' Malley et al., 2015).

At the same time, mitigation strategies can be not enough if there's a fallacious urban planning at the root: distance between buildings, structure height and other characteristics should be factored in when designing new areas or modifying existing ones. So, urban planning is paramount for the mitigation of the UHI, and it should be 'hand-fitted' to the case in question. Because of this, the UHI question sits at the intersection of multiple areas of research, needing answers from climate scientists, civil engineers, architects, policymakers, administrators, urban planners and more.

And the urgency of action is increasing: IPCC's Sixth Assessment Report claims that hot extremes have intensified in cities, with adverse impacts being more prominent among vulnerable residents. Cities now host more than half of the world's population and the proportion is estimated to reach 60% by 2030 (UN, 2018) 69% by 2050 (Qiu et al., 2013), so it is of crucial importance to mitigate the adverse effects that the UHI can generate.

The UHI leads to increased energy and water consumption, thermal discomfort, heat-related health risk caused by extended exposure to high temperatures, along with increased pollution (traffic, household, commercial and industrial emissions). Furthermore, the polluting aerosols, because of the UHI-altered circulation, can stagnate on cities and create a UPI (Urban Pollution Island), that leads to greater risk of cardiorespiratory disease for the citizens (Román et al, 2009).

Conclusively, the temperature anomaly induced by the UHI has multiple consequences, especially during hot periods, such as heatwaves.

1.1.2 Heatwaves

Heatwaves are periods in which recorded temperatures exceed quite significantly the climatology for the area and time in question. These events can last a few days or can persist for extended stretches of time. Deciding whether an event is a heatwave or not thus depends on the specific area of study and period of the year, along with the chosen approach for the election of a threshold of temperature, duration and other properties.

There isn't a univocal definition for heatwaves: the IPCC (2023) defines them as 'a period of abnormally hot weather, often defined with reference to a relative temperature threshold, lasting from two days to months', but the terms change based on where the heatwave happens. For example, in Adelaide, Australia it's defined as 'five consecutive days at or above 35°C, or three consecutive days at or over 40°C' (Australian Bureau of Meteorology, 2010), while in Ireland, a heatwave is declared when 'the daily maximum shaded air temperature is greater than twenty-five degrees Celsius (> 25.0°C) for five or more consecutive days' (MET Éireann, 2023). In general, to define a heatwave, it is important to consider the climatology of the region: the tropics, for example, exhibit less variability than the extratropics, and this behaviour must be factored in when defining a heatwave event.

Russo et al, 2014 developed a Heat Wave Magnitude Index that can be compared over space and time, as it considers duration, intensity and comparison with the distribution of the maximum temperature climatology, unlike other indexes. In fact, the study reports how some heatwave indices were found to be unrobust when comparing different regions or periods, since they can be constructed specifically for the region or be defined in absolute terms, omitting the comparison with the probability distribution of the reference period. Moreover, to define a heatwave, the definition can change from region to region: Perkins and Alexander, 2012 consider a period of 3 or more consecutive days above threshold to be an Australian heatwave, while for Europe, Fischer and Schär, 2010 defines it as a minimum of six consecutive hot days. Russo et al, 2014 states that, in a warmer planet (the analysed scenarios in the paper were RCP 8.5 and RCP 4.5), events as intense as the European 2003 heatwave or the 2010 Russian heatwave are projected to become the new norm, occurring as often as every two years in a few regions, including southern Europe.

Adil et al, 2025 estimates Italy to be on the top three of the most affected countries globally by climate-related extreme weather events, after Pakistan and Belize, in 2022. In that year, Italy suffered 18,000 fatalities, leading the ranking for deaths per 100,000 people (30.62/100,000). The fatalities were caused mostly by wildfires and severe droughts induced by the extreme heat, especially in the Po Valley. This data seems confirmed by ISTAT, 2022 that finds a +20% increase in deaths during July of 2022 and relates this anomaly to the summer heatwaves and their impacts. Garrido-Perez et al, 2024 further reports that Northern Italy was affected by severe drought conditions in June 2022, concurrent to heatwaves.

Heatwave events, particularly if prolonged and/or intense (extreme heat), lead to thermal stress and can pose a risk for health and economy (García-León et al, 2021), aggravate fire hazards, hinder food and water security through droughts and agricultural damages. Obviously, all these risks need to be weighted with the vulnerability of the region.

Heatwaves are being exacerbated by the warming climate: according to the Sixth Assessment Report of the Intergovernmental Panel on Climate Change, anthropogenic climate change is increasing the number, intensity and duration of heatwaves. Notably, ‘every additional 0.5°C of global warming causes clearly discernible increases in the intensity and frequency of temperature extremes, including heatwave intensity, frequency and duration’ (WMO).

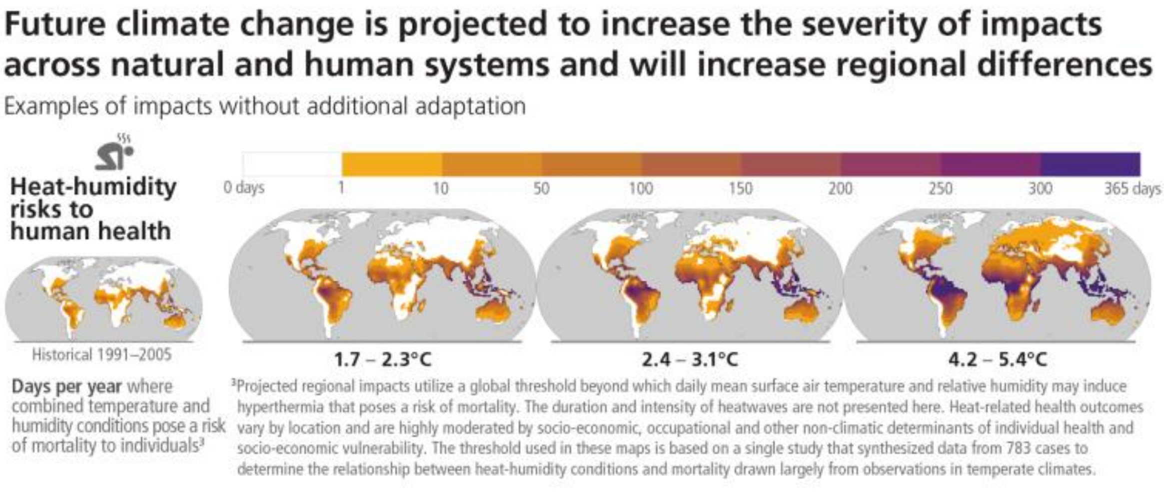

Figure 7 Evolution with increasing global warming of the number of days per year in which heat and humidity pose mortality risks (AR6 Synthesis Report: Climate Change 2023 (IPCC))

The 2023 summer in Europe, just two years ago, didn't have the highest average temperature, but showed great contrast: there were multiple extremes that couldn't be caught by the simple seasonal averages. Copernicus reported that 'heatwaves affected large areas, with multiple daily temperature records broken. At the peak of a heatwave in July, a record 41% of southern Europe was affected by 'strong', 'very strong' or 'extreme heat stress'.' (Copernicus, 2023)

Heatwaves are also known to cause reductions in productivity and consequent economic losses, this has been proven to be true also in Europe, especially in more vulnerable regions, that showed GDP losses even beyond 1% (García-León et al). If adaptive or mitigative measures aren't taken, the impacts could increase by up to a factor of almost five by 2060.

Areas subject to UHIs undergo an intensification of the risks associated with heatwaves, lessening the nocturnal cooling and eliminating the relief usually provided by the night (Possega et al, 2022). A study by Tan et al. (2010) highlighted how, as urbanization increases, the degree of warming increases too: UHIs become more extensive, thus leading to additional heatwave days in cities compared to rural areas. The same study finds increased heat-related mortality in urbanized areas from thermal stress caused by the UHI.

Heaviside et al. (2016) found out that 'the UHI contributed around 50 % of the total heat-related mortality during the 2003 heatwave in the West Midlands'. Additionally, they simulated a threefold increase in mortality for a medium emission scenario (UKCP09 Climate Projection) in 2080 compared to the 2003 rate, but there were no considerations regarding adaptation measures.

Conclusively, heatwave events and Urban Heat Islands will likely be intensified and exacerbated by the rising temperatures, posing a major risk for urban populations. Fortunately, adaptation and mitigation measures, like green areas, bodies of water or retro-reflective roofs, are proven to be effective at damping the negative effects of the UHIs, but need to be accurately tailored to the case in question, as numerous studies confirm. The risks posed by Urban Heat Islands and heatwaves across the world affect billions of people every year: this is why studying and analysing UHIs and heatwaves is of extreme importance.

Chapter 2

2 Methodology

In this chapter, the methodology for the data analysis and field campaign is described.

The first part concerns the climatology, clarifying the data processing procedure for the selected databases. Additionally, it explains the reasoning behind the choice of the datasets, specifically the ISPRA weather station records for the sake of the computation of the climatology and Urban Heat Island and ARPAE's Eraclito 91 reanalysis files for the UHI and heatwaves.

The second part details the setup of the field campaign and how it was conducted, followed by a description of the processing of the planar and frontal area indexes in QGIS, the calculation of the temperature and convergence velocity derived from the data collected with MeteoTrackers, and the object analysis operated on the infrared images.

2.1 Climatology

In the first part of the thesis, the climatologies of Bologna, nearby towns and the Emilia-Romagna region were computed to look for Urban Heat Island evidence. The climatology of Bologna and the close by area was first extracted from weather station datasets collected by ISPRA (Istituto Superiore per la Protezione e la Ricerca Ambientale). Secondly, the analysis was repeated in a broader way on a reanalysis dataset from ARPAE (Agenzia Regionale per la Prevenzione e Protezione Ambientale dell'Emilia-Romagna) to compare Bologna with the whole region and the surrounding area.

In the second part, from the same ARPAE reanalysis dataset (Eraclito 91), heatwave days and heatwave events for Bologna were analysed.

2.1.1 Urban Heat Island

2.1.1.1 ISPRA Weather Stations

The first analysis was conducted on ISPRA monitoring station monthly mean temperature datasets for the period 1991-2023. This specific timespan was chosen for two reasons: having at least 30 years of data, which is the standard for climate science and matching the Eraclito 91 dataset, that starts in 1991. Unlike the ARPAE dataset (1991-2025), the retrieved records from ISPRA had 2023 as the last obtainable year.

The utilized weather stations are located in Bologna and four nearby smaller towns or hamlets:

Table 2 Inhabitants as of March 2025 (ISTAT, 2025)

Place	**Bologna**	**Castel San Pietro Terme**	**Sasso Marconi**	**San Pietro Capofiume**	**Mezzolara**
Inhabitants	391,374	<21,000	<15,000	<2,000	<2,000

Table 3 ISPRA weather station information.

Weather station	**ISPRA name**	**Longitude**	**Latitude**	**Available period**
Bologna idrografica	BOLOGNAUFFID	11.34614	44.4999	1991-2012
Bologna regionale	Bologna Urbana	11.328789	44.500754	2006-2021
Bologna Borgo Panigale sinottica	BOLOGNA/BORGO PANIG	11.3	44.533	1991-2023
Castel San Pietro Terme idrografica	CASTSPIETROAGRO	11.59036	44.40475	2006-2023
Castel San Pietro Terme regionale	Castel San Pietro	11.597002	44.411113	2004-2021
Mezzolara idrografica	MEZZOLARAAGRO	11.53219	44.56725	2006-2023
Mezzolara regionale	Mezzolara	11.533782	44.571051	2004-2021
Sasso Marconi idrografico	SASSOMARCONAGRO	11.23687	44.43508	2006-2023
Sasso Marconi regionale	Sasso Marconi	11.240967	44.442754	1991-2021
San Pietro Capofiume idrografica	SPIETROCAPOAGRO	11.62262	44.65379	2007-2023
San Pietro Capofiume regionale	S. Pietro Capofiume	11.620434	44.657207	1991-2021

So, three stations for the main city and two station for each smaller town were elected, totalling 11 computed weather monitoring stations. The datasets were in .xlsx format and their columns contained information about the year, month, value of the monthly average temperature [°C], 2 standard deviations [°C] and the number of days from which the monthly average was calculated. The files were analysed in Python. Utilized libraries included: os, pandas, xarray, numpy, matplotlib and scipy.

The monthly average temperatures and STDs were plotted for each singular station with respect to time to check for gaps, inconsistencies and overall trend via linear regression (stats was used to find the linear fit and P-values). The threshold for significance was chosen as p-value ≤ 0.05, as is usual. The datasets included a few gaps, especially for some monitoring stations, such as San Pietro Capofiume or Sasso Marconi regionale. The records for each of the five locations were then overlapped to verify their coherence, as some stations could erroneously have misplaced data, delays or different trend.

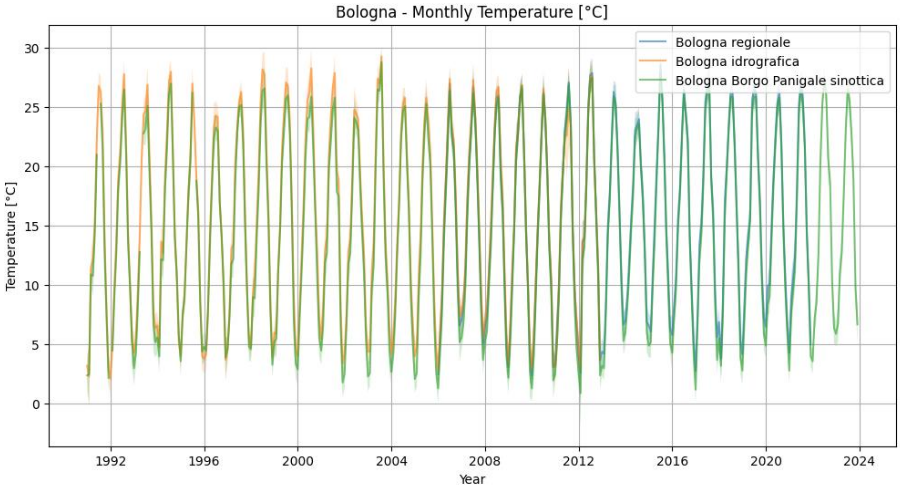

Figure 8 Overlapped data for Bologna (mean monthly temperature and STD).

After these preliminary checks, the datasets were averaged for each location, thus creating five records, that contained the mean of the average monthly temperature and the propagated STD for the mean, calculated as:

$$\sigma = \sqrt{\frac{\sum(x^2)}{N}}$$

With N being the number of STDs (x) to sum.

Overall, the covered periods for each place were:

Table 4

Place	**Bologna**	**Castel San Pietro Terme**	**Sasso Marconi**	**San Pietro Capofiume**	**Mezzolara**
Period	1991-2023	2004-2023	1991-2023	1991-2023	2004-2023

The temperature was plotted with respect to time and the linear best fit was computed with the corresponding p-value to attest the significance of the extrapolated trend [°C/month].

Then, the yearly and summer climatology for each weather station were computed. As for the summer climatology, the months of June, July, August and September were chosen, as opposed to the usual meteorological JJA, because the field campaign was carried out in the beginning of September and the astronomical summer lasts until the September equinox. To obtain the climatology, the values of all the years for each month were averaged.

The yearly and summer (JJAS) climatology was computed from the previously found town averages to find out which place was the warmest, to verify the Bologna Urban Heat Island hypothesis. The elected towns and hamlets are within a 30 km radius of Bologna, have similar elevation (except for Sasso Marconi, 200 m difference) and the climatic conditions in the plain are almost constant (same Cfa classification). The average of the average climatologies was also plotted to look at the bulk local temperature behaviour and observe where Bologna is placed with respect to it in the whole year and in summer (as the UHI is more present in this season). The STD was propagated too.

To analyse the evolution of the area's monthly temperatures, the average of the five towns' means (i.e. the Bologna mean was averaged with the means of Mezzolara, Sasso Marconi, etc.) for each year was calculated. All the years were then plotted in the same graph and the last three years were highlighted to compare them with the previous three decades. The process was repeated for the summer period. The STDs weren't displayed because the graph already appeared dense.

2.1.1.2 Eraclito 91

The second analysis was conducted on the ARPAE's Eraclito 91 reanalysis dataset of the Emilia-Romagna region for daily minimum and maximum temperatures (1991-present). The dataset is a 5 x 5 km resolution spatial interpolation of weather station data that has been filtered to comply with multiple requirements, such as spatial coherence, temporal consistency and statistical homogeneity (ARPAE).

Eraclito 91 was chosen instead of Eraclito 61 or ERG5 because it has a great accuracy for the computation of trends, because of the constant density of weather stations during the whole period, and it has a medium accuracy for local analyses and spatial accuracy. In short, it was elected because it's a good compromise between the two other ARPAE reanalysis datasets. The aim of the thesis is to compare Bologna with the surrounding area to find UHI evidence and compare the climatologies: to do so, it is necessary to have both spatial accuracy and good trend estimation.

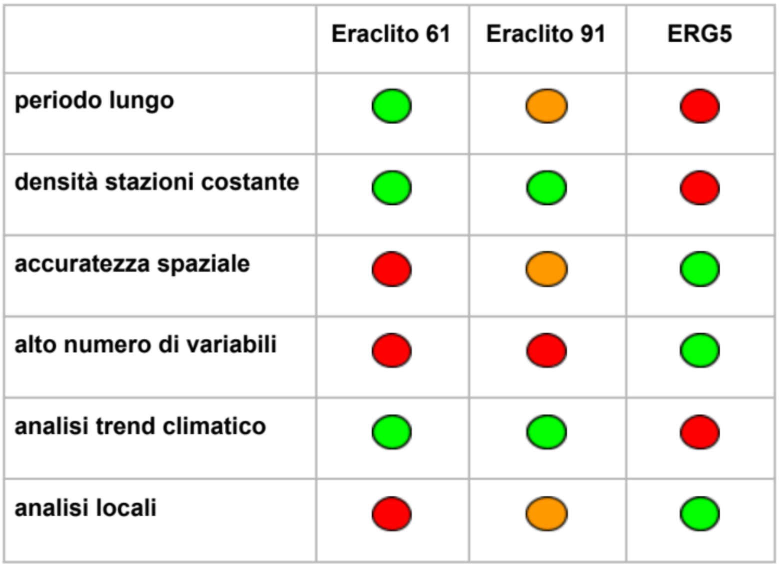

Figure 9 The table compares the characteristics of the ARPAE datasets: Eraclito 61, Eraclito 91 and ERG5. The left column reads 'long period', 'constant density of weather stations', 'spatial accuracy', 'high number of variables', 'climatic trend analysis' and 'local analysis'. (ARPAE, Guida agli open data meteo-clima)

The dataset on the ARPAE website can be found divided into .xlsx files, one for each year and each 5 x 5 km cell: to retrieve the 36,505 files (35 years, 1,043 cells), a parser elaborated from [simc-opendata-examples/erg5/README.md at master · ARPA-SIMC/simc-opendata-examples · GitHub] was modified and adapted to obtain the data locally. Each file contained four columns: 'PragaDate', 'DAILY_TMIN', 'DAILY_TMAX' and 'DAILY_PREC'. The files were named as the corresponding cell and year. The files were elaborated in Python, with the aid of the following libraries: os, pandas, xarray, numpy, matplotlib, scipy, argparse, io, zipfile requests and cartopy.

To map the data with cartopy, the coordinates were obtained in .geojson format from Index of /opendata/erg5v2/timeseries, as the cells of ARPAE's ERG5 dataset have the same coordinates of the Eraclito 91 dataset. For this file, the json library was also employed. The 'erg5v2.geojson' file was read, and it presented four keys ('type', 'name', 'crs' and 'features'). The 'features' key contained 17 properties, including latitude, longitude and number for all the cells of the Eraclito 91 dataset. In detail, the properties were ['Codice', 'Comune', 'Regione', 'Provincia', 'row', 'col', 'lat', 'lon', 'Name', 'UTM_X', 'UTM_Y', 'AvgHeight', '_mean', '_median', '_stdev', '_min', '_max', 'coordinates']. The values were stored in a pandas dataframe containing the information needed for all the 1,043 cells of the reanalysis grid, to then merge it with the already loaded Eraclito 91 files, thanks to the matching .xlsx name (which contained the number of the cell). Then, all the 36,505 files, now containing the coordinates for mapping, were merged into one for a more rapid use. Also, the data for the cell n. 1421, centred on Bologna, was merged into one, spanning from 1991 to 2025 (not the full year). For the computations, though, the year 2025 wasn't used, as it wasn't complete for obvious reasons.

With the objective of comparing them, the climatologies of daily minimum and maximum temperatures [°C] for Bologna (cell 1421) and for the whole region were computed for the full year (1991-2024) by averaging the values for each day. The STD was also determined as

$\sigma = \sqrt{\frac{\sum(x_i - \bar{x})^2}{N}}$ where x_i is the datapoint, $\bar{x}$ is the mean and N is the number of datapoints. The calculation was elaborated with built-in functions.

The 1991-2024 yearly means for Bologna and Emilia-Romagna were calculated for minimum and maximum temperatures to observe variability and linear trend with associated P-value. The procedure was repeated for each season (DJF, MAM, JJA, SON) with the aim of observing seasonal trends and summer minima in particular (for UHI evaluation) and maxima (for heatwaves).

Yearly anomalies were evaluated as $x_i - \bar{x}$, where $x_i$is the average of minima or maxima for a certain year i, and $\bar{x}$ is the 34-year (1991-2024) average of all yearly minima or maxima. Also, 'hot years' and 'cold years' were evaluated by comparing them to the average.

To analyse the data from the field campaign with respect to the climatology of the city and of the region, a 10-day climatology (1991-2024) centred on the 1st and 2nd of September was computed. So, daily minima and maxima for the days 28th of august to 6th of September were averaged for each day and the daily STD was estimated.

After the temporal analysis with the evaluation of trends and such, a spatial analysis was completed to look for temperature gradients and UHIs. To map the datapoints of the Emilia-Romagna region, the merged file with the coordinates retrieved from the .geojson file was utilized.

Mapping of the mean minimum and maximum temperatures was carried out (1991-2024) for average yearly values and average seasonal values (DJF, MAM, JJA, SON). Then, the slope of the linear trend for the minima and maxima temperatures evolution was mapped.

To observe in more detail the city of Bologna and the surrounding area, a square of 11 x 11 cells centred on the cell n. 1421 was chosen (or 55 x 55 km, roughly a 30 km radius circle – same scale of the ISPRA weather stations) and minima and maxima were mapped for the JJAS months. As the average of the daily minima can be deemed as representative of the night hours, i.e. the hours during which the UHI develops, the meridional and zonal section were plotted to confirm a UHI profile (which was found). In practice, the retrieved value for JJAS cell minima in the row containing Bologna was plotted with respect to the longitude (zonal section) and the same was done with the 'column' with respect to the latitude (meridional section).

2.1.2 Heatwaves

For the heatwave analysis, the Eraclito 91 database was kept as reference, because of the possibility of trend estimation and medium spatial accuracy. Please note that the heatwave evaluation was carried out only for the city of Bologna (cell n. 1421) and the dataset unfortunately provides only medium spatial accuracy. In fact, in its guide (Guida agli open data meteo-clima), ARPAE recommends ERG5 as the best dataset for local heatwave evaluation. But ERG5 doesn't have any accuracy for trend estimation. So, in the end, Eraclito 91 was preferred.

The adopted definition of heatwave is from Russo et al. (2014). In the paper, a heatwave is defined as at least three consecutive days with daily maximum temperature above a certain threshold, picked as the 90th percentile of the set of data:

$$A_d = \bigcup_{y=1991}^{2024} \bigcup_{i=d-15}^{d+15} T_{y,i}$$

where '$T_{y,i}$ is the daily maximum temperature of the day i in the year y' and the years of beginning and end (1991-2024) have been adjusted to the case at hand. In practice, each day of the year will have a specific threshold, that is calculated as the 90th percentile of all daily maxima contained in a moving window of 31 days centred on that specific day of the year.

In the thesis, three types of thresholds were chosen: 90th, 95th and 99th percentile. This was done to observe the trend and number of extreme heatwaves too.

In this part, only the daily maximum temperature from the merged dataset (1991-2024) of the cell n. 1421 was utilized. The involved Python libraries included: os, pandas, xarray, numpy, matplotlib and scipy.

At first, an absolute evaluation was conducted by counting and plotting a histogram of the number of yearly hot days in Bologna, that is, days with maximum temperatures above 30, 35 or 40 °C. Also, a trend and P-value estimation for each type of hot day was carried out.

Then, the Russo et al. definition was used, with the three thresholds. Two histograms were plotted to represent the number of yearly heatwave days for the whole year and for the JJAS months. Trends and p-values were estimated. Here, all days above a certain threshold were counted.

Only after, yearly heatwave events were counted (i.e. three or more consecutive days with maximum temperature above the threshold) for the whole year and for the JJAS months. Trends and p-values were estimated for the period 1991-2024.

To wrap up the heatwave evaluation, there's a focus on the duration of each heatwave event. Both for the full year and for the JJAS months, for each threshold, the number of yearly heatwave events for each duration (min. 3 days – calculated max. 11 days) was plotted in a stacked-bar histogram. Warmer colours represented longer heatwaves.

This assessment was carried out to measure if heatwaves exhibit a trend, and if heatwaves of different intensity (three thresholds) have different trends for the city of Bologna. Also, their duration was evaluated for each different type.

2.2 Field Campaign

The described methods were employed with the objective of comparing temperatures and phenomena at different scales. The climatology part regarded the investigation of regional and 'municipal' scales, while the experimental part will allow the examination of urban-rural scales (extra routes), intra-city scales (neighbourhood analysis from normal routes, planar and frontal indexes) and street-level scales (thermal imaging). An integration for the 'municipal' scale will be given by the convergence velocity.

2.2.1 The Experimental Sites

The field campaign was conducted in Bologna on the first and second day of September 2024, during a 24-hour period (09:00-09:00 CEST). The dates were chosen because of the probable presence of conditions favourable to heatwave formation, with the aim of observing the concurrent effects of the UHI and heatwave. Two sites were chosen for the measurements: the Prendiparte Tower (Torre Prendiparte - TP), 60 meters high and located in the historical city centre, and the Sant'Orsola hospital (Ospedale Sant'Orsola - SO), located outside of the historical walls of the city, composed of various buildings, a main tree lined street and multiple smaller alleys.

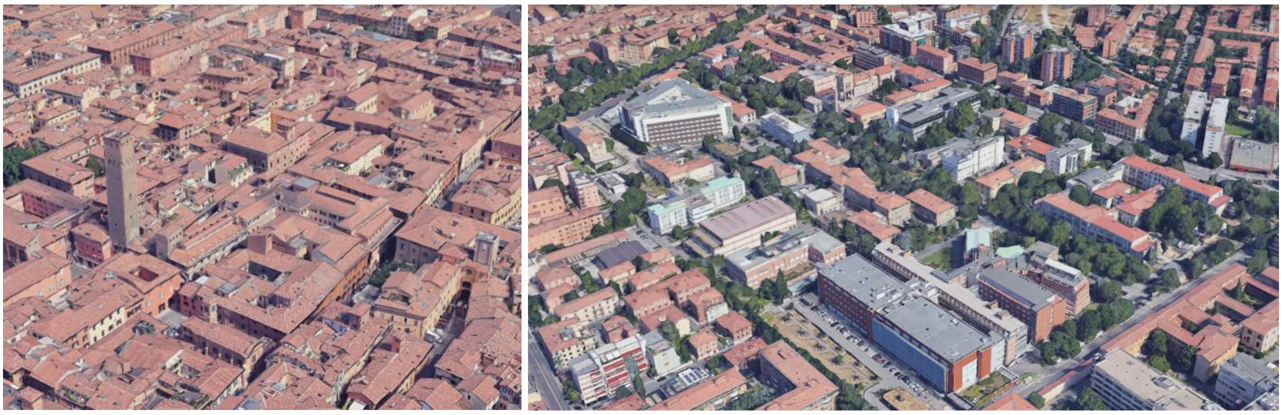

Figure 10 Views of the investigated neighbourhoods. On the left, the central district, a densely built area; on the right, the hospital district, outside of the historical city centre, a more sparsely built and tree lined area. (Google Earth)

A 24-hour period was chosen to collect information on the full diurnal trend of air and object temperatures, and on the evolution of their interactions and effects as the external conditions changed.

A few volunteers carried out measurements at ground level via MeteoTracker devices installed on bikes. Every hour, three volunteers headed out on an approximate 10-minute ride on their equipped vehicles on three different routes covering the two study areas: the Prendiparte zone was divided into an eastern and western route for ground measurements, while the Sant'Orsola zone was covered by a single volunteer per hour.

The route choice was made with the objective of gathering the most detailed ground temperature possible in a short amount of time, to have air temperature data that was comparable to the surfaces' temperature data collected with the FLIR thermal camera.

In fact. at the same time, as the three volunteers departed on their bike routes, two sets of 360° IR photos were taken from atop the tower, in open air. The first set covered the closest area by pointing the FLIR thermal camera at a lower inclination with respect to the perpendicular to the ground, and the second set covered the further 'ring' by maintaining a higher angle. For each set, the thermal camera was calibrated. To do so, the RH and air temperature was detected with the thermo-hygrometer (Extech MO297). The values were then used to measure the reflected temperature for the sky and for the buildings, with the distance parameter set to 0 and emissivity set to 1 (approximate blackbody radiation). This operation was carried out by pointing the camera to a piece of tinfoil at a particular angle, as metals are highly reflective (low emissivity) and the measured temperature is approximately equal to the reflected temperature, rather than to the real temperature of the object. After this, all the object parameters were determined, and the photos were taken. Only the distance was adjusted to 180 m for the lower set and 430 for the higher set. For the whole campaign the chosen camera temperature range was -40/120 °C to maximize detail.

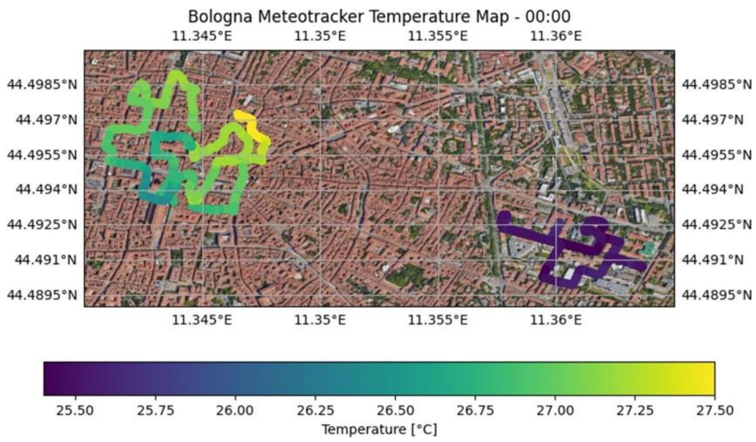

Figure 11 Tracks covered by the volunteers on the equipped bikes. On the upper left tracks representing the TP or Prendiparte Tower zone; on the lower right tracks representing the SO or Sant'Orsola Hospital zone.

2.2.2 The Experimental Equipment

Figure 12 MeteoTracker, FLIR T1020 IR camera, Extec MO297. (meteotracker.com, amazon.it)

The utilized instrumentation consisted of:

-MeteoTrackers: MeteoTrackers (MT) are mini-mobile weather stations.

The employed type is specific for the collection of data while in movement, and can be attached via a holder to the handlebars of a bike. After securing the MT with the louvers towards the direction of movement, as the sensors will be exposed to the flow of air passing through, it will be able to produce an array of data, such as air temperature [°C], relative humidity [%], atmospheric pressure [mbar], dew-point temperature [°C], potential temperature [K] and humidex index [°C].

At the start of the recording session, the device must also be connected to the mobile app MeteoTracker, that utilizes the associated phone's GPS and clock to locate both temporally and spatially the various point-like measurements, collecting date, hour, longitude, latitude, altitude and speed [km/h].

The humidex is defined as:

$$HDX = T + 0.5555(e - 10)$$

Where e is the water vapor pressure in hPa and the temperature is in °C. (Barbano et al., 2024)

MeteoTrackers are effective thanks to RECS technology (Radiation Error Correction System) that balances the necessity of fast measurement response and accuracy under strong solar radiation for mobile weather stations. RECS can correct the temperature data effectively at speeds of over 7 km/h. In general, the accuracy of the MT for important variables is reported in table 5:

*Table 5 *Under solar radiation and speeds > 7 km/h **for the initial value only (Barbano et al, 2024)*

Variable	Accuracy	Operational range
Air Temperature [°C]	± 0.5 °C *	-40/125°C
Relative Humidity [%]	± 2%	0-100%
Atmospheric Pressure [hPa]	± 3 Pa (relative) ± 50 Pa (absolute)	-
Altitude a.m.s.l. [m]	± 10 m **	-

-FLIR T1020: It's a high-performance IR thermal imaging camera with a thermal resolution of 1024 x 768 pixels. It has a temperature range that goes from -40 to 2000°C, a 30 Hz frame rate and it can be remotely controlled. It contains a Vox microbolometer and can detect temperature differences as low as 20mK (at 30°C). The temperature error is of ±2 °C or ±2% of the reading (the greatest one must be considered). It has six object parameters: external IR window compensation, object distance, atmospheric temperature, relative humidity, reflected temperature and emissivity (FLIR, 2016).

-Extech MO297:

It's a psychrometer with IR thermometer and Bluetooth. It measures the temperature [°C] and relative humidity [%].

2.2.3 Data And Methods

2.2.3.1 Planar and Frontal Area Indexes - QGIS

With the aim of evaluating the characteristics of the TP and SO areas, vector layers regarding the building and trees of Bologna were loaded on QGIS for the assessment of the planar and frontal area coefficients of the two zones ([Homepage — Geoportale]). The tree shapefile presented a gap in the trees inside of the Sant'Orsola Hospital, that were thus integrated by hand. The building and tree data to analyse was exported in .xlsx format, by selecting only the area covered by the bike routes (see Figure 13). The obtained spreadsheets were elaborated in Python (libraries: os, pandas, xarray, numpy, matplotlib).

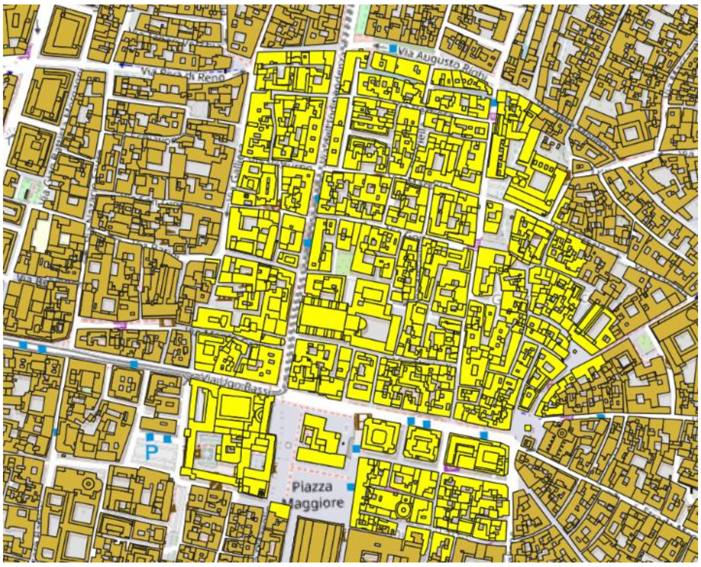

Figure 13 Selection operated in the TP district (yellow buildings).

The .xlsx data for the buildings was composed of 19 columns, out of which four were employed: building area, height, perimeter and volume. As for the trees, the only utilized variable was the number of trees in each area; the diameter was approximated to 5 m and the height to 15 m. To calculate the coefficients, a paper from Barbano et al. (2020) was taken as reference.

The planar area fraction coefficient represents the ratio of the surface occupied by buildings to the lot area:

$$\lambda_p = \frac{A_p}{A_d}$$

Where A_p is the occupied planar area. This value was estimated for buildings only and for buildings and vegetation, respectively A_p^b and A_p^v:

$$A_p = A_p^b$$

$$A_p = A_p^b + (1 - P)A_p^v$$

$$A_p^v = n \cdot \pi \cdot r^2$$

The first equation represents the planar coefficient for buildings only and the second one also factors in trees, that are approximated to porous cylinders of 2.5 m radius. P is the porosity of the tree crown, taken equal to 0.56 and n is the number of trees in the district of study. A_p^b was taken equal to the area value of the buildings' shapefiles.

The frontal coefficient can be defined as:

$$\lambda_f = \frac{A_f}{A_d}$$

$$A_f = A_f^b$$

$$A_f = A_f^b + P_v A_f^v$$

Where A_f is the occupied frontal area. The second equation is for the case in which vegetation isn't considered. P_v is the ratio between the vegetation and building drag coefficient, taken equal to 0.24.

$$A_f^v = n \cdot h \cdot r$$

A_f^v is the tree frontal area, where r is always equal to 2.5 m and h to 15 m, n is the number of trees in the district of study.

Please note that a neighbourhood or any area has two frontal coefficients: one to account for the drag on the N-S winds and one for the E-W winds. So, the area A_f^b of the buildings and the area A_f^v should be different for the two directions (i.e. EW that acts as the impact surface for NS winds and NS that acts as the impact surface for EW winds). In this case, the trees were approximated to cylinders, so their value is the same in both cases. Conversely, for the buildings:

$$A_f^b = \sum_i \frac{h_i \cdot l_i \cdot \Delta_j}{\bar{\Delta}}$$

where h_i is the height of the i[th] building, l_i is the width of the i[th] building for the EW or NS direction, Δ_j is the domain length for the direction of the impacting wind and $\bar{\Delta}$ is the mean domain length.

As the shapefiles didn't provide the values of the length of the façades, but only the height h, volume, perimeter and base area, two approaches for the computation of the oriented façades were attempted:

- $l = \sqrt{A}$ approximating the base of the structures to a square. In this way, the NS and EW values would be equal, but the perimeter wouldn't be 'respected', because the buildings actually do have specific shapes (not clarified in the files);

- $l = l$ where l was estimated from the system of equations provided by the relationships between area, volume, perimeter and height for a parallelepiped. The two obtained values for l (NS and EW) were then randomly selected to represent the NE or SW side of the buildings. This approach was more realistic, but the coefficient would change enormously, as the choice of the side length is random. In the end, the values didn't seem realistic, so they were discarded.

The frontal coefficients shown in the Results chapter are thus the ones obtained with the first approach. λ_p and λ_f give information on the drag force that the air sustains when crossing the two neighborhoods, given their density, and on heat transfer. Higher values indicate hindered ventilation and usually a higher amount of entrapped heat.

2.2.3.2 MeteoTracker Routes Monitoring Protocol for Temperature Mapping

Monitoring for the temperature mapping was conducted by three volunteers each hour, continuously for the whole 24-hour period. The bike routes covered the areas of interest, i.e. the Prendiparte central area and the Sant'Orsola zone, delimited in figure 14.

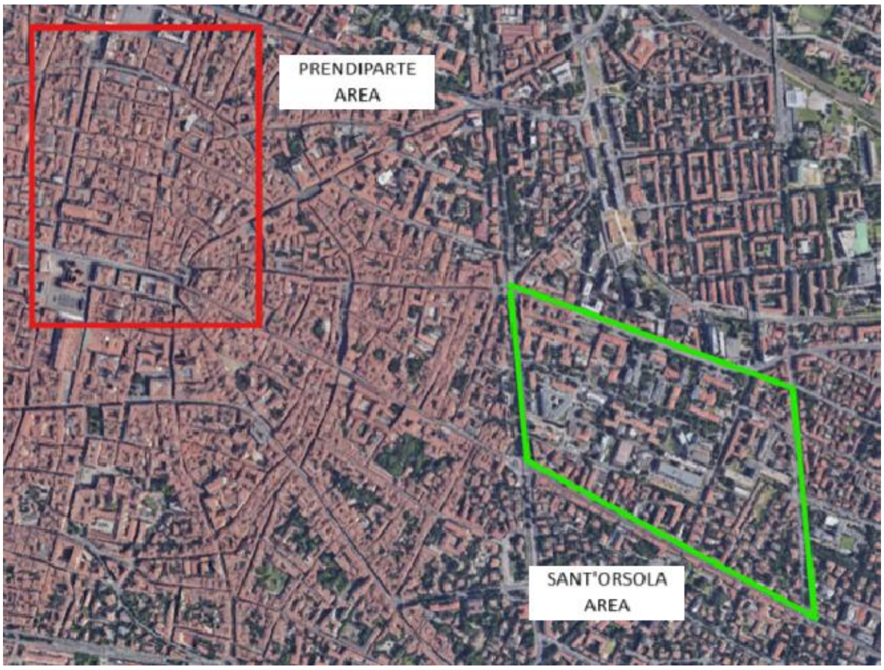

Figure 14 Google Earth

After having characterized the two zones to confirm their different nature with respect to the UHI, the data collected by the volunteers was downloaded from the MeteoTracker platform in .xlsx format and catalogued by hour and route (TP east, TP west and SO).

The files had 12 columns (usually, as it depends on the model of phone connected to the MT): time (date and time with second resolution), latitude, longitude, altitude [m], speed [km/h], radiation, air temperature [°C], relative humidity [%], atmospheric pressure [mbar], dew-point temperature[°C], potential temperature [K] and humidex index [°C].

The data recollected in the field campaign was analysed in Python. The utilized libraries were: os, xarray, numpy, matplotlib, pandas, cartopy, pykrige, scipy and geopy.

The files were first filtered to remove outliers, caused by the adjustment time of the MT to the air conditions (f.e. if the MT was taken from a colder enclosed space to open air). Air temperature values that were either:

$$x < Q_1 - 1.5\ IQR$$

or

$$x > Q_3 + 1.5\ IQR$$

were considered outliers. Q_1 is the first quartile of the dataset and Q_3 is the third one, IQR is the difference between the third and first quartile. (Barbano et al., 2024)

After filtering, the datasets were first simply plotted via scatterplot onto the area, using the coordinates and the air temperature to reveal eventual problems with the temperature range or match with the coordinates. To verify the latter, a satellite image [11.34°, 11.365°, 44.489°, 44.50°] was layered under the MT temperature data.

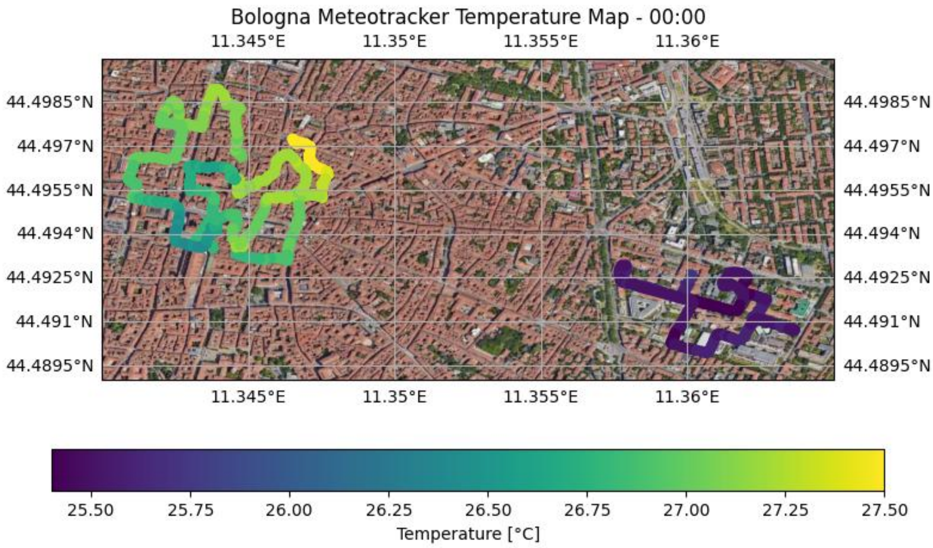

Figure 15 Example of a scatterplot of MT data for 00:00.

After this first phase, that already revealed significant differences between the two areas during the night (UHI), the data was spatially interpolated to investigate the temperature distribution in the urban fabric. To do so, a kriging interpolation with linear variogram was operated for the two separate zones (TP and SO) and for the full extent of the area. This choice of kriging was made to obtain an accurate interpolation in the two areas, layered over a less accurate kriging operated over all the data for that hour.

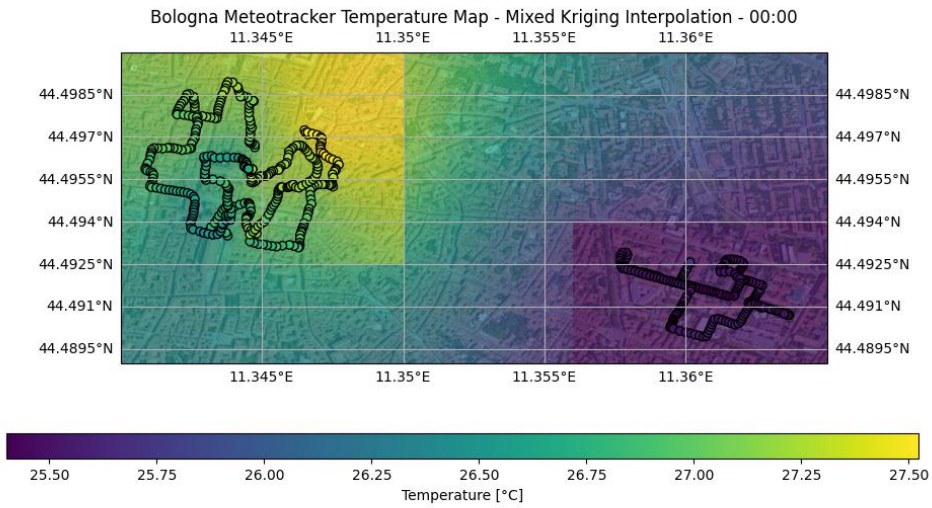

Figure 16 Example of the 'mixed' kriging map.

In the figure 16, the top left 'boxed' kriging was computed from the TP tracks of that hour, while the bottom right 'boxed' kriging was computed from the SO data for that hour. The extent of each box interpolation was chosen based on the area that the tracks covered and on the position of the walls of the city, that coincide approximately with the left limit of the SO box. Under the two interpolations, another one was operated on the merged data from both SO and TP for the whole extent of the figure. The values of the data were concatenated to look for the minimum and maximum to get only one colour bar, valid for all the temperatures shown.

The spatial interpolation was computed for the 'extra' tracks, i.e. nocturnal itineraries that didn't follow the usual routes. These extra tracks allowed a great visualization of the Urban Heat Island of the city, reaching night temperature differences of more than 6 °C in the span of a bit more than 2 km in one case. The kriging for these datasets was operated on the area that they approximately covered.

To relate the recorded temperatures with the terrain and the distance from the dense city centre, some of the extra routes were utilized to compute their temperature difference against distance. To make them more 'readable', the temperature differences were averaged for every 500 m. In particular, a quite straight route was chosen to compare the terrain with the spatial changes in temperature to find correlations.

For the next sections, the mean for each hour for the two zones (TP and SO) was computed to obtain the hourly average temperatures for the whole field campaign duration (from 09:00 of the 1st to 09:00 of the 2nd of September). Because of a few problems and because of the voluntary nature of the campaign, there were some gaps in the diurnal data, which luckily wasn't too central to the UHI investigation. Standard deviations were also computed for every hour and location.

The newly attained data from the MTs was compared with data from two Bologna weather stations (Asinelli and idrografico) and one weather station in Mezzolara, a town close by (already mentioned in the climatology part). From all three stations, instant 2 m temperature data for the 24-hour period was plotted, after adjusting it to the right time zone (as it was in UTC, 2-hour difference with CEST). For the monitoring stations located in Bologna, the hourly climatology for a 10-day period centred on the 1st and 2nd of September was also plotted for the available period, which was 2006-2024 for Asinelli and 2016-2024 for idrografico. The used data is available on ARPAE's Dext3r platform. As the databases for the stations had instant values, the temperatures were averaged to get the hourly mean. For the 10-day climatology, the standard deviation was also estimated. In the end, the plotted data was useful to compare MT data with instant Bologna station data for the same 24-hour period to assess the compatibility and solidity of the temperatures collected with the portable MeteoTracker sensors, and to decide whether it was valid to use for further analysis instead of station values. In short, this was done to see if the MT data could be used as an accurate synthesis of the temperature in Bologna. Secondly, the comparison with Mezzolara could show how much slower Bologna cools down at night because of its Urban Heat Island. Thirdly, the difference between the MT temperatures and the Bologna climatologies could confirm the 1st September as a heatwave day again. In general, the comparison with the three climatologies allowed for the contextualization of the field campaign temperatures with respect to the local climatology. Lastly, the Asinelli station (2006-2024) climatology was also computed for the same period of the idrografico station (2016-2024), both for observing an eventual increase from the previous time range and for the comparison between the two monitoring stations, that are at different heights above ground (Asinelli is higher, 60 m above ground).

2.2.3.3 UHI Convergence Velocity from Permanent Monitoring Networks around Bologna

After this, hourly temperature data for the 24-hour period from seven rural weather stations encircling the city was examined, with the objective of evaluating the UHI and calculating the convergence velocity. For Bologna, the MT TP data was utilized, as it seemed to represent quite accurately the city centre's temperature during the day. In fact, the here utilized coordinates of Bologna correspond to the Prendiparte tower, an extremely central place in the city walls, and the altitude is an average of the altitudes of the historical part of the city.

Table 6

	Coordinates	**Altitude a.s.l. [m]**
Bologna	(44.495833, 11.344444)	65
Zola Predosa	(44.496142, 11.200059)	65
Sasso Marconi	(44.439668, 11.241251)	275
Settefonti	(44.40274, 11.46209)	321
Castel San Pietro Terme	(44.411115, 11.597005)	58
Mezzolara	(44.571053, 11.533793)	20
Padulle Sala Bolognese	(44.627752, 11.290563)	25
Saletto	(44.632318, 11.441136)	18

All monitoring stations belong to ARPAE except for the Saletto one, that belongs to the Emilia-Romagna region. The TP MT data was interpolated to estimate the 18:00 CEST missing value. The following processes for convergence velocity assessment were done both for non-lapse-rate-adjusted temperatures and for lapse-rate-adjusted temperatures. The utilized lapse rate was the environmental lapse rate, commonly taken equal to 6.5 °C/km (ICAO).

$$\Gamma = -\frac{dT}{dz} = 6.5\ °C/km$$

$$T_{adj} = T_0 + \left(\frac{h_{adj} - h_0}{1000}\right) \cdot \Gamma$$

T_{adj} is the adjusted temperature, T_0 is the non-adjusted temperature, h_{adj} is the reference altitude (Bologna in this case) and h_0 is the altitude of the data that has to be adjusted.

The temperatures for all stations and for Bologna were plotted to look for more UHI evidence. As the heat island develops at night, the Sasso Marconi station was discarded because most of the nocturnal values were missing. The delta of the temperatures and the normalized delta was plotted too, where the normalized temperature was equal to ΔT divided by the maximum value of ΔT.

To find the convergence velocity induced by the temperature difference due to the UHI, a formula from Di Sabatino et al. (2020) was adopted:

$$U_r = C\sqrt{g\alpha|\Delta T_{u-r}|L}$$

where C = 0.08 (Colomer et al.,1999), g is the gravitational acceleration, α is the thermal expansion coefficient (for air at the investigated temperature it's = 3.38×10^{-3}), ΔT is the difference between the urban and rural temperature and L is the distance between the two places.

The distances between Bologna and the weather stations were calculated to estimate the convergence velocity for each location.

Table 7

Station	**Zola Predosa**	**Settefonti**	**Castel San Pietro**	**Mezzolara**	**Padulle Sala Bolognese**	**Saletto**
Distance[km]	11.5	13.9	22.2	17.2	15.3	17.0

The wind values were thus interpolated (kriging) for the area surrounding Bologna, for the adjusted and for the non-adjusted temperature differences.

2.2.3.4 Surface Thermal Imaging

From now on, the methodology for the analysis of the infrared photos will be described. During the field campaign, as previously stated, two sets of 360° captures were taken from the top of the 60 m high Prendiparte tower for each hour. The .jpg files were post-processed in FLIR Tools: objects considered typical for the city were selected from the photos, adjusted and examined. The set of objects that was chosen was: roofs, façades, streets and trees. Furthermore a 'roof mix', that is a 'box' selection containing various objects (roofs, façades, windows, etc), was selected for each exposure to account for the bulk response of the urban canopy to the SW and LW radiation.

This selection was done for four exposures (N, E, S, W) and for all objects. The adjustments were implemented for all the objects elected for the analysis. The boxes in each photo were chosen to be as homogeneous as possible, except for the roof mixes, to immediately obtain an accurate representation of the response and temperature of that certain object.

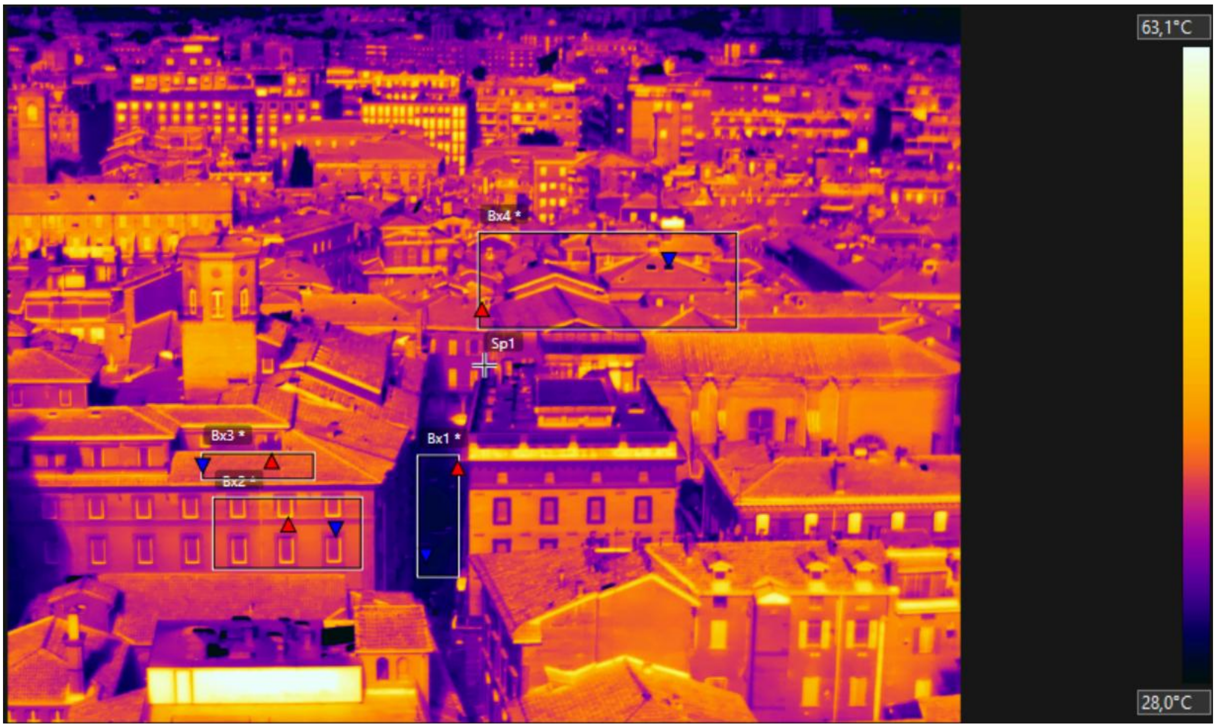

Figure 17 Example of a selection in FLIR Tools: Bx1 was chosen as the reference for a E-W street, Bx2 is an east-facing façade, Bx3 is an east-facing roof, Bx4 is the reference for the east-facing 'roof mix'. This photo was taken at 09:00 CEST, the temperature range is on the right.

Table 8 Corrections operated for the objects in post-processing.

map ref	type	subject	coordinates	emissivity	notes	distance
1	tree	via del Monte-Donzelle E	44°29'46"N 11°20'37"E	0.98	avg leaf emissivity	103
2	tree	Montagnola park N	44°30'05"N 11°20'47"E	0.98	avg leaf emissivity	602
3	street N-S	via Albiroli N-S	44°29'48"N 11°20'42"E	0.94	old (asphalt 0.9-0.98)	117
4	street E-W	via Manzoni E-W	44°29'47"N 11°20'32"E	0.92	smooth cotto tiles	199
5	roof N	San Pietro N	44°29'45"N 11°20'36"E	0.92	rough earthenware brick	108
10	(roof E)	via Indipendenza	44°29'46"N 11°20'34"E	0.92	rough earthenware brick	158
6	roof E	San Pietro E	44°29'44"N 11°20'38"E	0.92	rough earthenware brick	85
7	roof S	via Goito	44°29'48"N 11°20'41"E	0.92	rough earthenware brick	94
8	roof W	via Oberdan	44°29'45"N 11°20'45"E	0.92	rough earthenware	112

					brick	
9	façade N	via Rizzoli	44°29'40"N 11°20'39"E	0.91	plaster	187
10	façade E	via Indipendenza	44°29'46"N 11°20'34"E	0.91	plaster	158
7	façade S	via Goito	44°29'48"N 11°20'41"E	0.91	plaster	94
8	façade W	via Oberdan	44°29'45"N 11°20'45"E	0.91	plaster	112
11	tower façade N	San Pietro N	44°29'43"N 11°20'37"E	0.91	*sagramatura*	98
11	tower façade E	San Pietro E	44°29'43"N 11°20'37"E	0.91	*sagramatura*	98
12	mix N	ref. Dome L		0.92	avg	216
13	mix E	ref. Manzoni R		0.92	avg	270
14	mix S	ref. Montagnola R		0.92	avg	294
15	mix W	ref. chimneys		0.92	avg	150

The table 8 reports the local parameters adopted for the selected boxes in post-processing. The roof mixes were kept with the mean emissivity of the city (0.92), but the distance was adjusted.

Figure 18 Reference map for the objects. (Google Earth)

The hourly mean temperature for each object was plotted in two ways: one grouping together same exposure surfaces and one grouping together the same object type. The former graph was computed to compare directly how different materials and types of surfaces respond to the same approximate exposure to radiation during the day and the night; whereas the latter graph was plotted to observe how the same type of object changes its temperature according to the direction it's facing.

The aim was to examine how the typical city surfaces are influenced and influence the Urban Heat Island, as they absorb and re-emit radiation in the urban canopy.

To compare the evolution of the temperatures of surface materials and air, some objects' diurnal and nocturnal trend was compared with the air temperatures recorded via MeteoTrackers.

In the last part, this analysis was brought further, by investigating the correlation and trend between the nocturnal MT temperatures and the nocturnal IR camera temperatures. This process was first carried out for MT mean hourly temperatures (mean of all the temperatures recorded by the two volunteers in that hour in the central district) and for the full range of MT hourly temperatures. As the resulting correlations and linear best fits were almost equal, the two approaches were synthesized into one.

Overall, the Prendiparte MeteoTracker data was plotted against the IR camera object temperatures. Only the TP MT values were used because the infrared survey was conducted only in the central district. Each plot contains the IR data for a certain exposure and the subplots contain the scatterplots of the surface types, ordered from highest to lowest (roof, roof mix, façade and street). The closest to the ground an object is, the most heat it keeps: this is because of the multiple reflection, absorption and emission processes it goes through. Obviously, the material and its properties further affect these interactions. So, the graphs exhibit how this behaviour correlates with the air temperature in the Urban Heat Island. The correlation and the P-value for each subplot were calculated, as well as the best fit.

In this chapter, the methodology for the multi-scale investigation of the UHI in Bologna was clarified, both for the climatological review, operated both on the mean temperatures provided by the ISPRA weather stations and on the minimum and maximum temperatures provided by the Eraclito 91 reanalysis dataset; and for the design and processing of the urban campaign. The elaboration of the thermal imagery and temperature datasets collected during the field campaign was schematized, showing the reasoning behind the employed choices.

Chapter 3

3 Results

Starting from the climatology of the surrounding area (ISPRA monitoring stations) and of the Emilia-Romagna region (ARPAE Eraclito91 dataset), there's the transitioning towards the field campaign, as the results show clearly that the city of Bologna exhibits higher temperatures (minimum and maximum – respectively relevant for UHI and heatwaves - Eraclito 91, mean – ISPRA). This seems to be a direct consequence of the UHI, as no other factor could really cause this phenomenon (altitude, etc). The climatological analysis thus moves to smaller and smaller scales, exploring the neighbourhood and street level responses to the changes in external conditions, thanks to the data recollected during the field campaign. Furthermore, findings on morphological coefficients and UHI dynamics are reported.

3.1 Climatology

3.1.1 Urban Heat Island

To confirm the UHI of Bologna, data from weather stations and reanalysis data was examined.

3.1.1.1 ISPRA Monitoring Stations – Municipality, Local scale

Weather station datasets recollected from the ISPRA institute for five locations were plotted to look for differences in temperature between Bologna and its surroundings. As explained in the Methodology chapter, the values for each location are the result of the integration of available weather station data for the area.

The table 9 displays the linear best fit slope for the periods at hand. Even if the trends aren't all directly comparable due to the different recording years, Bologna still seems to have a quite contained coefficient. Nonetheless, the area has a clear warming trend, greater than the estimates of the IEA for Italy (0.04 °C/year), which is already bigger than the world average (0.03°C/year) (please note that the IEA trends refer to the 2000-2020 period). It is important to consider the P-value, as it is far from optimal, and that the data from weather stations suffers from various gaps.

Table 9

	Period	Trend [°C/month]	P-value
Bologna	1991-2023	0.003	0.4
Castel San Pietro Terme	2004-2023	0.006	0.4
Mezzolara	2004-2023	0.006	0.4
Sasso Marconi	1992-2023	0.005	0.2
San Pietro Capofiume	1991-2006	0.007	0.1

Anyways, the climatology should be able to better represent the average regime of the Bologna area, simply thanks to the very nature of climatology computation.

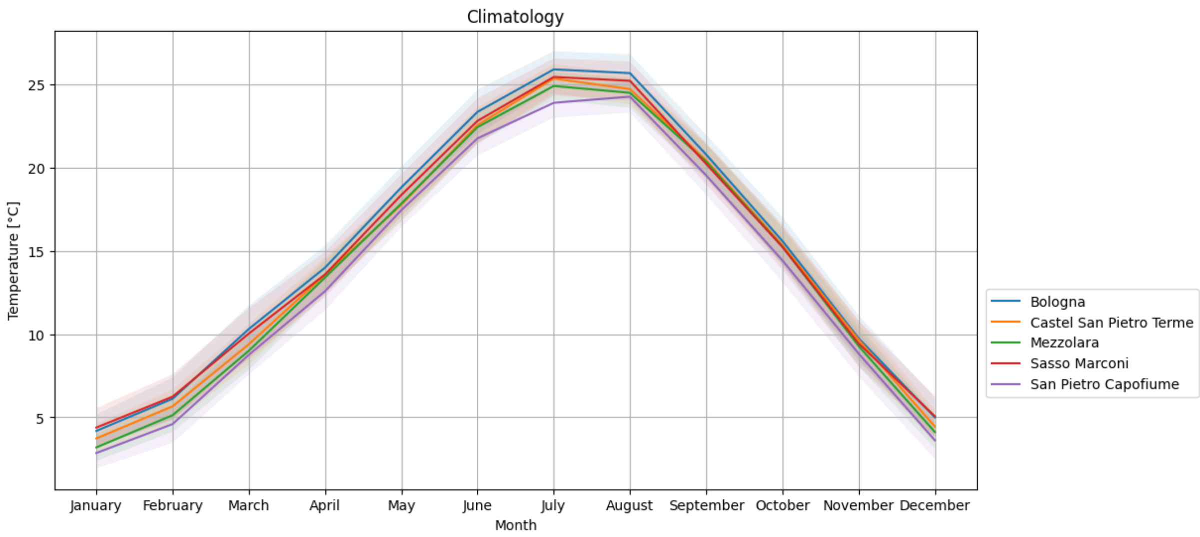

Figure 19

The climatology for the group presents the lowest values during January (3°C) and the highest during July (25°C). At the same time, Bologna results as the warmest city in the area, given its bigger Urban Heat Island. The effect seems prevalent during the summer months, as during the winter the city's climatology is at times surpassed by the Sasso Marconi one. This consideration can be further confirmed by the JJAS climatology:

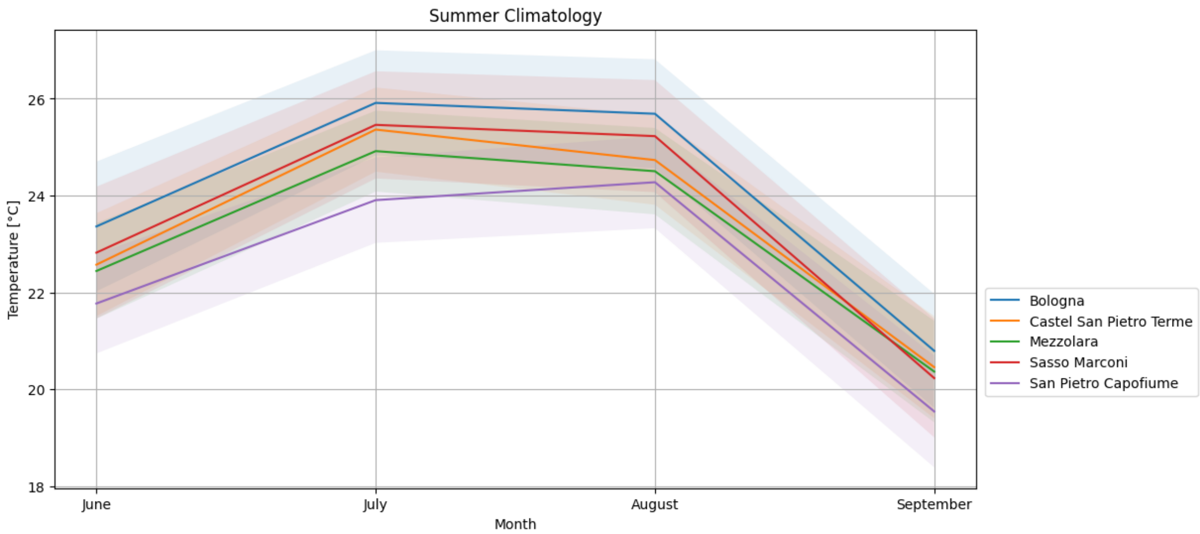

Figure 20

It can be clearly seen that Bologna exhibits the hottest summer in the area, with monthly average temperatures reaching 26 °C in July.

A further investigation was conducted on the evolution of the average temperature of the area. It can be noted that the last years (highlighted in the graphs) appear to be warmer than average, especially during the summer season. July recent temperatures position themselves among the hottest in the last 30 years.

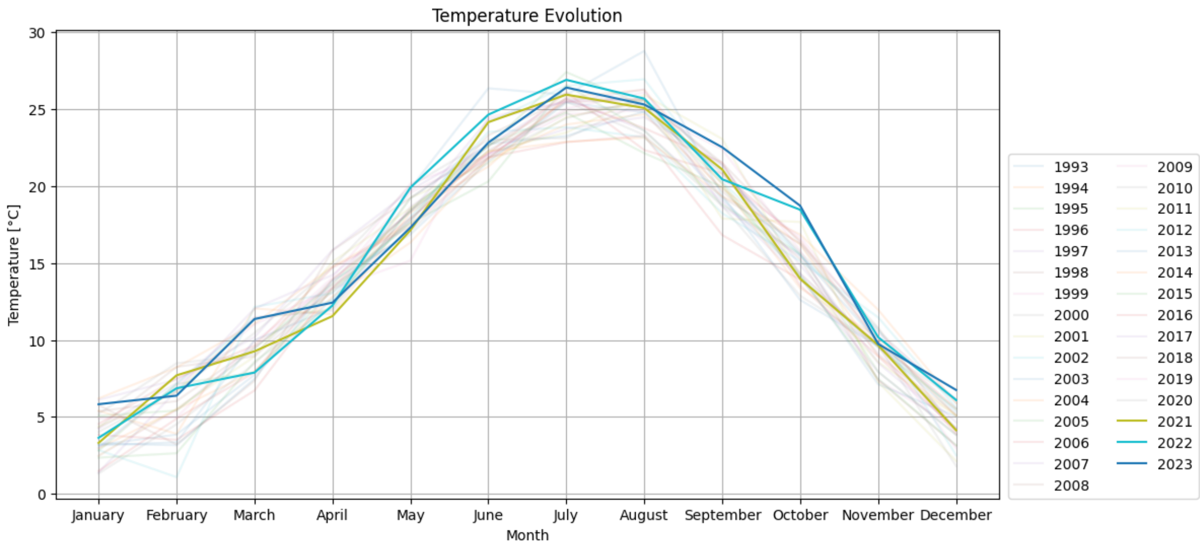

Figure 21

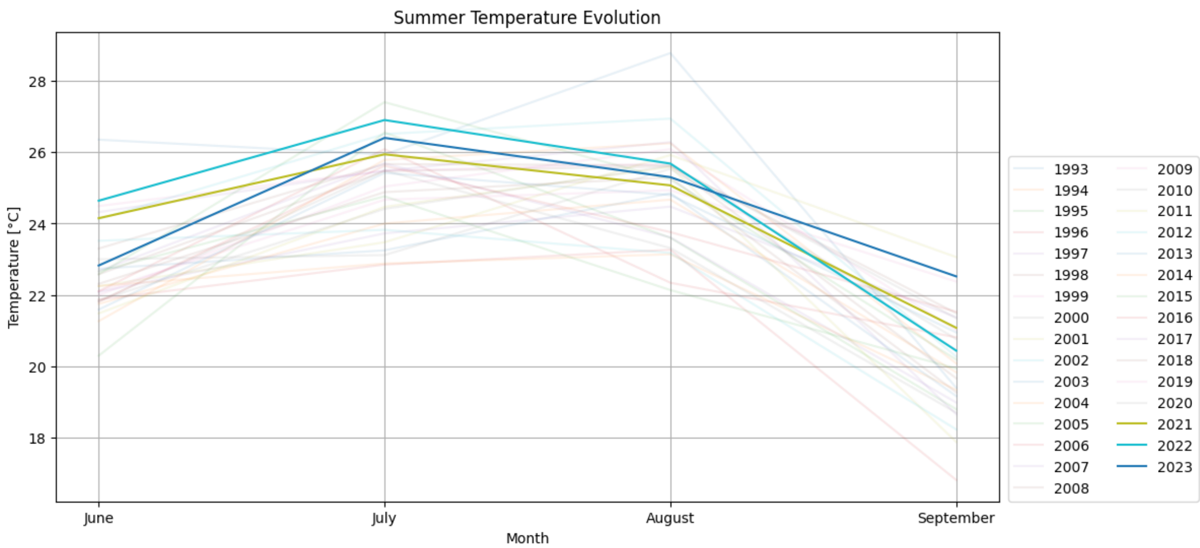

Figure 22

3.1.1.2 Eraclito 91 reanalysis – Region, Meso- and local scale

To acquire a deeper understanding of the climatology of the area, additional information on minimum and maximum temperatures is necessary. From the ARPAE Eraclito91 dataset, an analysis of the minimum and maximum daily temperature climatology and trend was carried out for the available time period (1991-2024) for the whole Emilia-Romagna region and for the city of Bologna. The Eraclito91 data for Bologna refers to data retrieved from the 5x5 km cell centred on Bologna.

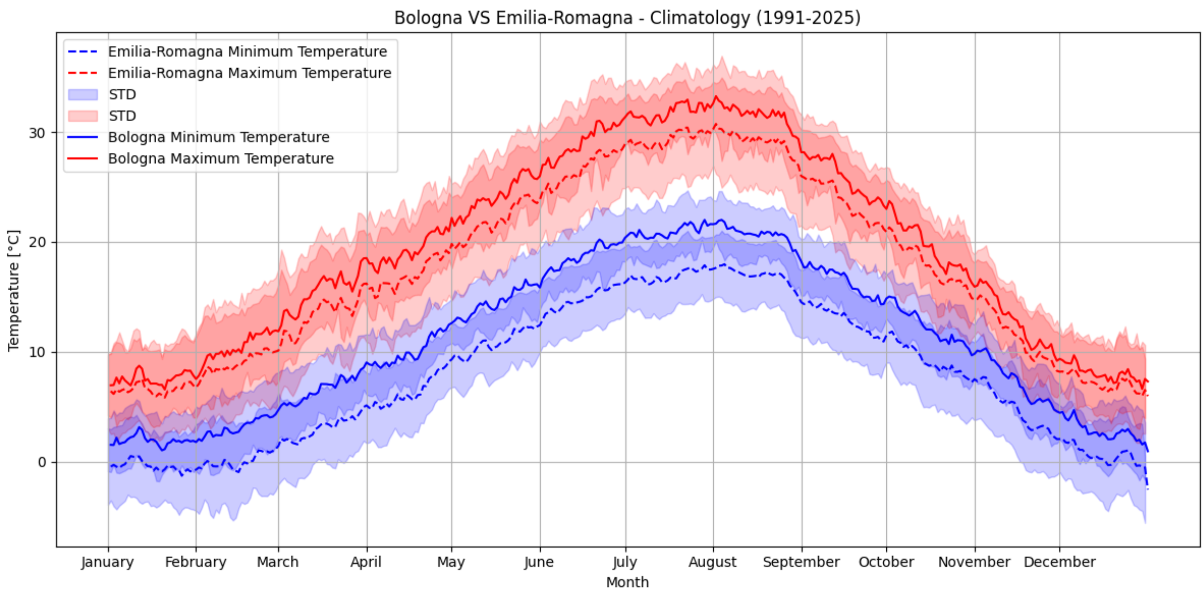

Figure 23

The previous findings from the analysis of the weather stations are confirmed, even at a regional level (Emilia-Romagna), so at a larger scale. Bologna continues to be warmer than its surroundings, particularly its minima. The city's minimum temperatures during the summer present the largest difference with the regional values, proving how the nocturnal UHI affects its urban zone. Nonetheless, it is important to consider that the regional averages include mountainous areas and coastal areas, that aren't directly comparable to the plain climate.

As the Eraclito91 dataset is considered apt for the computation of temporal trends, given the constant weather station density, linear best fits for minima and maxima have been computed for the region and for the city of Bologna. (ARPAE, Guida agli open data meteo-clima)

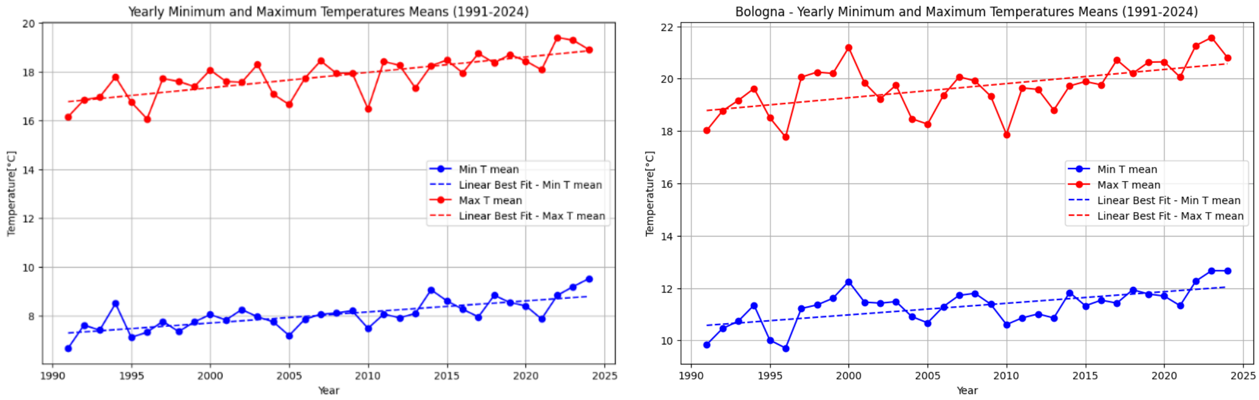

Figure 24

The graph 24 displays the yearly average value of minima and maxima for the region (left) and for Bologna (right). Bologna reasonably seems to experience higher variability than that of the whole region and shows values that are on average higher by 2°C. For example, in 1991, the region had an average minimum of less than 7°C, while in 2024, it reached almost 10°C; Bologna had an average minimum temperature of 10°C in 1991 (which was one of the lowest values for the last three decades), then reaching almost 13°C in 2024. Furthermore, the year 2000 for the grid cell of Bologna hit extremely high temperatures (both minimum and maximum), only comparable to the last five years.

Table 10

	Minimum Temperature Slope [°C/year]	**Associated P-value**	**Maximum Temperature Slope [°C/year]**	**Associated P-value**
Emilia-Romagna	0.045	0.00	0.063	0.00
Bologna	0.044	0.00	0.054	0.00

The trends for the minimum temperatures for Bologna and Emilia Romagna are almost equal while, for maximum temperatures, the region is experiencing a highest rate of warming (high confidence, P-values = 0.00). This is the same conclusion that was drawn with the simple weather station data (average temperature). In general, maxima will likely increase at a faster pace than minima. ARPAE found that, for 1961-2023, the regional maxima trend is 0.5°C/decade and the minima one is 0.2°C/decade: the different values could originate both from the dissimilar periods or from a different database of reference. If we suppose a similar dataset (likely Eraclito61), the comparison between the two sets of values leads to hypothesise an increase in the rate of warming.

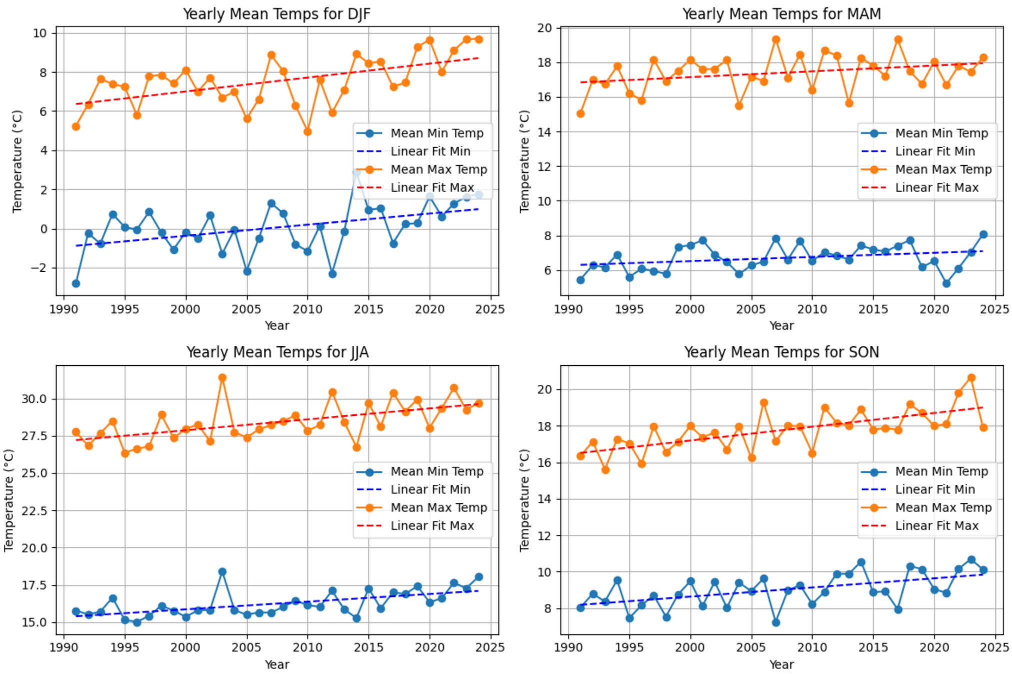

Figure 25

The graph 25 regards the whole Emilia Romagna and computes its seasonal trends. In the JJA section, the 2003 summer stands out as the hottest for the last three decades. There's a clear warming trend for all seasons, with spring being the one with the lowest rate (0.02 °C/year for minima and 0.03 °C/year for maxima) and similar rates for all the other seasons (0.05-0.06 °C/year and 0.07 °C/year). The p-values are all optimal, expect for the MAM one.

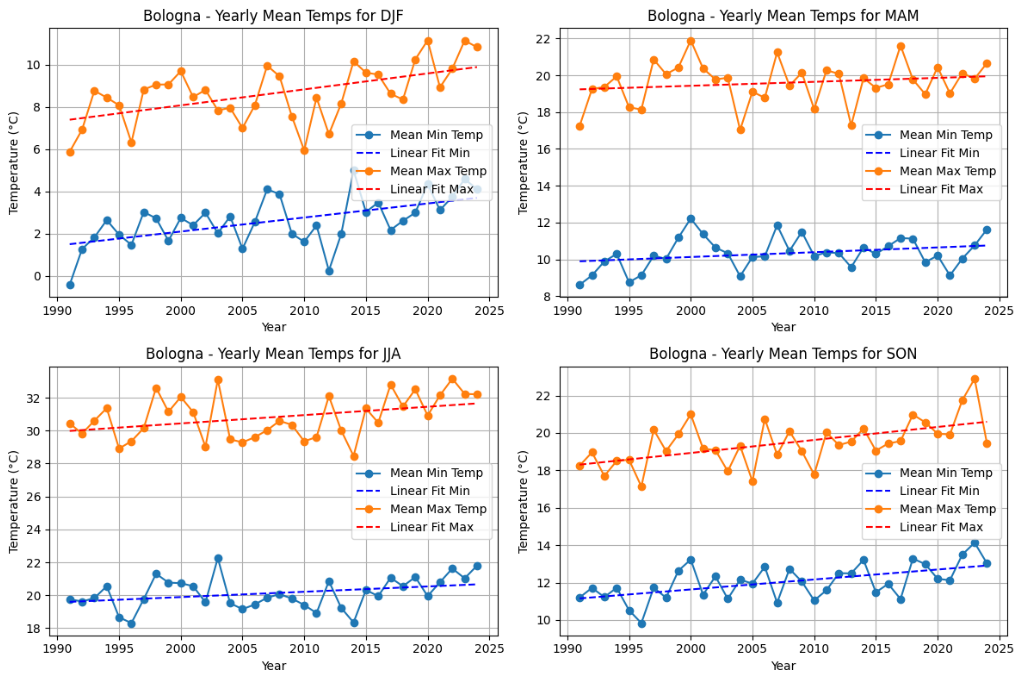

Figure 26

As for Bologna, the best fit coefficients are bigger for all minima, except for the summer value, while the maximum temperature slope suggests a slower warming rate for all seasons except for winter. The comparison between minimum temperatures in Bologna and in the region can provide some information on the UHI, whereas the comparison for the maxima can be useful for heatwaves and their relationship with the UHI.

Table 11

	Emilia-Romagna		**Bologna**		**Emilia-Romagna**		**Bologna**	
	Min. T Slope [°C/year]	P-value	Min. T Slope [°C/year]	P-value	Max. T Slope [°C/year]	P-value	Max. T Slope [°C/year]	P-value
DJF	0.057	0.00	0.066	0.00	0.071	0.00	0.075	0.00
MAM	0.024	0.06	0.026	0.09	0.033	0.06	0.021	0.29
JJA	0.051	0.00	0.032	0.05	0.073	0.00	0.050	0.03
SON	0.050	0.00	0.053	0.00	0.075	0.00	0.069	0.00

Figure 27 report the yearly anomalies for the region and for Bologna: Emilia Romagna has undergone smoother warming from 1991, while Bologna shows higher variability with the year 2000 being a prime example. 2023 seems like the hottest year so far for the city. The growing number of red dots in the last years (hotter than average) exemplifies how the area is moving to progressively higher heat, that can have as consequences increased UHI intensity and heatwave frequency and intensity.

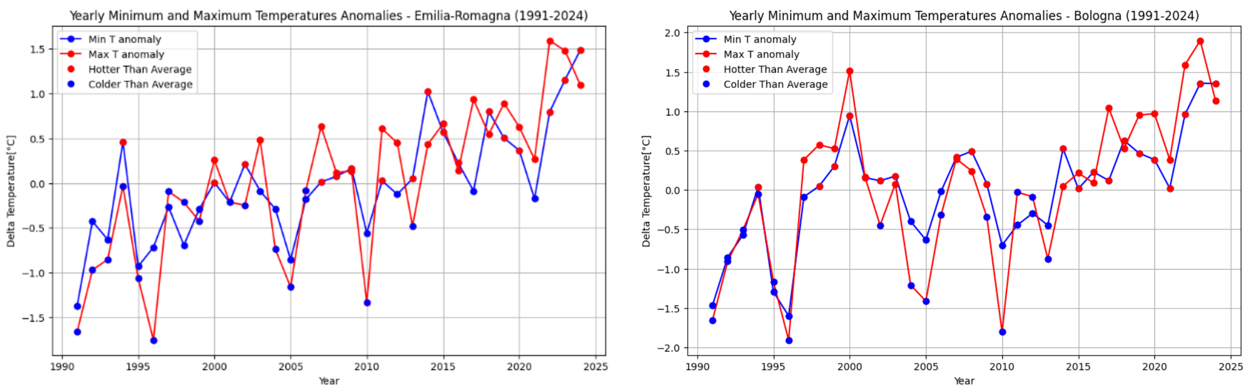

Figure 27

3.1.1.3 Climatology for the field campaign

The following is the climatology of ten days centred on the 1st and 2nd of September, the days of the field campaign. High discrepancies between the urbanized Bologna and the region are clear, even more so for the minimum temperatures. Bologna presents 1991-2024 maxima around 26-30 °C and minima around 17-20 °C. The values recorded on the 1st and 2nd September 2024 in the central district via MeteoTrackers had a range of 25-33 °C, above the climatology (even when considering the STD). In fact, the first day of the field campaign was a heatwave day for Bologna, as will be clarified later in the thesis.

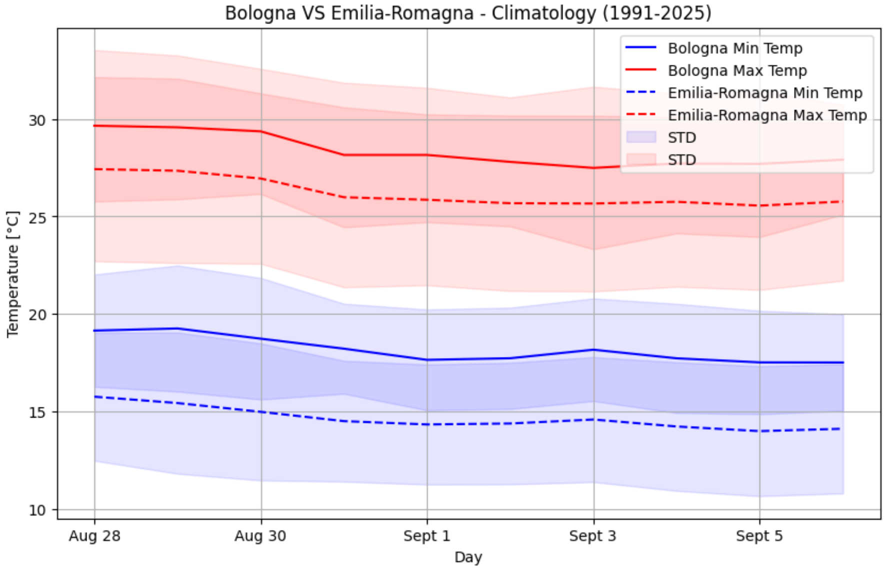

Figure 28

3.1.1.4 Regional Maps – Meso- and Local scale

To have a better grasp of the temperature gradient between Bologna and the Emilia Romagna region, the Eraclito91 dataset was mapped. Figure 29: the maps for the 1991-2024 mean minimum temperature and mean maximum temperature clearly display differences: average minima are higher in Bologna (approx. 44.5°, 11.35°) and in other major cities (the 'yellow dots' coincide with cities like Imola or Modena) and are lowest in the mountainous region; similarly, average maxima are still higher in the cities, even if less clearly.

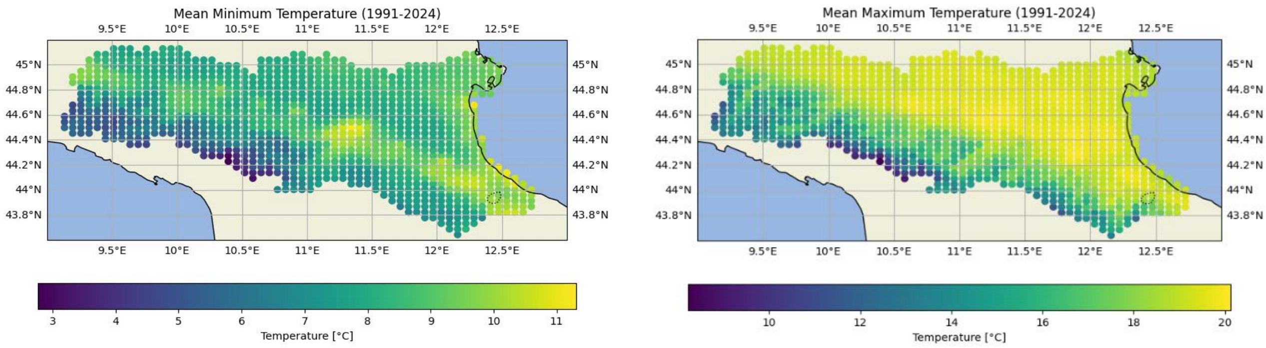

Figure 29 Eraclito 91 regional maps: on the left, minimum T average (3-11°C range); on the right, maximum T average (9-20°C range).

The trends computed from the historical reanalysis don't identify a specific spatial value for the region, but indicate a prevailing warming trend, with values oscillating between -0.02 and 0.08 °C/year for minimum temperatures, while the maximum temperatures exhibit a steeper best fit slope that sits between 0.01 and 0.12 °C/year. Overall, the maxima will likely become higher and higher, posing a threat especially during the summer season.

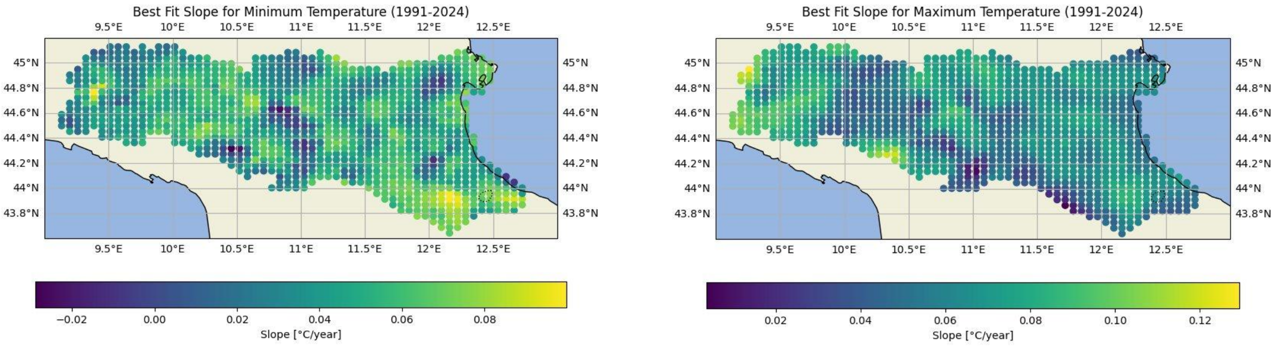

Figure 30

The summer (JJA) map (Figure 31) reiterates the already known fact that the average minima are higher in cities (or coastal areas, obviously). When restricting the scale of analysis to the immediate surroundings of the cities in question, this phenomenon is almost certainly a direct consequence of the Urban Heat Island, as no other factor like altitude, presence of bodies of water, currents or other could be at the root of the high gradient. Other seasonal graphs and more can be found in the Appendix.

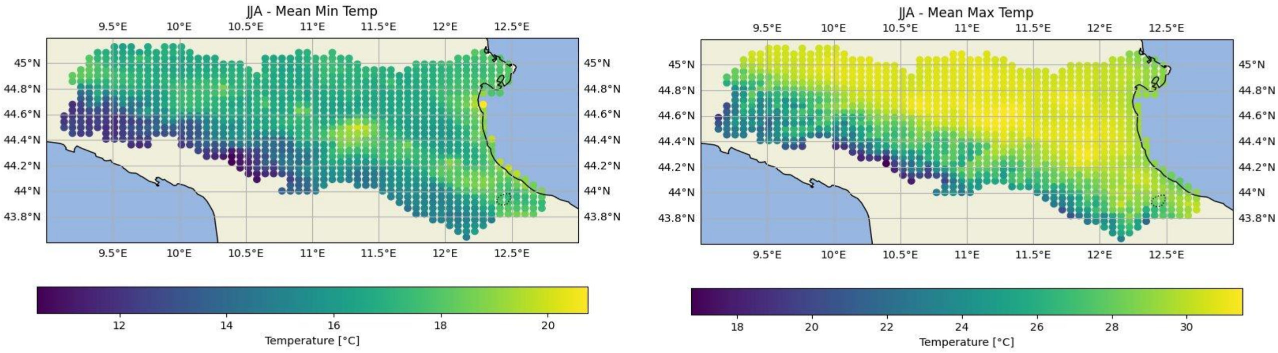

Figure 31

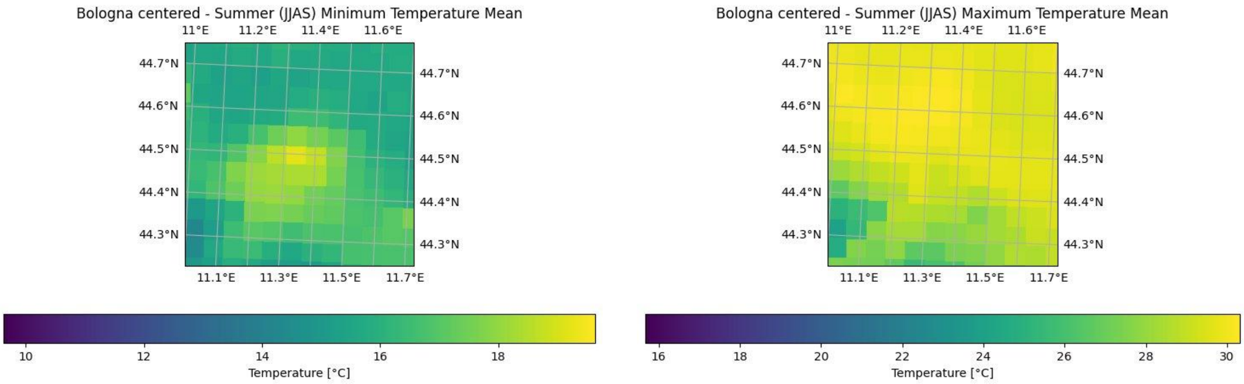

Figure 32

Figure 32 shows the JJAS (September is added to the previous computation) minimum and maximum temperatures for a 0.6° x 0.7° cell centred on Bologna, displaying a steep gradient for the minima, thus suggesting that, at night, the city undergoes slower cooling than its surrounding area. The last plot for the section intuitively displays the zonal and meridional section of the minimum summer temperature, which is a typical UHI trend.

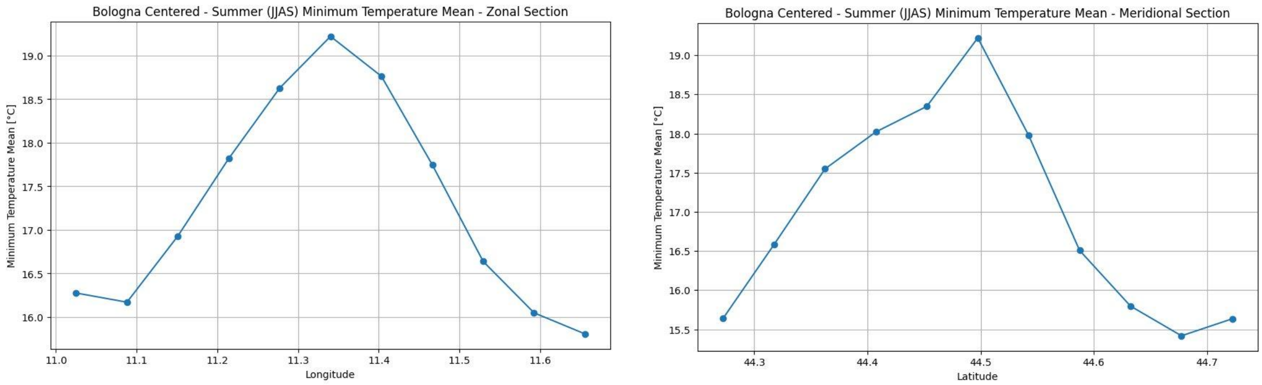

Figure 33

Conclusively, Bologna shows evidence of its Urban Heat Island in both climatological analyses conducted on the local weather stations and on the regional reanalysis Eraclito91.

3.1.2 Heatwaves

Thermal comfort is also modulated by heatwaves, along with Urban Heat Islands, as described in the first chapter, and the concurrence of the two can exacerbate extreme consequences, especially during summer. Given this premise, it's fundamental to analyse heatwaves in the city of Bologna. Eraclito91 was kept as the chosen dataset, considering its fitness for trend computation; at the same time, ARPAE warns the users about its medium accuracy for smaller spatial scales, so this is a matter that must be kept in mind. The variable of reference was the daily maximum temperature for the 5 x 5 km cell centred on Bologna.

Firstly, an absolute approach was taken: the histogram 34 counts the number of days with temperatures above a fixed threshold (30 °C, 35 °C and 40 °C) for the whole year (likely it comprises mostly summer days).

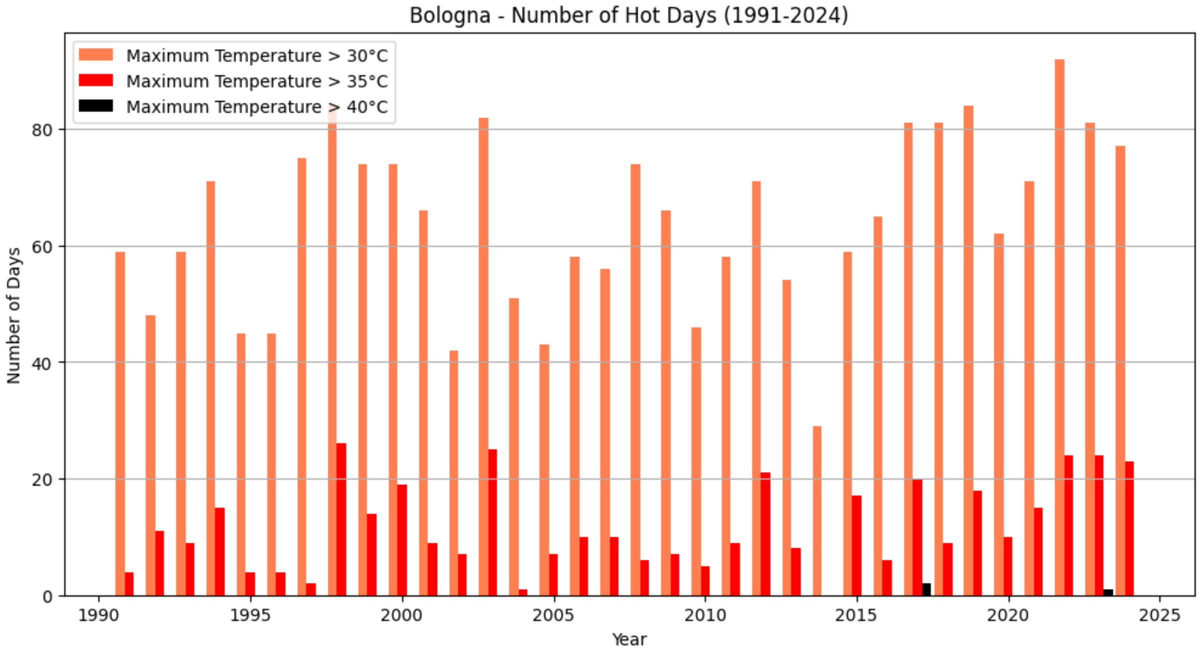

Figure 34

Hot days may look like they are evenly distributed, but the trends say otherwise: the best fit slope is positive for all three cases, with the steepest one found for the days with maximums above 30 °C. The most reliable value is the increase of 0.3 days/year for days with temperatures that reach above 35 °C (p-value = 0.05). Additionally, the only dates going over 40 °C are in the last years.

Table 12

	Slope [#/year]	(R-squared)	P-value
30°C	0.5	0.11	0.06
35°C	0.3	0.12	0.05
40°C	(0.01)	0.08	0.11

From now on, the comparison becomes relative to the climatology. The utilized method is from Russo et al. So, each date maximum is positioned in the distribution of the 1991-2024 climatology centred on that day, becoming specific for the time of the year and area.

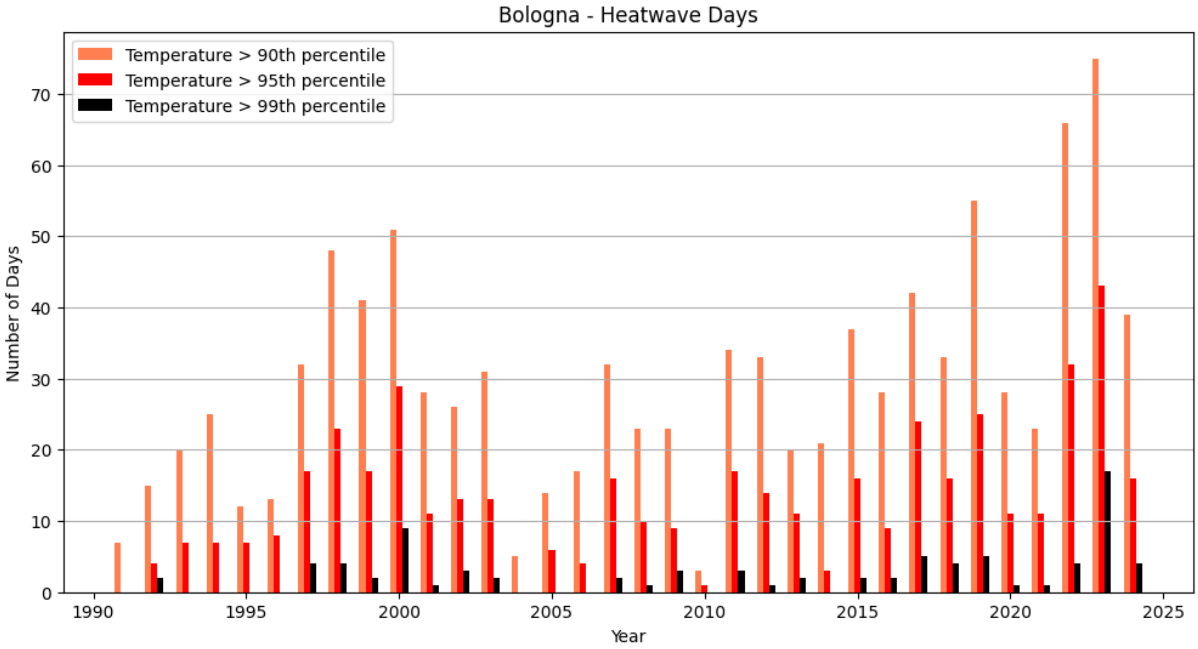

Figure 35

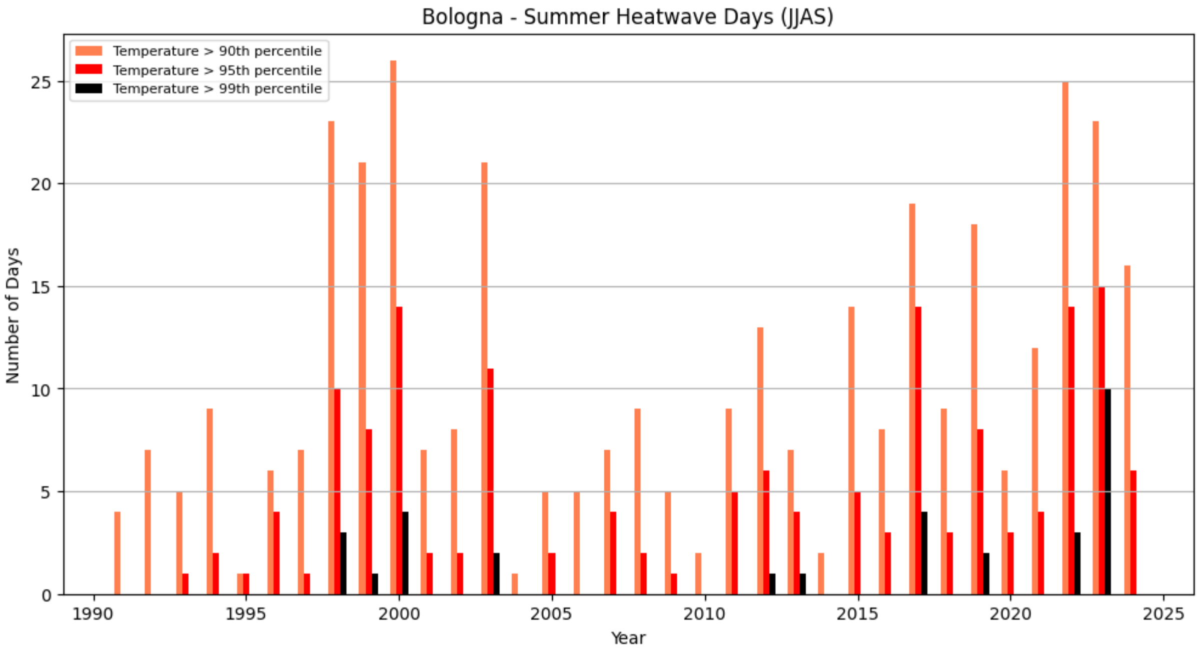

Figure 36

The heatwave days exhibit an evident increase for the yearly values, while they are bimodal for the JJAS values, with the year 2000 presenting a high number of them (along with 1998, 1999 and 2003). At the same time, the most extreme temperatures (above 99th percentile) are found in the year 2023, in line both with the ARPAE statement that 2023 was the hottest recorded year since 1961 (regarding mean and maximum temperatures) and with the Copernicus finding about the great contrast of the summer of 2023, with heatwaves affecting 41% of southern Europe and causing 'strong', 'very strong' or 'extreme' heat stress. Copernicus also claimed that 2022 provided the hottest summer ever in Europe, which is reflected here in the histogram, as the year possesses one of the highest numbers of heatwave days.

Table 13

	Bologna – Full Year Heatwave Days		Bologna – Summer Heatwave Days	
Percentile	Slope [# days/year]	P-value	Slope [# days/year]	P-value
90th	0.8	0.00	0.2	0.01
95th	0.4	0.01	0.2	0.03
99th	0.1	0.03	0.06	0.09

The trend for heatwave days is positive in all cases, with the bigger values found for less extreme days (above 90th percentile). The coefficient is luckily smaller for summer heatwave days rather than for the full year. All numbers have P-values below 0.05, except for the summer dates above the 99th percentile.

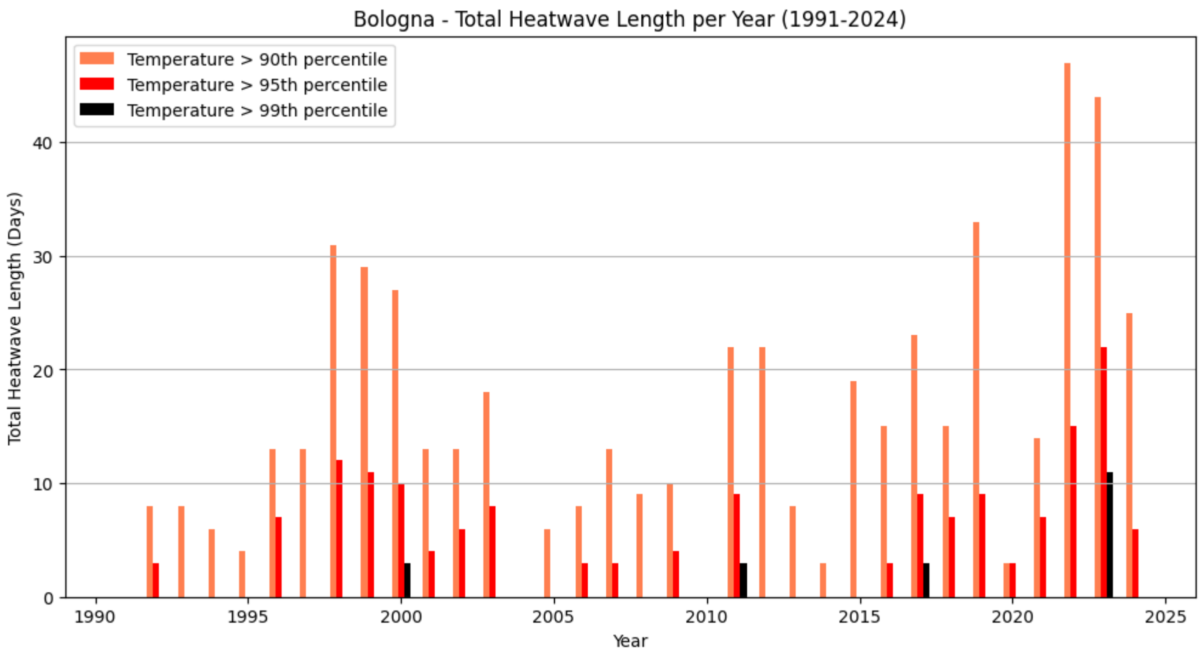

Figure 37

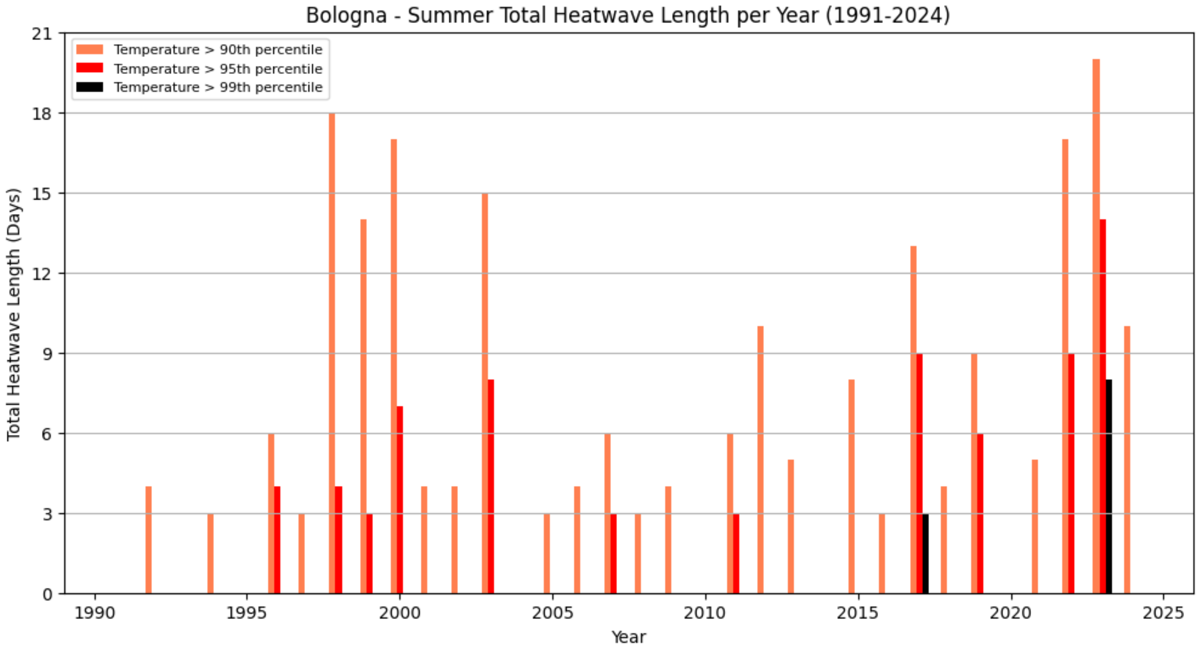

Figure 38

The two graphs (37, 38) represent the total length of heatwave events, so periods of three or more consecutive days in which every day exhibited temperatures above the same nth percentile. With this different concept, the yearly and summer histograms appear to be bimodal, but with a strong increase in extreme values in the last years, especially for the summer season. The summer of 2023 had 20 dates in the four months (JJAS) above the 90th percentile, 14 above the 95th percentile and 8 above the 99th percentile.

Table 14

	Bologna – Full Year Heatwave Event Length		**Bologna – Summer Heatwave Event Length**	
Percentile	Slope [# days/year]	P-value	Slope [# days/year]	P-value
90th	0.5	0.01	0.2	0.15
95th	0.2	0.04	0.1	0.13
99th	0.1	0.11	0.0	0.06

The linear best fit slopes for the heatwave events in Bologna exhibit positive values. Significant results are found for the full year (90th and 95th percentile) with coefficients of 0.5 and 0.2 days/year respectively.

Histograms 38 and 39 for the number of heatwave events over the nth percentile are plotted by duration, with warmer colours representing longer events and cooler colours representing events closer to three days.

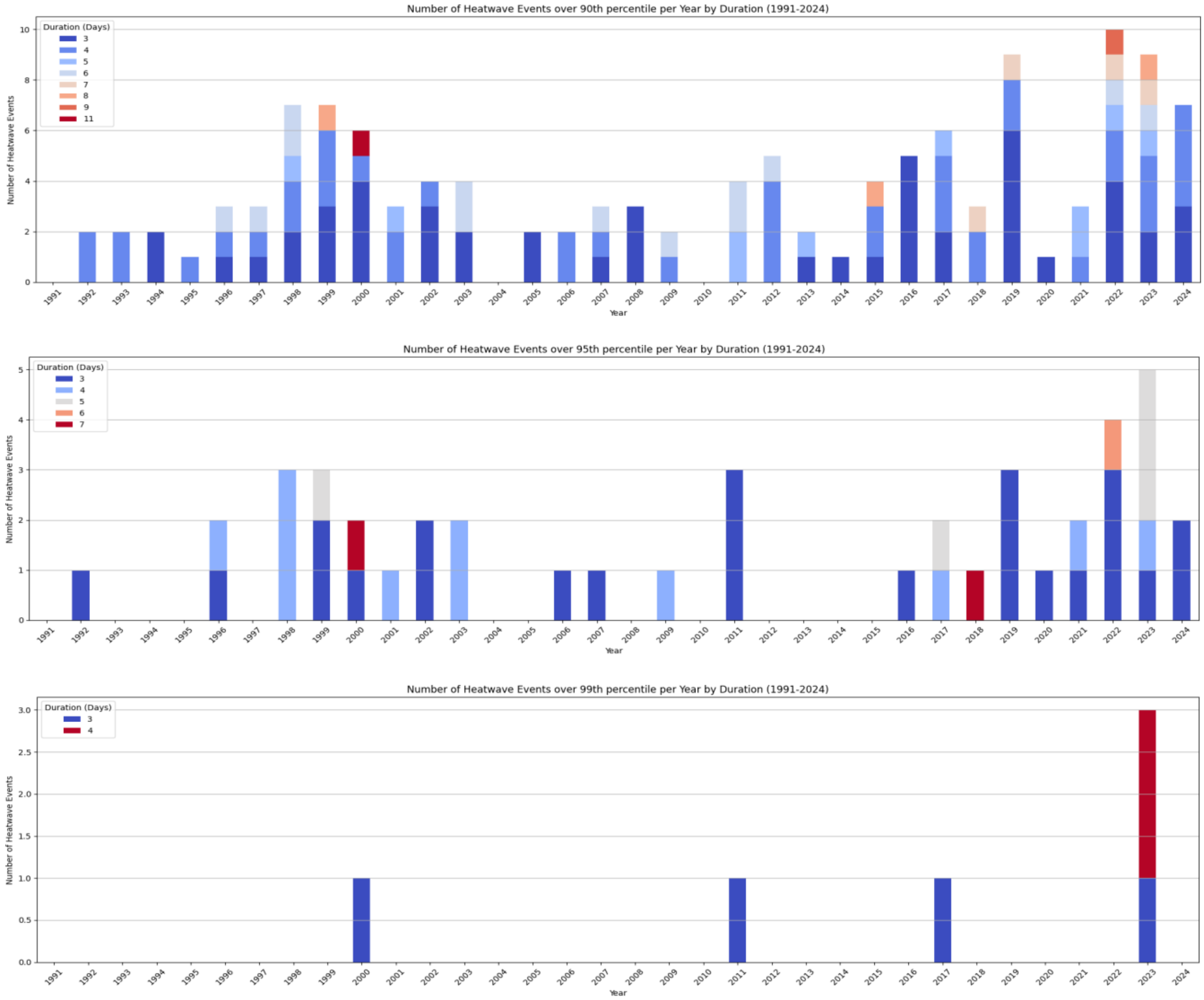

Figure 39 Full Year Number of Heatwave events over nth percentile per year by duration (1991-2024). The percentile threshold increases going down (90th, 95th, 99th)

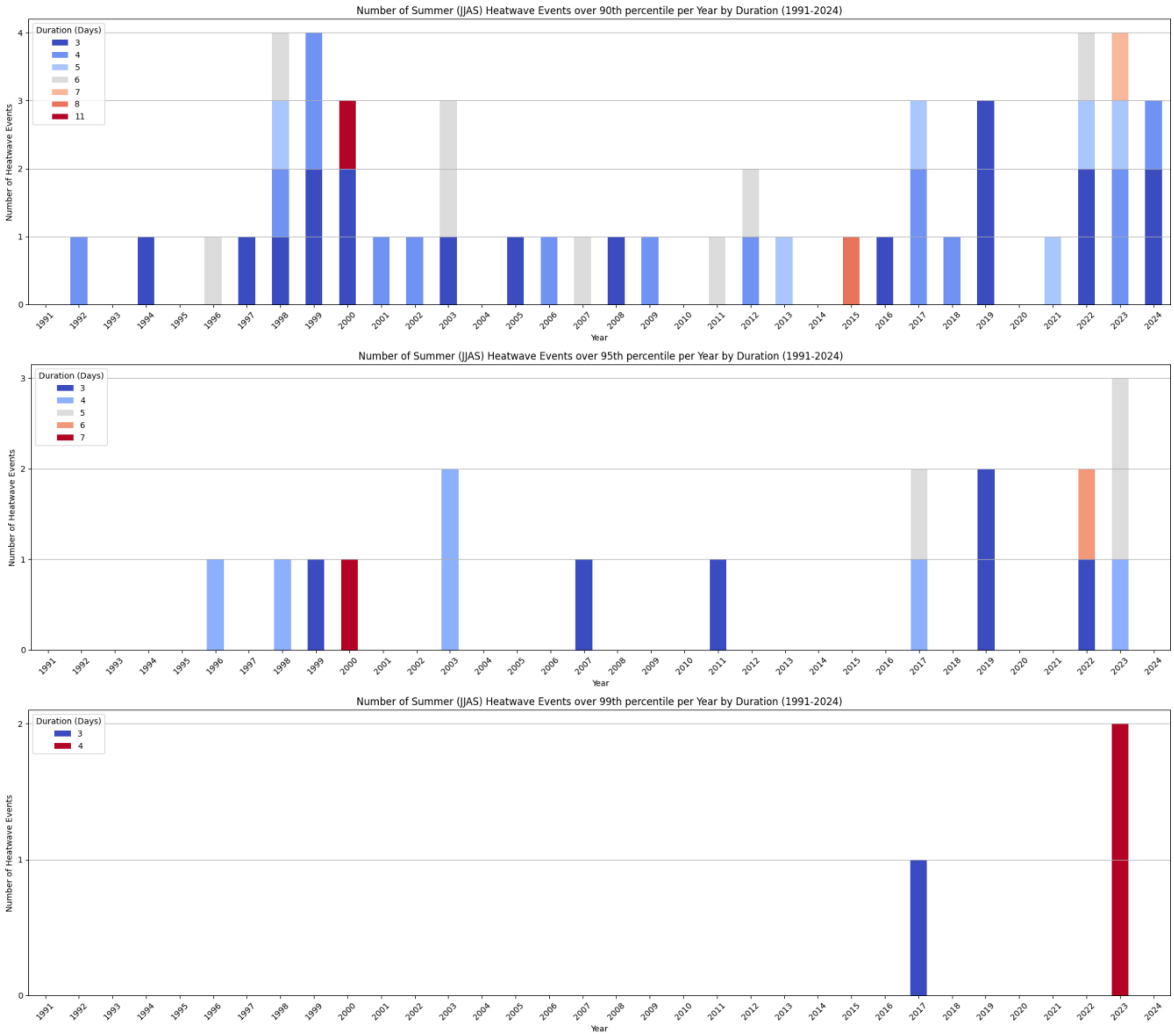

Figure 40 Summer (JJAS) Number of Heatwave events over nth percentile per year by duration (1991-2024). The percentile threshold increases going down (90th, 95th, 99th)

The previous graphs (39, 40) still show the two peaks around the year 2000 and the last years, with more extreme values appearing only recently, particularly for the summer months. The 2003 heatwave seems now normalized, as the 2022 and 2023 summer months, for this heatwave definition and period, exhibit greater durations and intensities. This finds confirmation in some of the papers reviewed in the first chapter, such as Russo et al, 2014 or Copernicus, 2023.

Long heatwave events are not a new phenomenon, but extremely hot consecutive days (for example above the 99th percentile) are becoming more common because of global (and local) warming. Extended heatwave periods combined with UHIs, because of the continued exposure to heat, can lead to multiple negative consequences during summer, especially for more vulnerable people.

Among other heatwave days and events, the 1st of September 2024, first day of the field campaign, was highlighted as part of a 3-day heatwave event over the 90th percentile of the Eraclito91 1991-2024 maxima climatology, with the day belonging to the field campaign being the last one of the period, that had begun on the 30th of august 2024. Furthermore, the thermometer on the abovementioned first day (30th) reached a maximum value over the 95th percentile. As the utilized definition of heatwave is supplied by Russo et al, 2014, that utilizes maximum temperatures, and the nocturnal UHI responds to the diurnal maximum temperatures above the 90th percentile of the previous day, the measured quantities can be considered as gathered under heatwave conditions.

Table 15 Partial view of the table computed for days with maxima above the 90th percentile of the climatology. Left column: date; centre: maximum temperature of the day from Eraclito91; right: 90th percentile of the maxima climatology for that day (calculated as explained in the Methodology chapter). The rows in bolds show the heatwave event discussed here.

Date	Maximum Temperature	Threshold (90th percentile)
2024-08-24	35.4	35.1
2024-08-30	**35.6**	**34.4**
2024-08-31	**35.3**	**34.2**
2024-09-01	**34.9**	**34.1**
2024-10-31	21.9	21.4

Table 16 Partial view of the table computed for days with maxima above the 95th percentile of the climatology. Left column: date; centre: maximum temperature of the day from Eraclito91; right: 95th percentile of the maxima climatology for that day (calculated as explained in the Methodology chapter). The row in bold shows the heatwave day discussed here.

Date	Maximum Temperature	Threshold (95th percentile)
2024-08-13	38.0	37.0
2024-08-30	**35.6**	**35.5**
2025-01-27	17.1	14.5

3.2 Field Campaign

The field campaign was conducted on a heatwave day, as the 1st of September 2024 presented a maximum temperature above the 90th percentile of the climatology extrapolated from the Eraclito91 database, thus representing a useful case study for very hot summer days and the combined effects of heatwaves and UHIs.

3.2.1 Planar and Frontal Area Indexes – QGIS – Intra-city scale

The two surveyed areas present different characteristics, as stated before and as further confirmed with the analysis of the urban structure of the neighbourhoods. The area density coefficients were calculated for both zones, with and without vegetation:

$$\lambda_f = \frac{A_f}{A_d} \quad with \quad A_f = A_f^b + P_v A_f^v$$

$$\lambda_p = \frac{A_p}{A_d} \quad with \quad A_p = A_p^b + (1 - P) A_p^v$$

(More detailed formulas can be found in the Methodology chapter.)

The results of the computations are written in the table 17. The Prendiparte zone has significantly higher coefficients, that increase heat absorption during the day and slow down its release at night. Ventilation is also greatly hindered in the central district because of the high density of the buildings. Conversely, the Sant'Orsola district has quite low values because of the sparser distribution of the built-up areas; there's also more vegetation, so the coefficients change more between the 'barren' scenario and the vegetated one.

Even though they increase the frontal and planar area, trees, shrubs and plants in general can help in UHI mitigation, thanks to evapotranspiration, shade and pervious surface provision (though these effects are not considered in this specific calculation).

Table 17

	Prediparte district	Sant'Orsola district
Planar area fraction coefficient	0.61	0.33
Frontal area fraction coefficient N-S	0.70	0.17
Frontal area fraction coefficient E-W	0.50	0.26
Planar area fraction coefficient with vegetation	0.61	0.35
Frontal area fraction coefficient N-S with vegetation	0.71	0.21
Frontal area fraction coefficient E-W with vegetation	0.51	0.30

These coefficients contextualize how morphologically different the two probed neighbourhoods are, thus providing a baseline for the following findings.

3.2.2 MeteoTracker Maps – Intra-city and microscale

To analyse more deeply the interplay between the two different urban neighbourhoods and the UHI intensity, the data collected via Meteotrackers mounted on the volunteers' bikes was mapped and interpolated as explained in the Methodology chapter.

The figures 41 and 42 were chosen as representative maps of the study areas for the day. The recorded values at 14:00 and 15:00 CEST don't show any significant difference between the districts, only local discrepancies can be seen between individual streets or segments of street in each area. This phenomenon could be caused by microscale thermal inhomogeneities generated by building shades, HVAC systems, vicinity to green areas, etc.

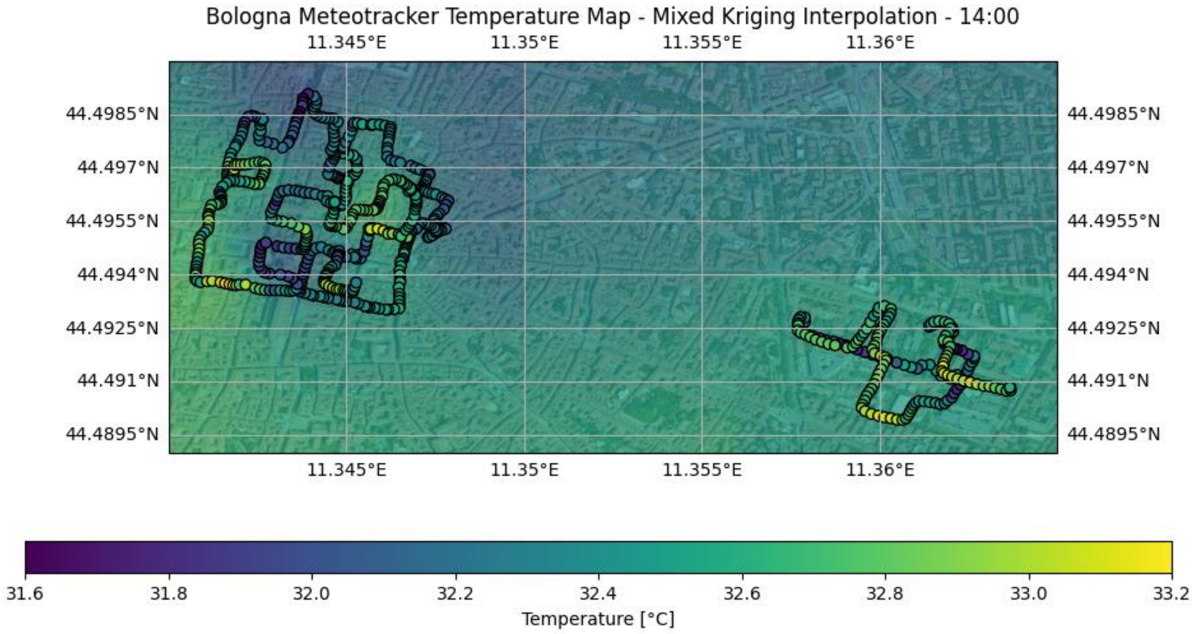

Figure 41 Map for 14:00. No significant difference between the Meteotracker recorded temperatures in the two districts. Upper left: central district, with bike tracks centred on the Prendiparte tower; lower right: Sant'Orsola district, tree lined and less densely built.

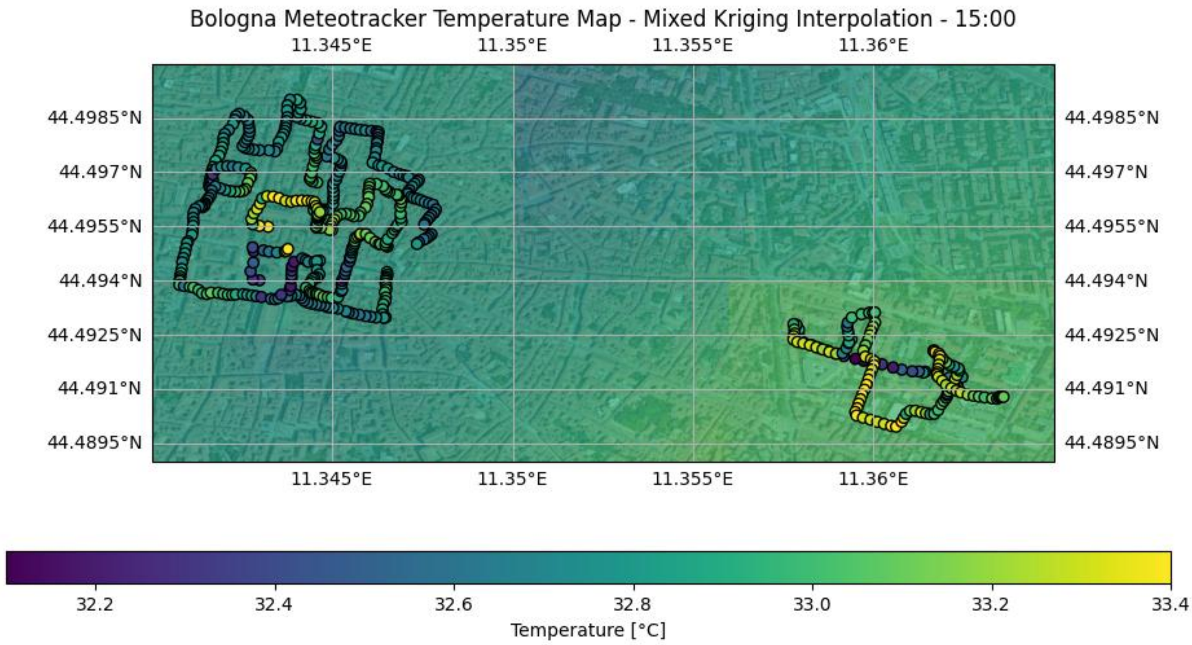

Figure 42 Map for 15:00. No significant difference between the Meteotracker recorded temperatures in the two districts. Upper left: central district, with bike tracks centred on the Prendiparte tower; lower right: Sant'Orsola district, tree lined and less densely built.

At night, the situation changes drastically, as the two representative maps (43, 44) shown here highlight the UHI effect in the central area. The Sant'Orsola district undergoes an evident more rapid cooling during the hours after sunset, thanks to the lower planar and frontal area fraction coefficients, while the central area keeps more heat trapped. The difference is of about 2°C at both 00:00 and at 03:00 CEST. This difference originates from the different building densities and vegetation presence. As clarified previously, the SO site is composed by a larger central tree-lined street, multiple green areas and open spaces with less buildings, that are distanced between each other. On the contrary, the TP site has really densely packed buildings and almost no pervious surfaces or trees. The central site isn't mitigated, while the hospital zone can be considered mitigated, as it is also characterized by lower planar and frontal area coefficients (consequences of this fact were already discussed in the previous chapters and are applicable in this case). The smaller planar coefficient of SO lowers the exposure of high thermal capacity materials (buildings), diminishing heat emission at night; while the smaller frontal coefficients allows for nocturnal ventilation and heat release via convection, along with decreased thermal interactions during the day (multiple reflections, absorptions and re-emissions of radiation are increased if vertical surfaces are dense – this phenomenon leads to augmented entrapped heat, which is what happens in the TP zone).

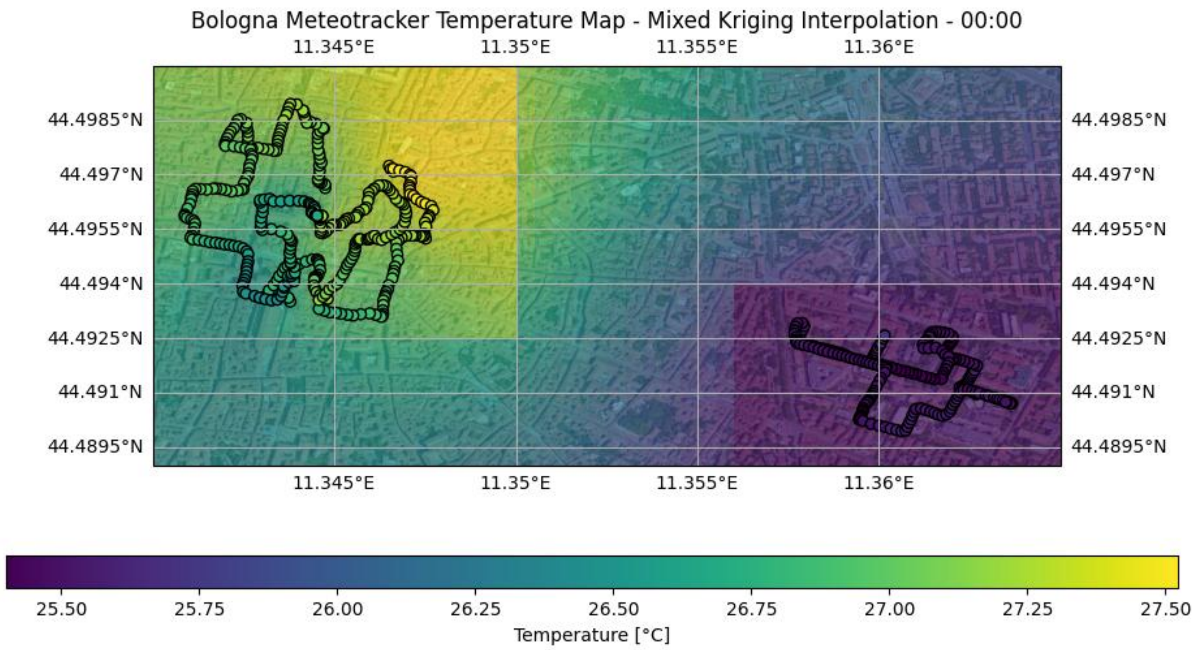

Figure 43 Map for 00:00. Clear difference between the Meteotracker recorded temperatures in the two districts. Upper left: central district, with bike tracks centred on the Prendiparte tower; lower right: Sant'Orsola district, tree lined and less densely built.

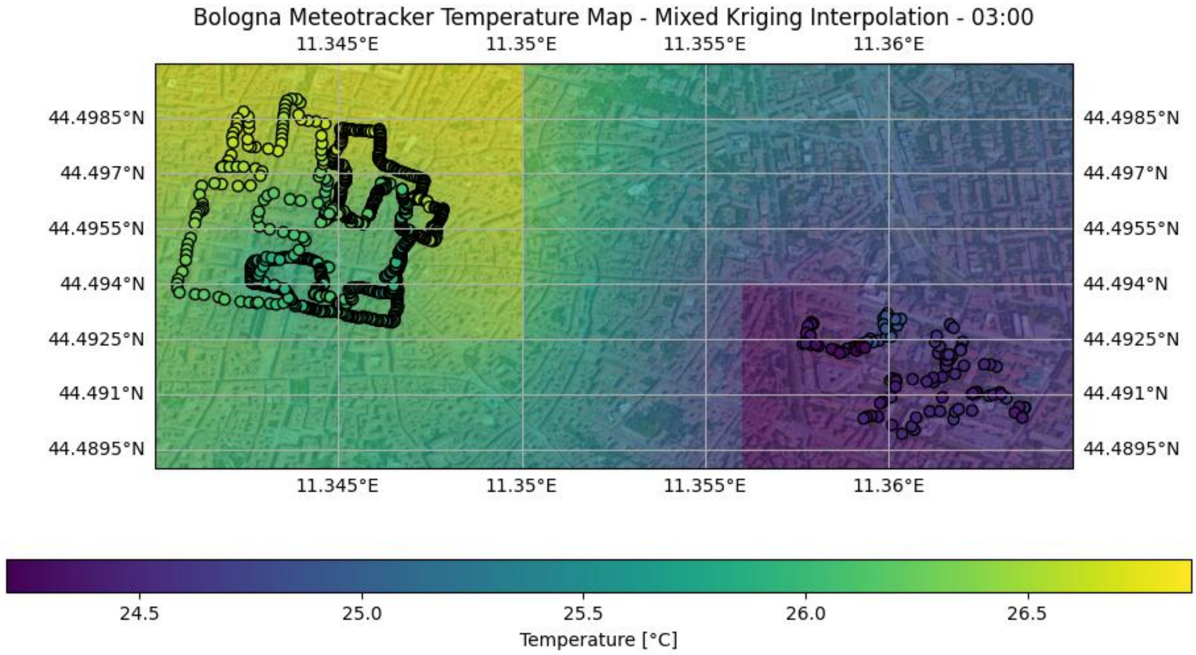

Figure 44 Map for 03:00. Clear difference between the Meteotracker recorded temperatures in the two districts. Upper left: central district, with bike tracks centred on the Prendiparte tower; lower right: Sant'Orsola district, tree lined and less densely built.

(maps for the rest of the field campaign can be found in the Appendix)

3.2.3 MeteoTracker Maps – Extra Routes – City and Intra-city scale

Extra tracks were also collected, with volunteers heading out on different routes than those planned, during their rest time. The results showed clearly a strong UHI at work on the whole city of Bologna, with temperatures on the actual outskirts being lower by over 6°C when compared with those recorded in the centre.

In figure 45 the route (02:30 CEST) moves from the city centre to a slightly higher elevation green zone of Bologna, with an almost 7 °C difference between the two areas. The linear distance between the start and finish point is of around 2 km, thus revealing an extremely high mean gradient of 3.5 °C/km. The clear sky conditions of the field campaign night and the extremely light wind, accompanied by the heatwave of the previous day, probably allowed for conditions similar to those described by Oke, 1973, in which the maximum UHI could be measured. By solving the equation (assuming a population of 390,000):

$$\Delta T_{u-r(max)} = 2.01 \log P - 4.06 = 7.2\ °C$$

With an STD of 0.9 °C. This seems reasonable and quite similar to the measured value of ≈ 7 °C.

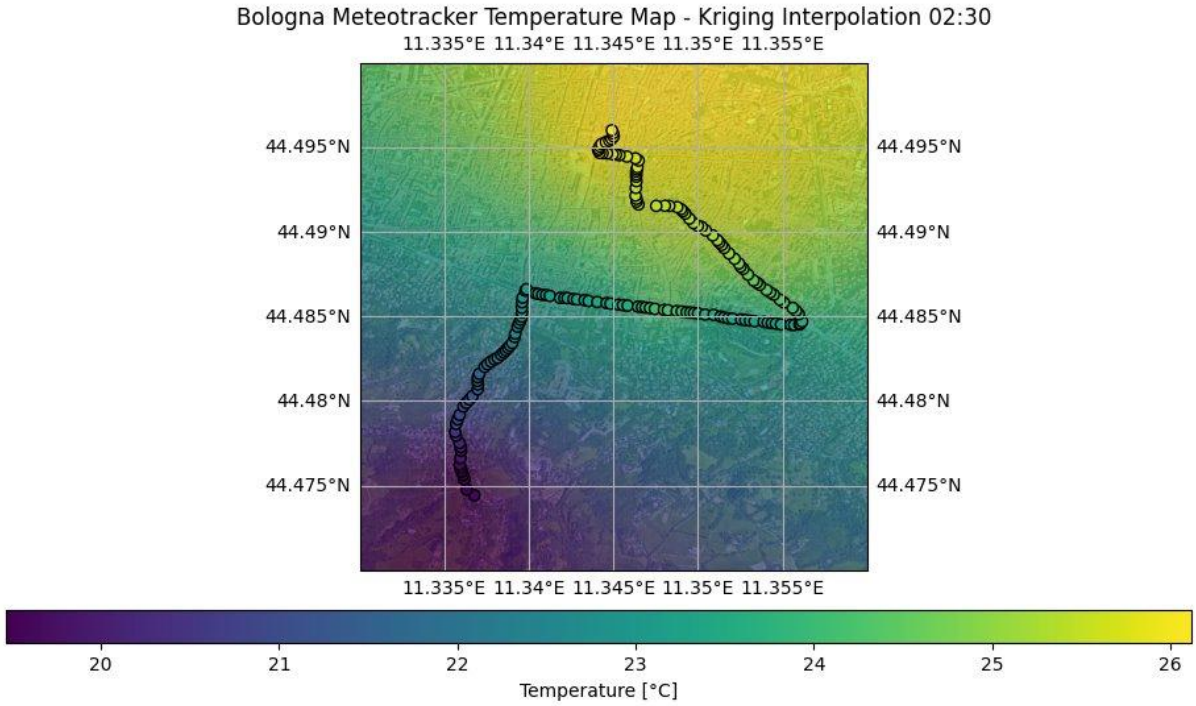

Figure 45

Figure 46 shows another extra route (03:15 CEST) that covers an area that goes from the city centre to the north-eastern outskirts of the city, that lie at the same height of the centre, approximately. So, no altitude difference effects are involved in the > 6 °C difference. In this case, the linear distance is of around 5 km, hence determining a gradient ≈ 1,2 °C/km or ≈ 1/3 of the previous gradient. This is probably caused by the greater number of buildings and impervious surfaces of this specific suburban neighbourhood and by the absence of elevation difference. Still, the UHI is of almost the same magnitude.

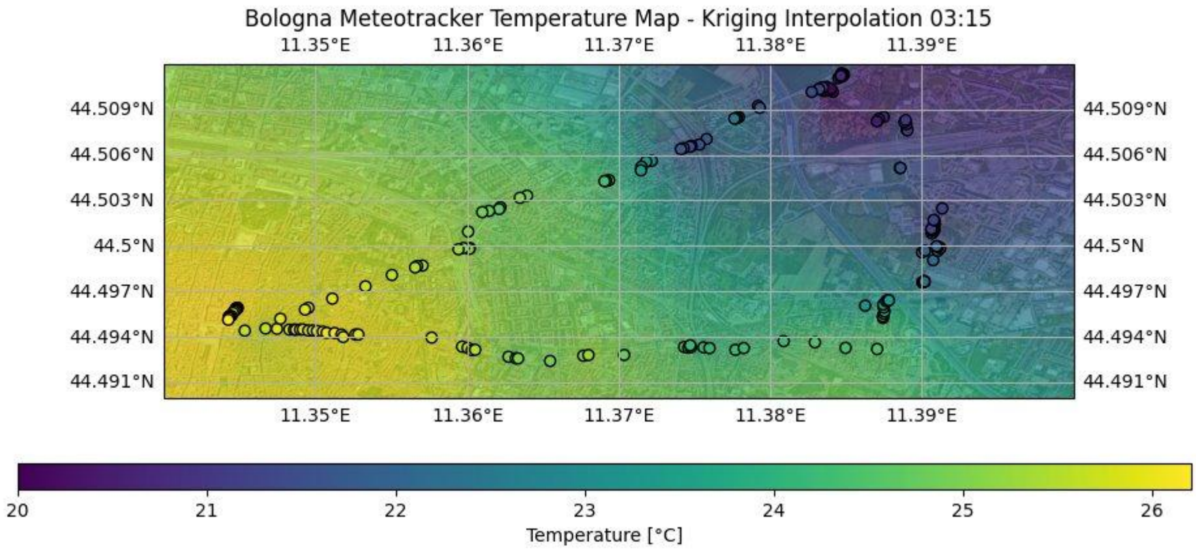

Figure 46

These two datasets were collected in the span of approximately one hour (from 02:30 CEST) and offer a clear picture of Bologna's UHI: the extent of the tracks covers two opposite sides with respect to the reference Prendiparte tower (SW and NE) and both show an extremely high temperature gradient in the span of less than 5 km.

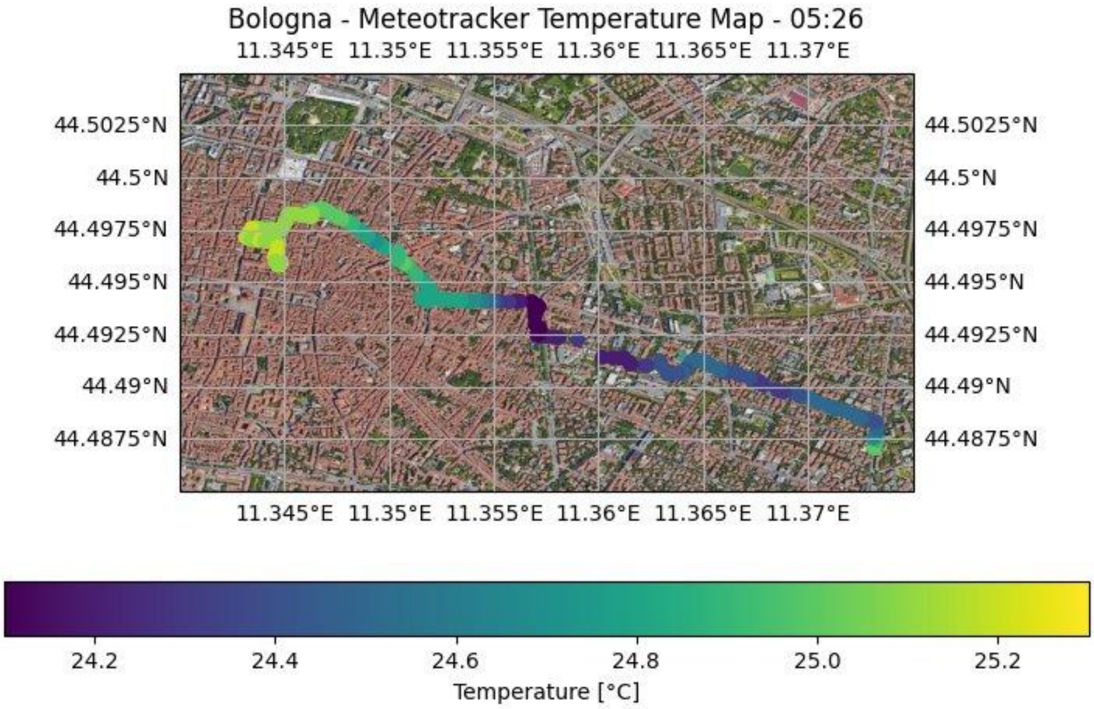

Figure 47

The picture 47 shows how the SO area is cooler than its surrounding neighbourhoods during the night (end of), confirming the supposition that it's a 'mitigated' zone thanks to its less dense buildings and higher percentage of green areas.

These extra tracks were crucial to determine the UHI of Bologna, that reached values of 6-7 °C during the peak hours of the night.

To further quantify the spatial evolution of the air temperature moving from the city centre towards the outskirts, horizontal temperature differences were computed and analysed alongside a selected straight itinerary between the Prendiparte and Sant'Orsola sites. In this case, the volunteer headed out at 05:56 CEST, when the Prendiparte and other central districts had cooled down more compared to the 2 or 3 a.m. routes.

Nonetheless, a steep difference of almost 4 °C remained.

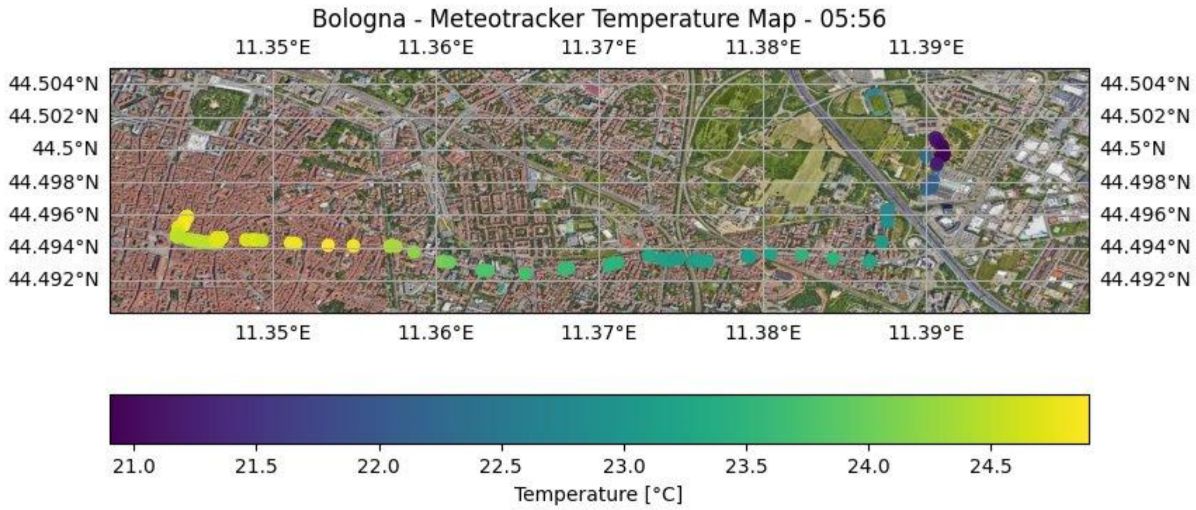

Figure 48

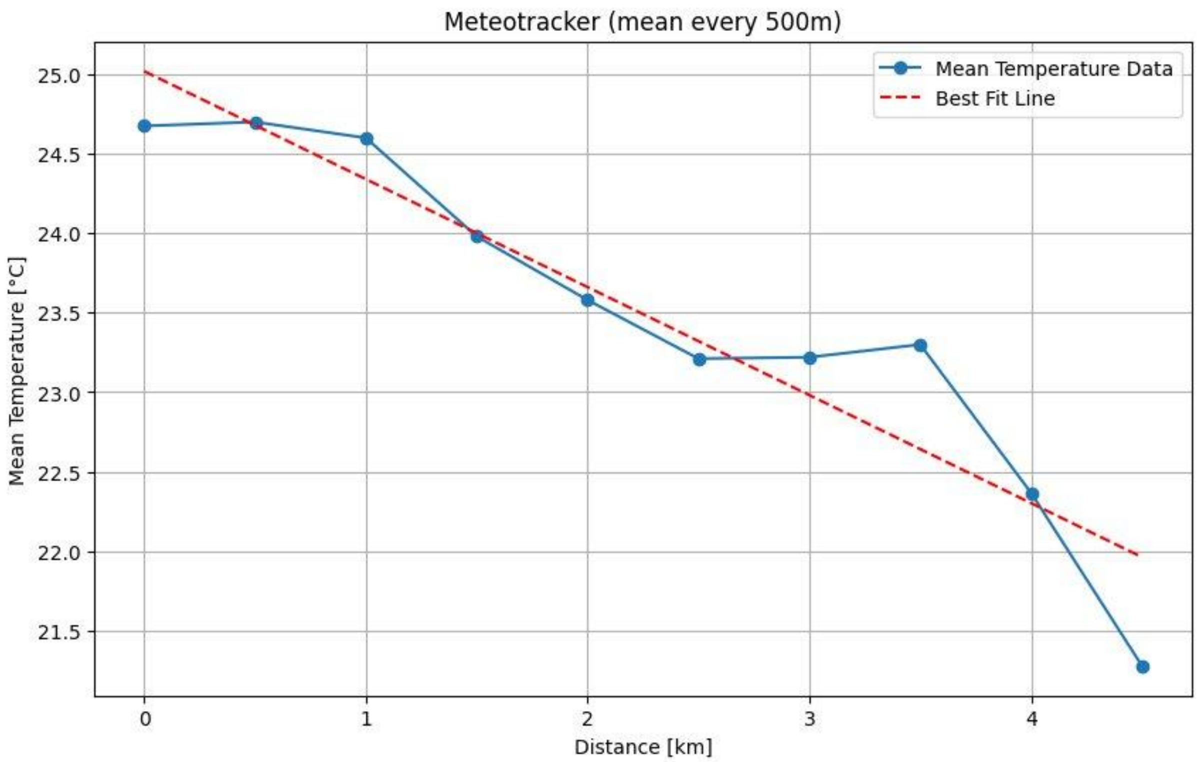

Figure 49

The mean temperature best fit has a slope of -0.68 °C/km, but it is important to observe that the linear regression isn't fully representative of the reality, even though it's a good approximation for the radius of the city in the majority of directions: in fact, the first kilometre has an almost constant temperature, because it was recorded inside of the historical city walls, where the density of buildings is high. Outside of the historical walls, the temperature drops consistently, before hitting a temporary plateau from 2.5 to 3.5 km.

This consideration aids in understanding how much the local density of the urbanization can affect the cooling of a city at night. On the bright side, the part of the city that is extremely developed doesn't have a large radius and its UHI seems limited in its size, even though it influences greatly the thermal comfort in the centre, where a large number of people live. Finding mitigative solutions for the Prendiparte district and close by areas, even if not large, would benefit a large portion of the city population.

This approach can be extended to larger scales: cities are densely populated areas that occupy a small percentage of the Earth's land but host billions of people worldwide. Adapting mitigation strategies at city scale would better more than half of the planet's population.

The Sant'Orsola district partially represents a mitigated neighbourhood, because of the larger portion of vegetated areas. Still, its initial urban design is different from the Prendiparte district and promotes ventilation and convective cooling at night.

3.2.4 MeteoTrackers and Climatology

The graph 50 shows the hourly averages computed from the MeteoTracker datasets for the two zones, once again confirming the faster cooling of the hospital neighbourhood after the sunset (19:50 CEST). The SO site reaches mean hourly night temperatures that are up to 2 °C lower that those recorded in the TP site. The Prendiparte area exhibits a slower cooling, hence why the area manages to take on values similar to the SO ones only right before dawn (06:15 CEST). Conversely, during the day, the two areas reported similar measurements. The collected datasets have various gaps, given the voluntary nature of the campaign.

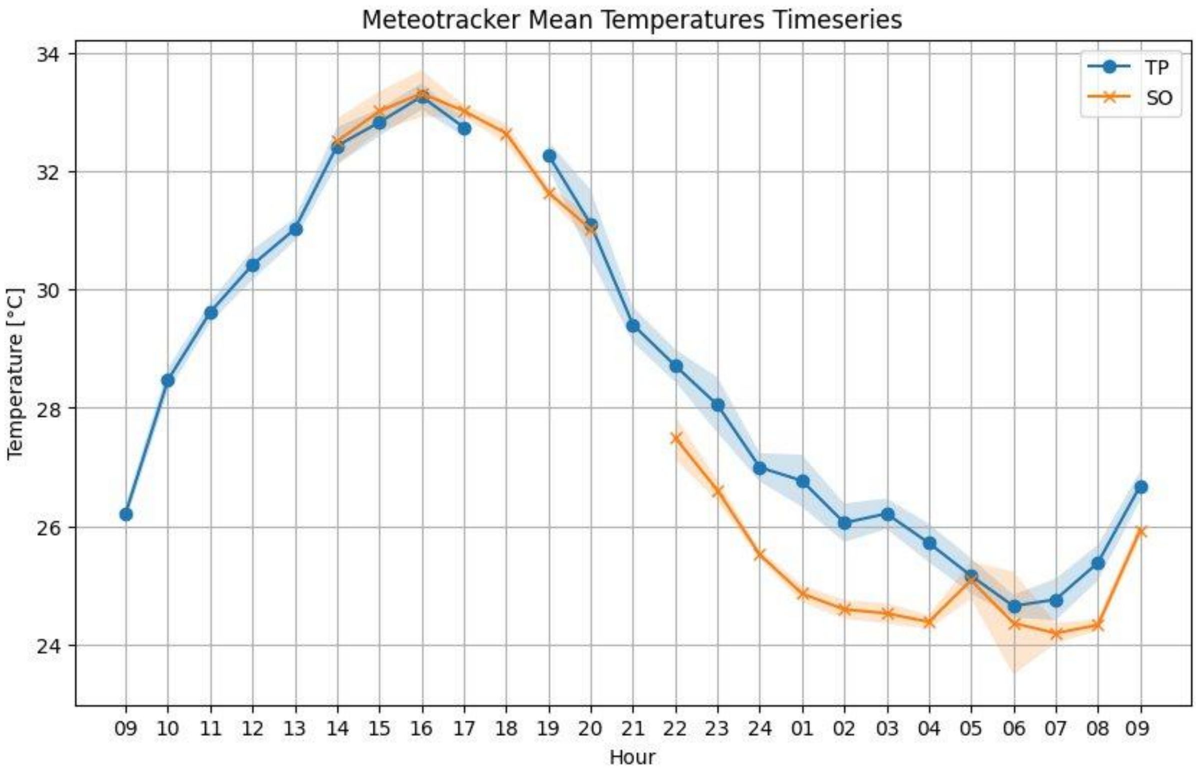

Figure 50

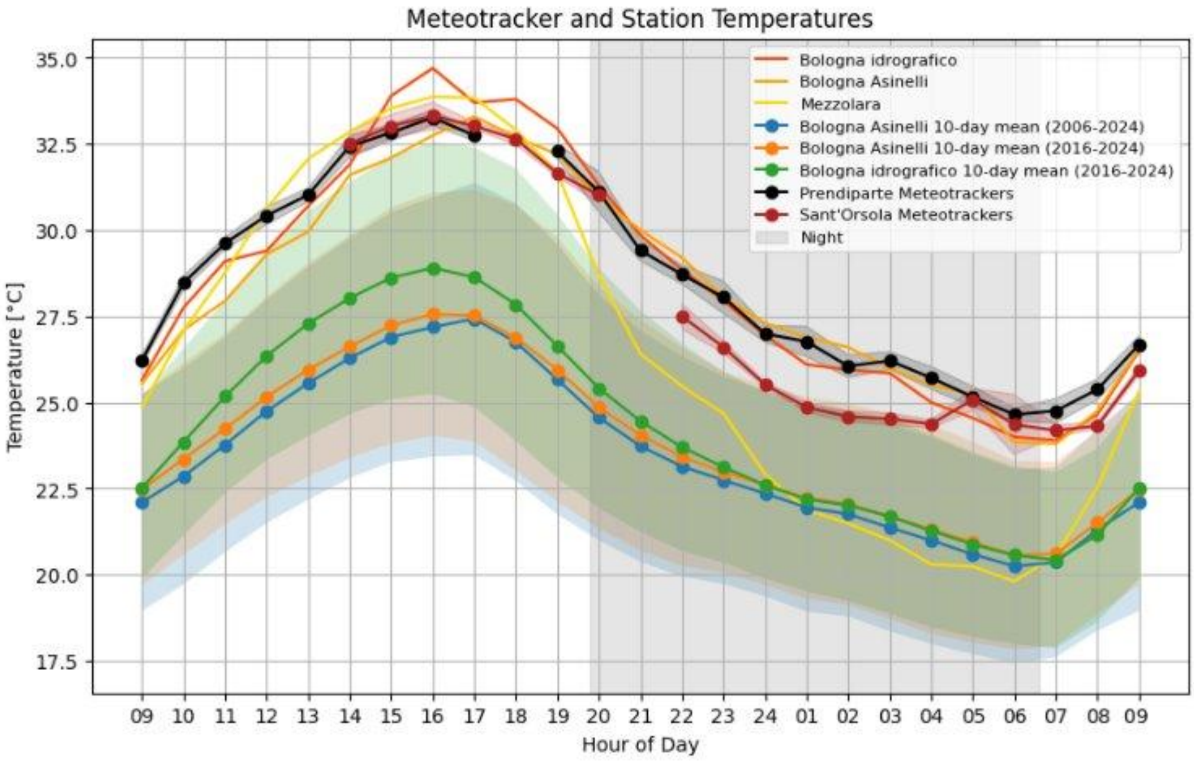

Figure 51

The daytime values of the ground temperature (MeteoTracker) coincide with the data from the weather stations (Bologna idrografico, Bologna Asinelli and Mezzolara), with peaks around 16:00 CEST, whereas the nighttime values for Mezzolara, which is a small town of 2000 people to the North East of Bologna, start diverging rapidly at sunset, reaching temperatures that are 5 °C lower than those collected in Bologna. The bottom bands represent the hourly maximum temperature climatology for ten days centred on the 1st and 2nd of September, operated on the Bologna Asinelli and Bologna idrografico stations: the field campaign values are well above, thus confirming the 1st of September as a heatwave day. The main objective of this graph, in fact, was to contextualize the field campaign temperatures with respect to the local climatology. Another reflection can be done on the two plots for Bologna Asinelli, as the climatology was calculated for two different periods (2006-2024 and 2016-2024): there's a slight increase for the more recent averages, that shows the warming of the last years. Furthermore, the two Bologna monitoring stations can be compared for the period 2016-2024, where the idrografico data results warmer during the day, because of the position closer to the ground of the instrumentation (Asinelli is placed at 148 m while idrografico is placed at a.s.l. 84 m a.s.l.).

3.2.5 MeteoTrackers and Monitoring Stations - Convergence Velocity

In the attempt to calculate the theoretical nocturnal wind that would be caused by the thermal difference between Bologna and its surroundings (within a 22 km radius), multiple weather stations distributed in the vicinity of the city were chosen.

Table 18 Prendiparte coordinates were chosen as the Bologna coordinates, because the data utilized originates from the TP Meteotrackers.

	Coordinates	**Altitude a.s.l. [m]**
Bologna	(44.495833, 11.344444)	65
Zola Predosa	(44.496142, 11.200059)	65
Sasso Marconi	(44.439668, 11.241251)	275
Settefonti	(44.40274, 11.46209)	321
Castel San Pietro Terme	(44.411115, 11.597005)	58
Mezzolara	(44.571053, 11.533793)	20
Padulle Sala Bolognese	(44.627752, 11.290563)	25
Saletto	(44.632318, 11.441136)	18

Data from seven towns was used for the comparison, but Sasso Marconi was then discarded because of the lack of night measurements (gap from 23:00 01/09/2024 to 04:00 02/09/2024), which are fundamental for the UHI and consequent convergence velocity.

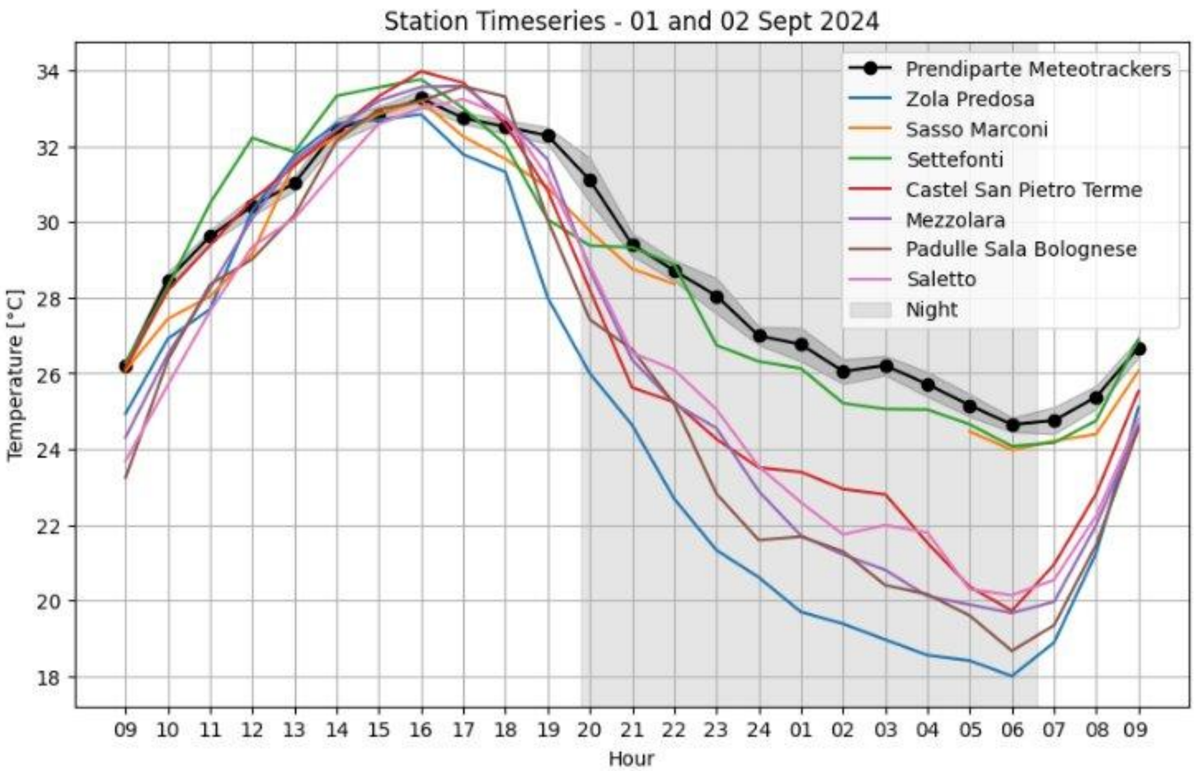

Figure 52

The data was lapse rate adjusted to the reference Bologna altitude, as explained in the Methodology chapter, and showed similar trends during the daytime and lower nocturnal values, especially for five weather stations. The city resulted warmer by more than 6 °C when compared to the nightly temperature values of all the other towns (except for Settefonti at 22:00 CEST).

The output of the computations is displayed below (Figures 53, 54) and clearly shows how Bologna cools down much slower at night in comparison to its surroundings, given that the daylight temperatures were in the same range, with some towns being even hotter than Bologna.

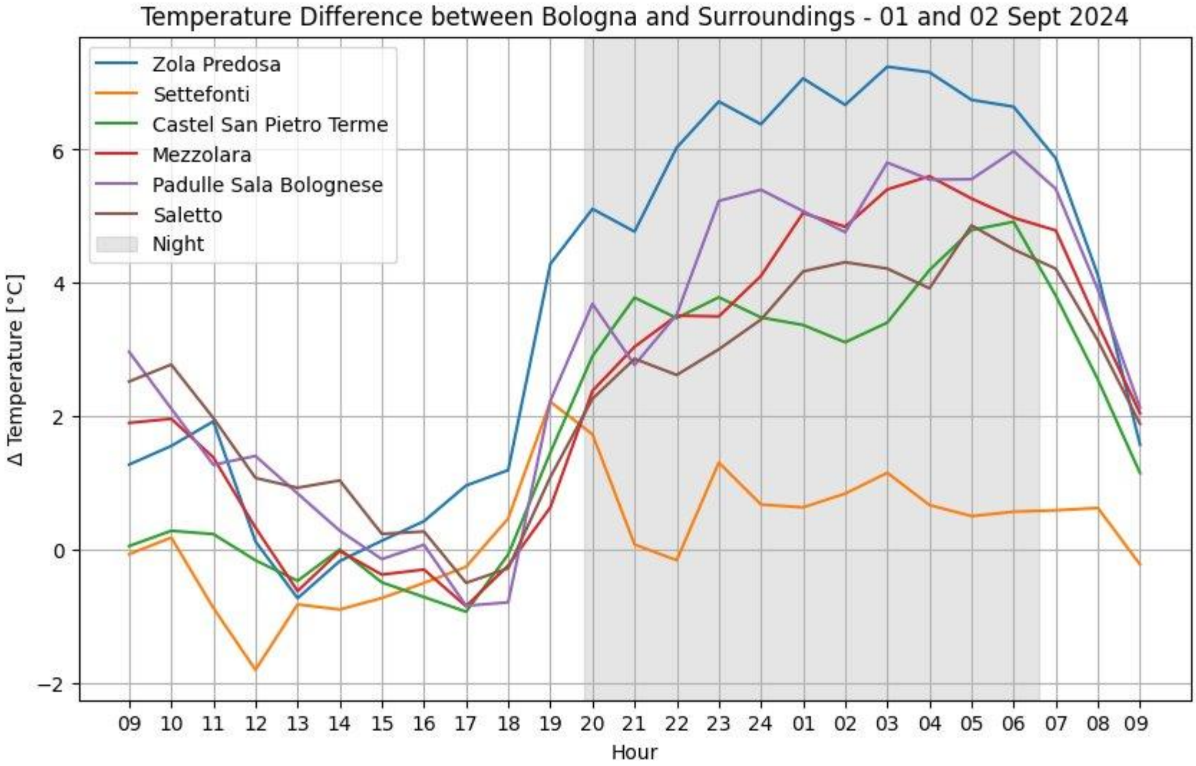

Figure 53

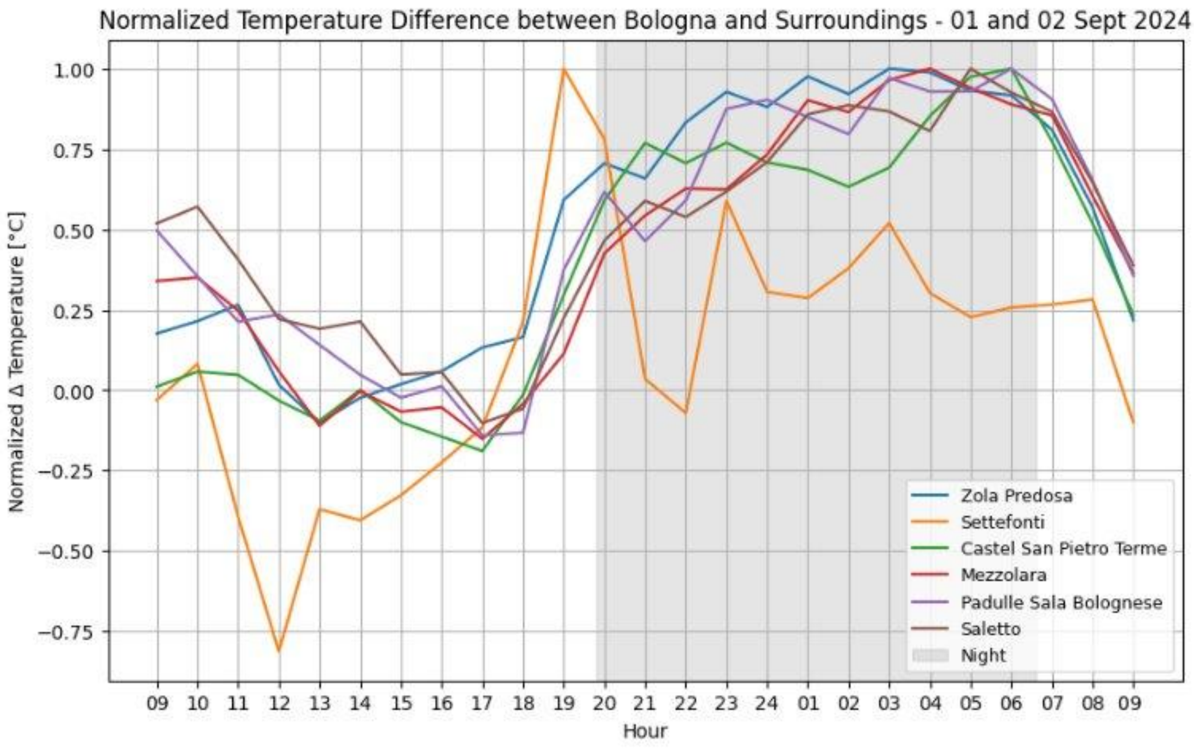

Figure 54 Temperatures normalized by the maximum value of ΔT

The convergence velocity induced by the UHI was calculated via the formula $U_r = C\sqrt{g\alpha\Delta T_{u-r}L}$, that represents the theoretical ground wind that would blow in the absence of inertial forcing.

The winds for the area are largely directed towards the city during the hours of the night, with an average value of around 4 m/s with the exception of Settefonti.

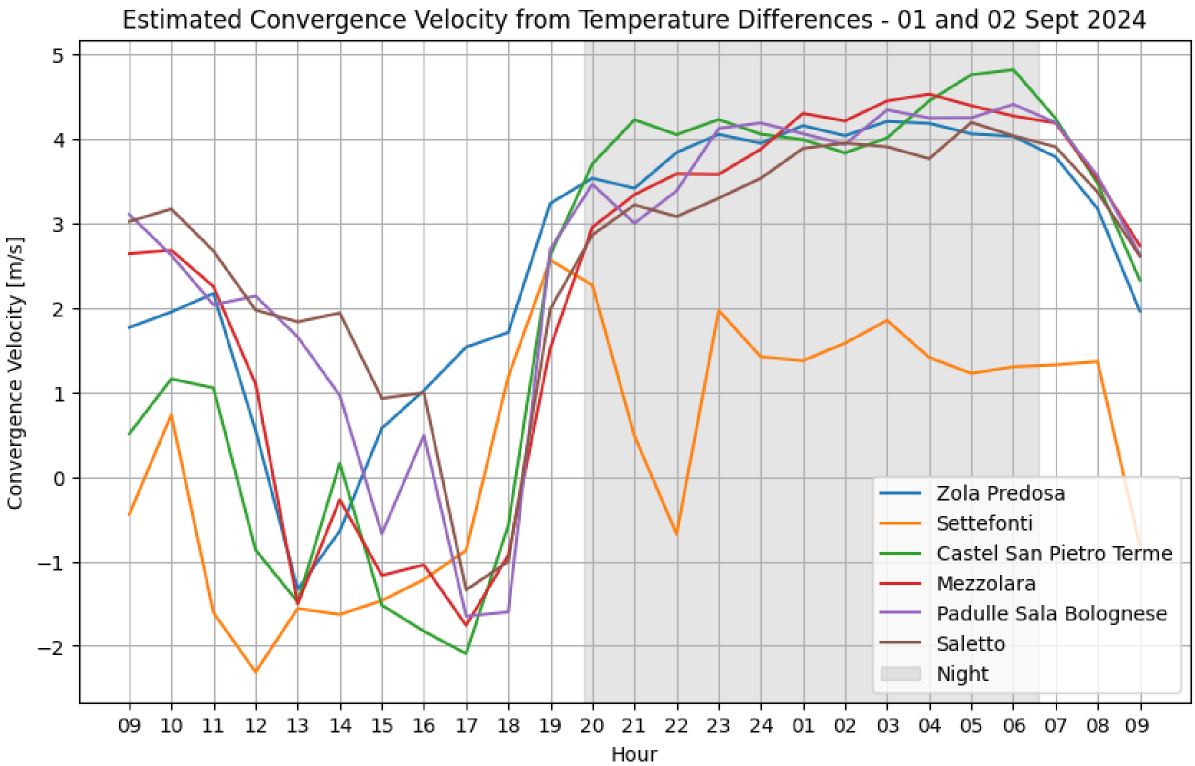

Figure 55

The convergence velocities were averaged over two exemplifying periods that represent the formation of the UHI and the beginning of its induced wind (20:00 - 23:00) and the plateau that is sustained at night (03:00 - 06:00). The weaker UHI in the first hours after sunset gives rise to a convergence velocity of ≈2 m/s, stronger in the northern section. As the UHI stabilizes, the theoretical wind intensifies and reaches ≈3 m/s or more on average. The precise values will be schematized later.

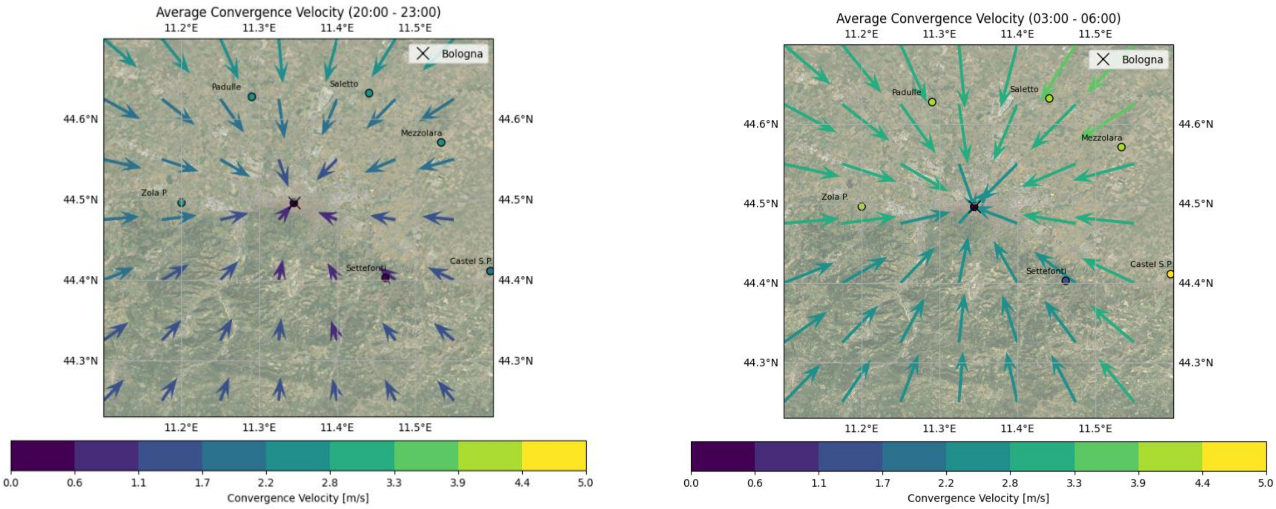

Figure 56

The same computations were repeated without adjusting the datasets to the lapse rate, as the utilized formula isn't specific for UHI convergence velocities and a clear literature on the necessity for lapse-rate adjustment isn't present. In this case, the resulting convergence velocities are more uniform than in the previous computation and the Settefonti station, which sits at the highest altitude of 321 m a.s.l., is in better agreement with the other locations.

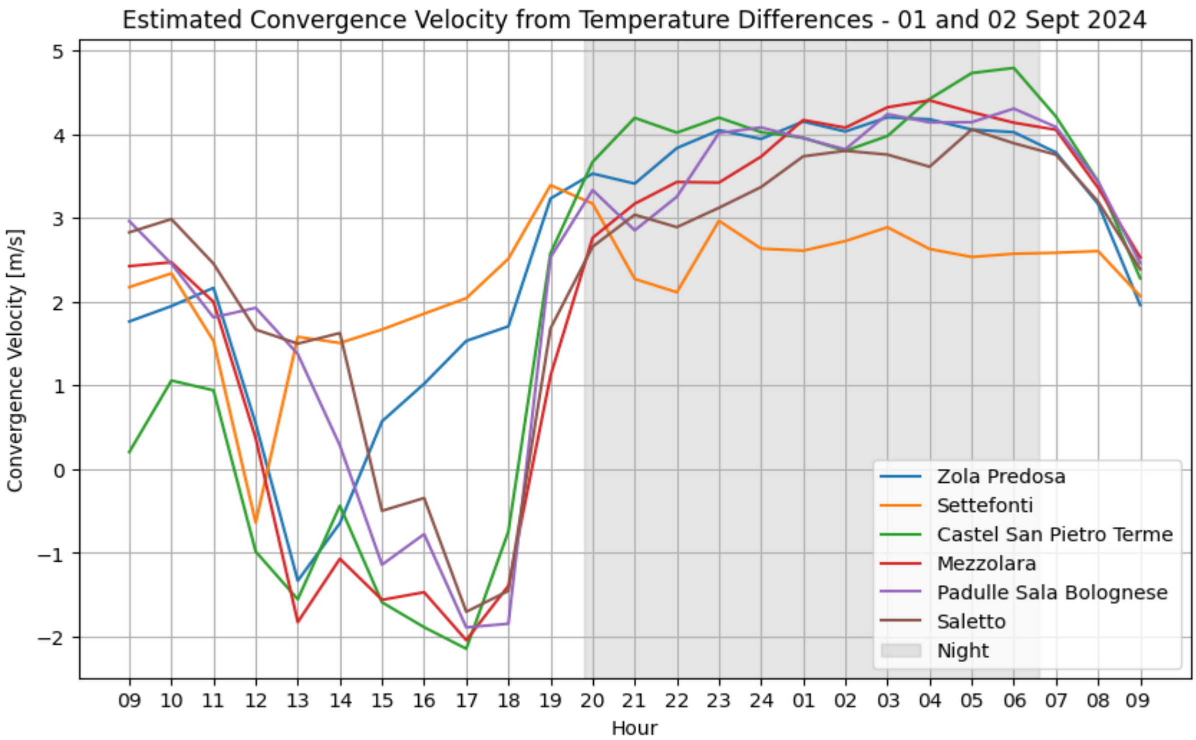

Figure 57

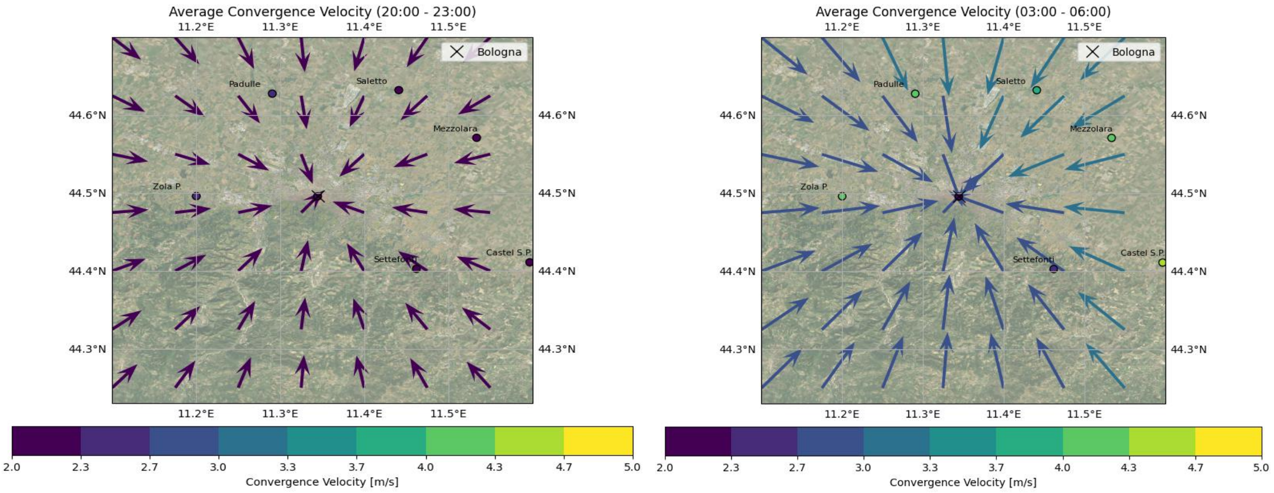

Figure 58

In the non-adjusted scenario, the wind blows towards Bologna more uniformly from all directions and gets to higher speeds than the adjusted case. The airflow is caused by the warm urbanized Bologna, that induces the thermal circulation.

Table 19

	Adjusted w.r.t. Lapse Rate		**Non-Adjusted w.r.t. Lapse Rate**	
Station	Convergence Velocity [m/s] (20:00-23:00)	Convergence Velocity [m/s] (03:00-06:00)	Convergence Velocity [m/s] (20:00-23:00)	Convergence Velocity [m/s] (03:00-06:00)
Zola Predosa	2.59	4.11	2.59	4.11
Settefonti	0.38	1.44	2.25	2.66
Castel San Pietro	2.13	4.50	2.05	4.48
Mezzolara	2.29	4.40	2.03	4.28
Padulle	2.62	4.30	2.39	4.21
Saletto	2.63	3.97	2.32	3.83

The table 19 schematizes the theoretical wind speed originated by the calculated temperature differences. The non-adjusted case displays values that are more similar to each other.

3.2.6 Surface Thermal Imaging and Object Analysis - Microscale

The field campaign included the capture of 360° infrared photos taken from atop the Prendiparte tower. In this way a comparison between the temperatures of the urban surfaces, like roofs, façades and streets, could exemplify how thermal radiation is emitted from these objects during the day and the night. In the analysis, mixes of objects of different types were also taken into account, to mimic 'urban mixes' and serve as a sample of how an average of the various materials and orientations of surfaces in the neighbourhood would react to the daytime solar radiation and nighttime radiative and convective cooling. Also, two of the very few trees in the zone were isolated and selected from the numerous IR pictures to plot their temperatures.

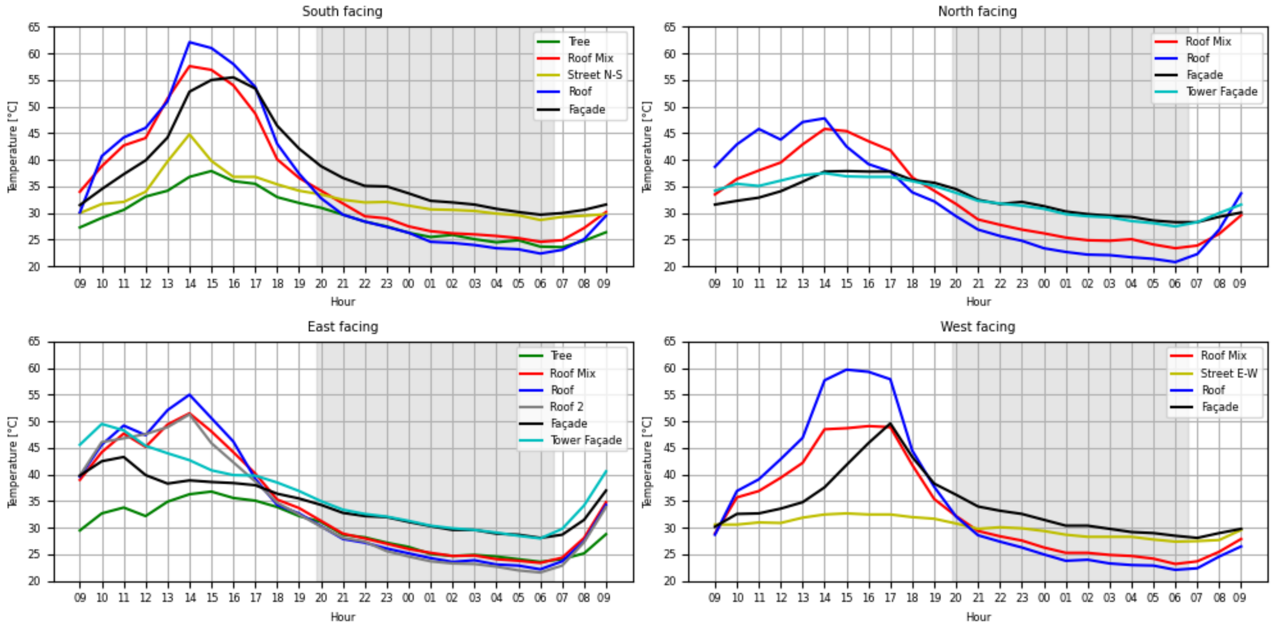

Figure 59

The plots from figure 59 are divided in four subplots that display one group of objects for each exposure (i.e. south-facing, etc…). It can be seen that the south-facing surfaces emitted more infrared radiation (so they were warmer), which obviously correlates with the longer and stronger exposure to the sunlight; on the contrary, north-facing objects clearly recorded the lowest temperatures. The peaks are dependent on the exposition, in fact, west-facing surfaces were recorded with the most thermal radiation later than the others. Out of all the different items, trees were the ones found at the lowest day temperatures (also, there's the possibility that, being that trees are porous mediums, the shade behind them was photographed, which is an interesting measure), whereas roofs reached the highest recorded temperatures.

There's a specific order in which diurnal temperatures appear and it coincides with the height of each object and the duration of the exposure to the sun. From highest to lowest values, the surfaces are: roofs, roof mixes, façades and streets. It's evident that roofs, being high up and receiving shortwave radiation for the longest period, absorb much more heat than a street that is shaded for a lot of time, thanks to the dense urban design of the city centre.

At night, the objects reach values closer to each other while cooling and some surfaces cool down faster than others: roofs are able to cool down thanks to thermal radiation and convective radiation quite efficiently, as they are usually not entrapped in the urban canopy and the heat that they emit is transferred away faster. Also, roofs are more exposed to wind and the greater ventilation guarantees a rapid convective cooling. For street surfaces, the opposite is true: radiative cooling isn't effective, as a lot of the radiation gets reflected back or absorbed by close by objects (façades or other structures) and the wind hardly reaches the ground.

The following plots (figure 60) are grouped by type of object, to focus on the comparison between different exposures.

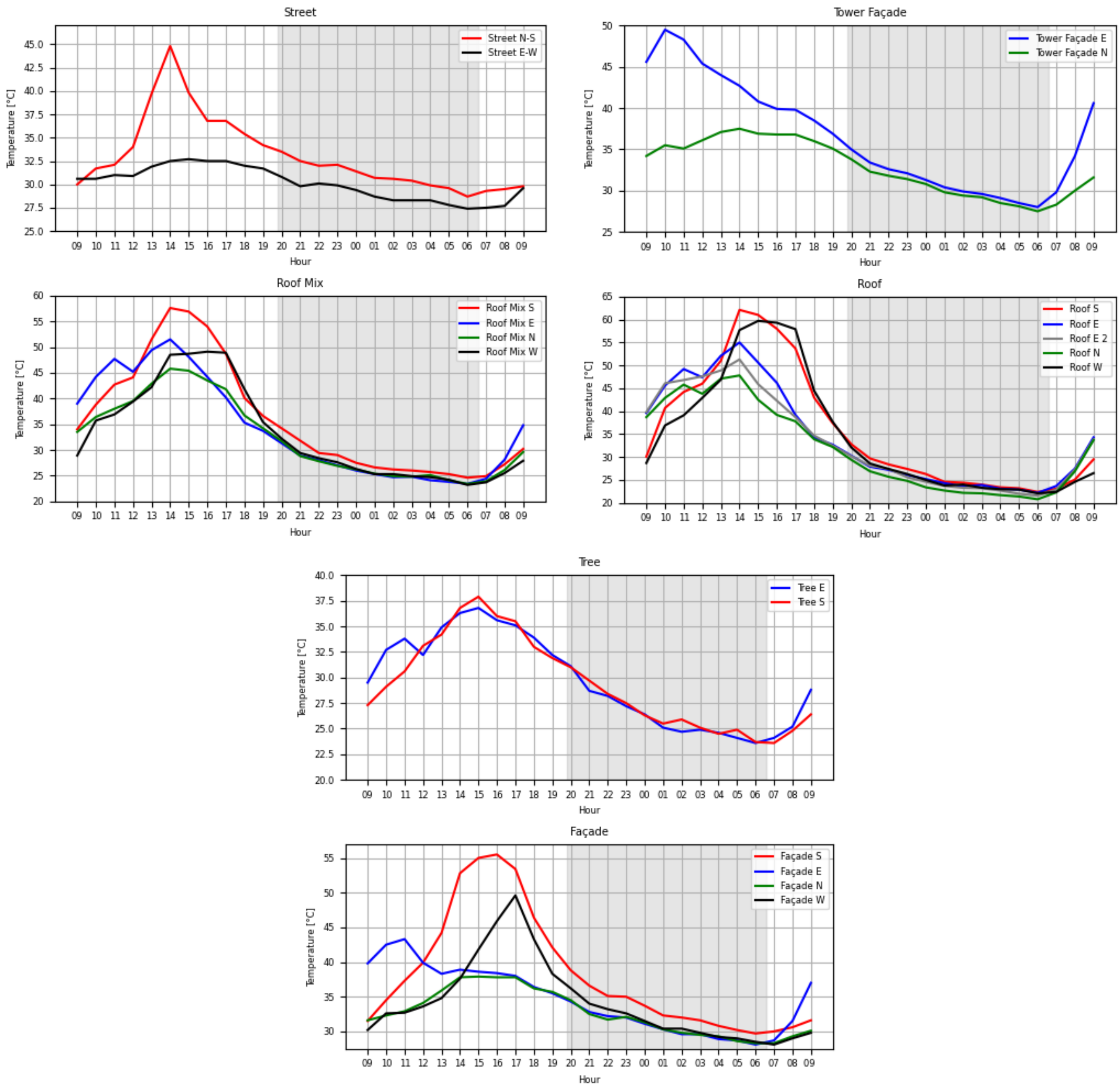

Figure 60

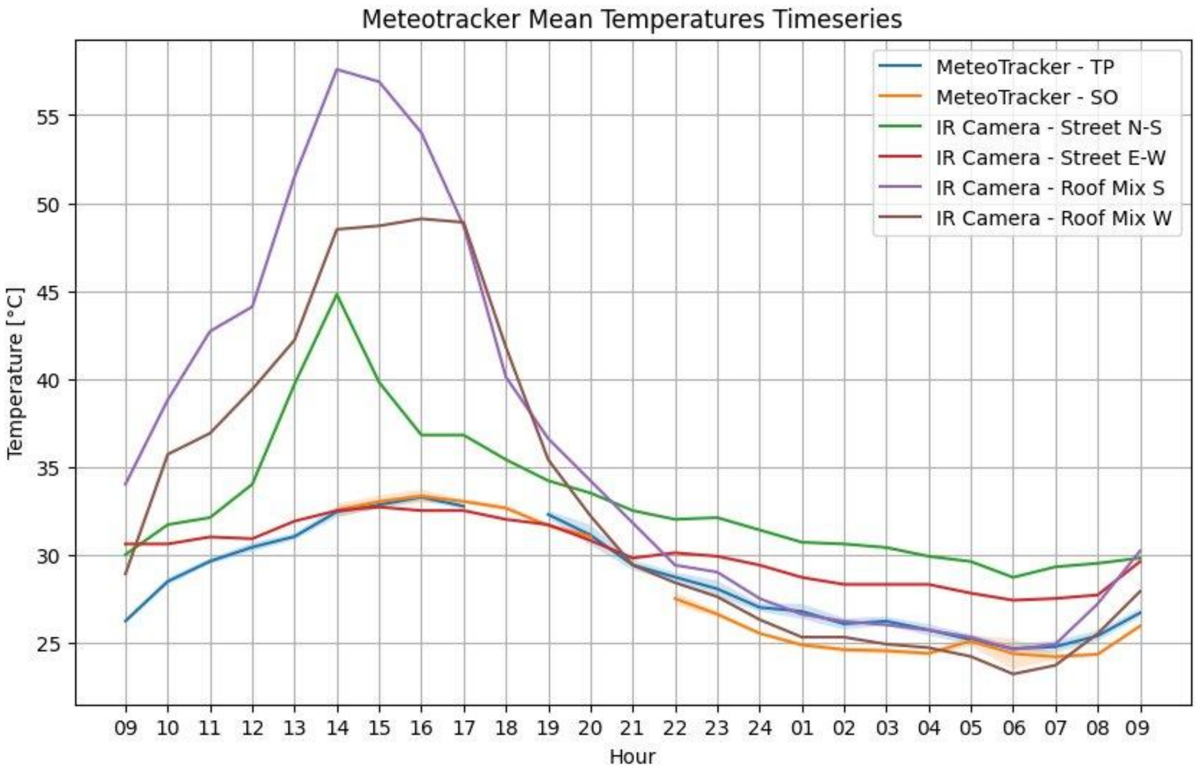

Figure 61

Figure 61 compares the ground air temperatures recorded with the MeteoTrackers in the two districts with the IR radiation emitted by some of the objects in the central area. It is evident that there is a bigger thermal excursion for the surfaces and for the roof mixes in particular (roofs would have an even greater excursion but are not plotted here) than for the air, fortunately. As the urban surfaces usually have lower albedos, they absorb a large part of the SW radiation, that is thus converted to heat, leading to the high measured temperatures. At night, as the shortwave radiation is no longer there, they start to cool down quite rapidly (but still at a lower rate than rural areas) via radiation and convection. The air, on the contrary, even if entrapped in the urban canopy, still mixes with the cooler air above during the day (turbulence), while at night it is partly heated up by the heat released by the city (hence the higher nocturnal urban air temperatures).

A more exhaustive evaluation can be carried out by plotting MeteoTracker data against IR camera data. Only the Prendiparte measures were utilized as the photos were taken only in the central district. The resulting graphs are shown in the following pages, with the linear best fit, correlation and p-value for the correlation displayed in the legend. The bars cover all the air temperature datapoints collected by the volunteers and the dot is the intersection between MT means and IR values. The plots are divided by exposure to facilitate a more direct grasp of how each type of surface responds to changes in temperature and vice versa, with the mediation of the presence or absence of sun radiation. They are intuitively arranged from the highest one (roofs) to lowest one (streets). The graphs can be interpreted as a temporal evolution ordered in the opposite way, because higher temperatures coincide with the first hours after dusk and lower ones were recorded right before dawn. All hours from sunset to sunrise are displayed (20:00 – 06:00).

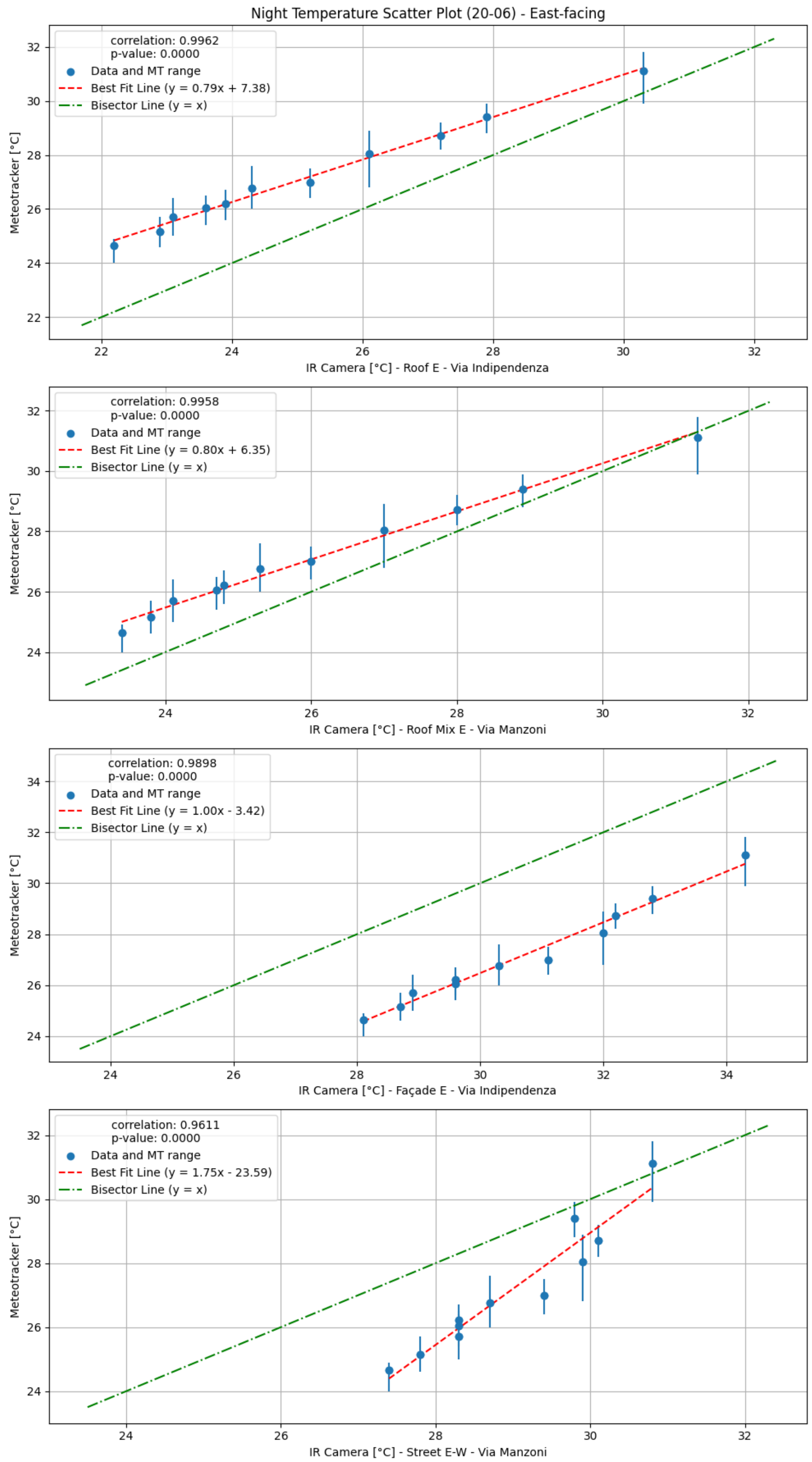

Figure 62 East-facing surfaces captured via thermal camera. Nocturnal temperatures (20:00 CEST to 06:00 CEST). Correlations ≈ 1 for all objects. Roof and roof mix (top 2) present a faster cooling compared to air, thanks to effective radiative emission. Façades exhibit the same rate of cooling as that of the air, while the street undergoes hindered cooling because of the increased number of thermal interactions it's subject to (position in the urban fabric). In fact, the street diminishes its temperature only by 3 °C in the full 11-hour period.

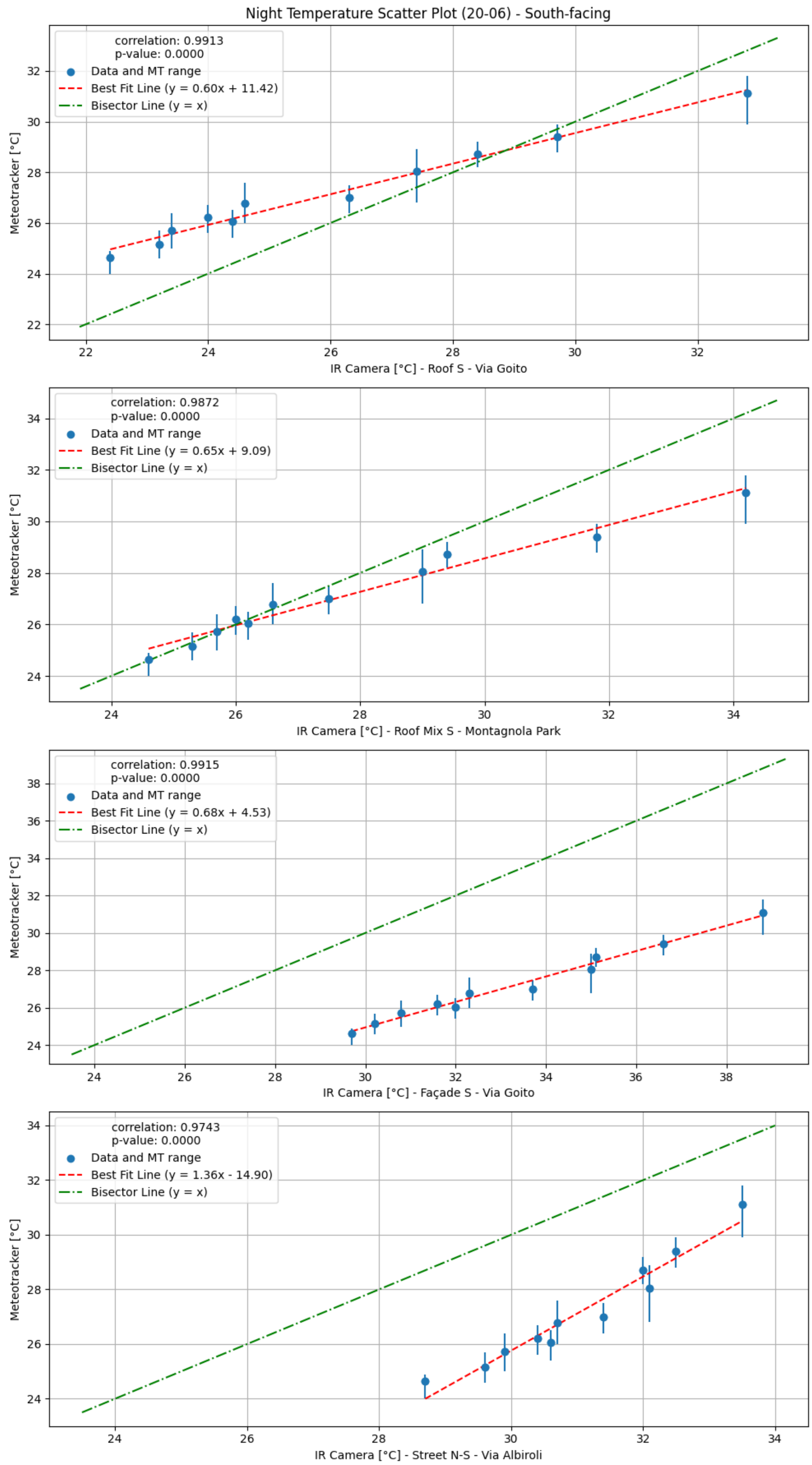

Figure 63 South-facing surfaces captured via thermal camera. Nocturnal temperatures (20:00 CEST to 06:00 CEST). Correlations ≈ 1 for all objects. Roof, roof mix and façade (top 3) present a faster cooling compared to air. The street has a slow cooling because of thermal interaction. Starting temperatures are the highest among all objects because of the orientation and exposure to South.

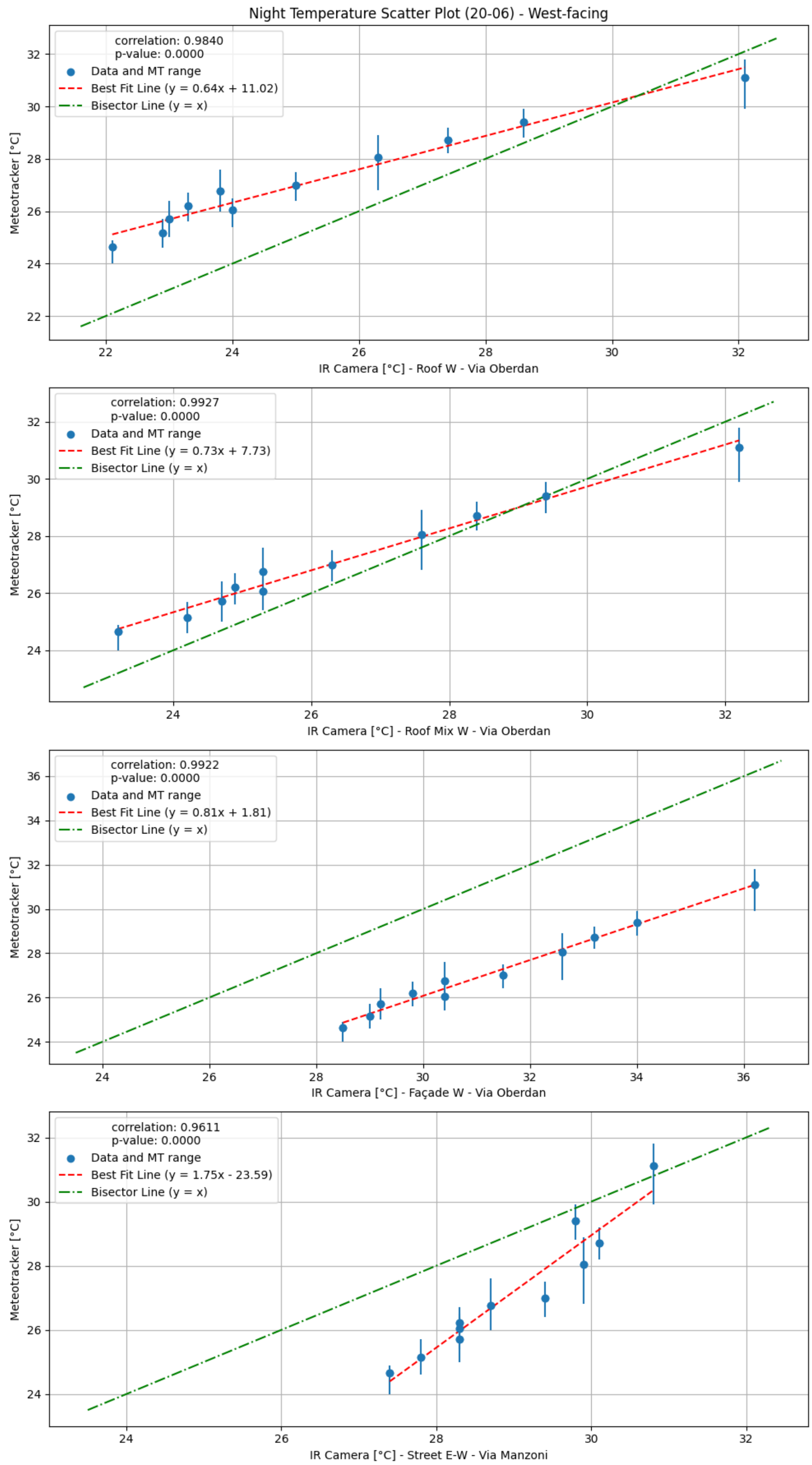

Figure 64 West-facing surfaces captured via thermal camera. Nocturnal temperatures (20:00 CEST to 06:00 CEST). Correlations ≈ 1 for all objects. Roof, roof mix and façades (top 3) present a more efficient cooling. The street presents a slower rate.

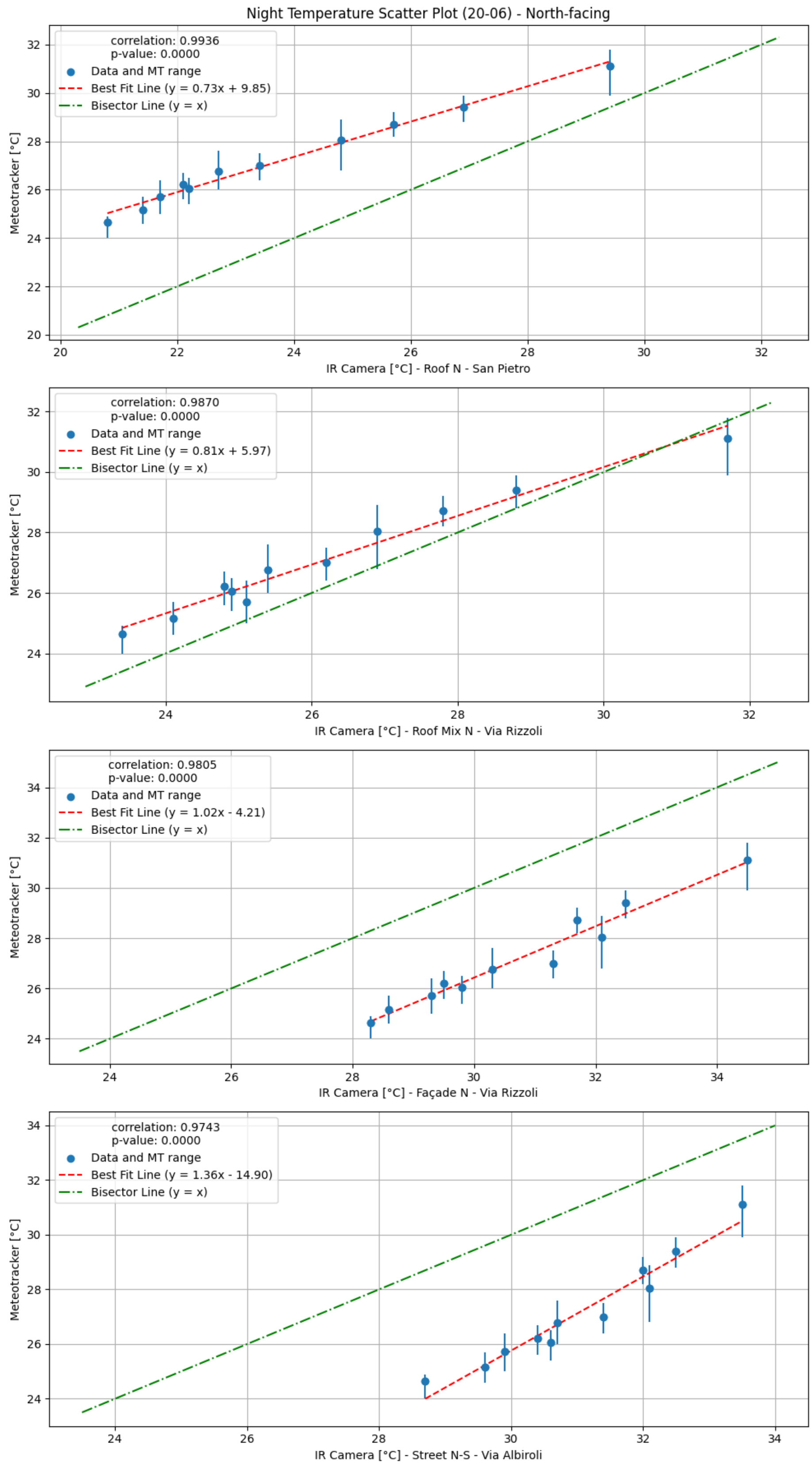

Figure 65 North-facing surfaces captured via thermal camera. Nocturnal temperatures (20:00 CEST to 06:00 CEST). Correlations ≈ 1 for all objects. Roof and roof mix (top 2) present a faster cooling compared to air, thanks to effective radiative emission. Façades and streets undergo hindered cooling probably because of the increased number of thermal interactions they are subject to.

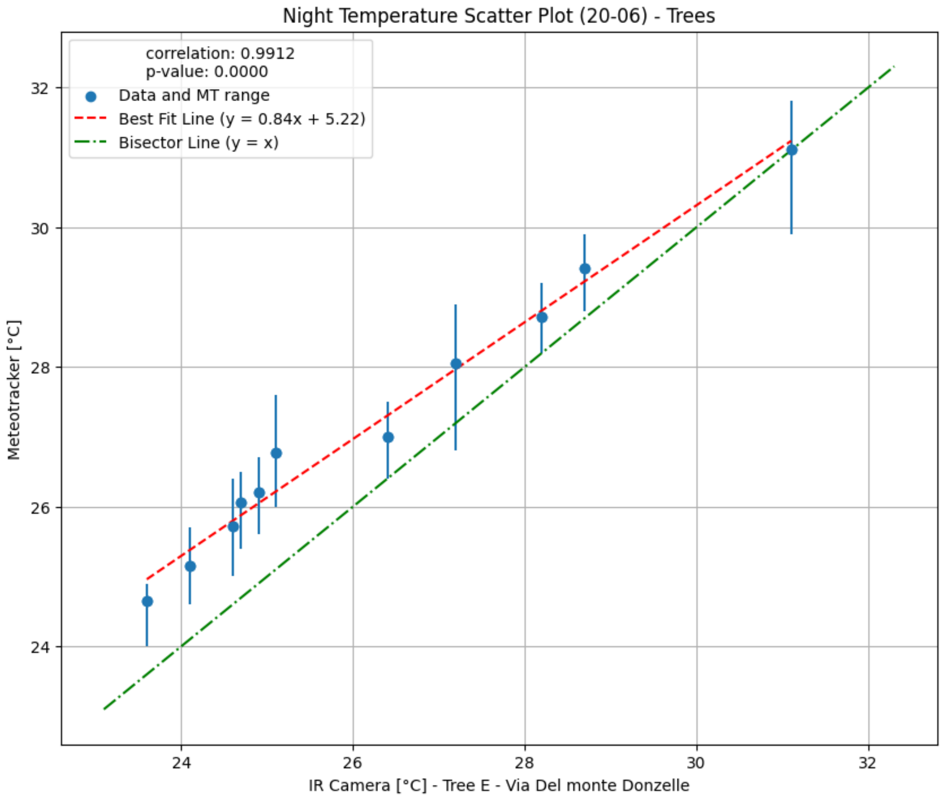

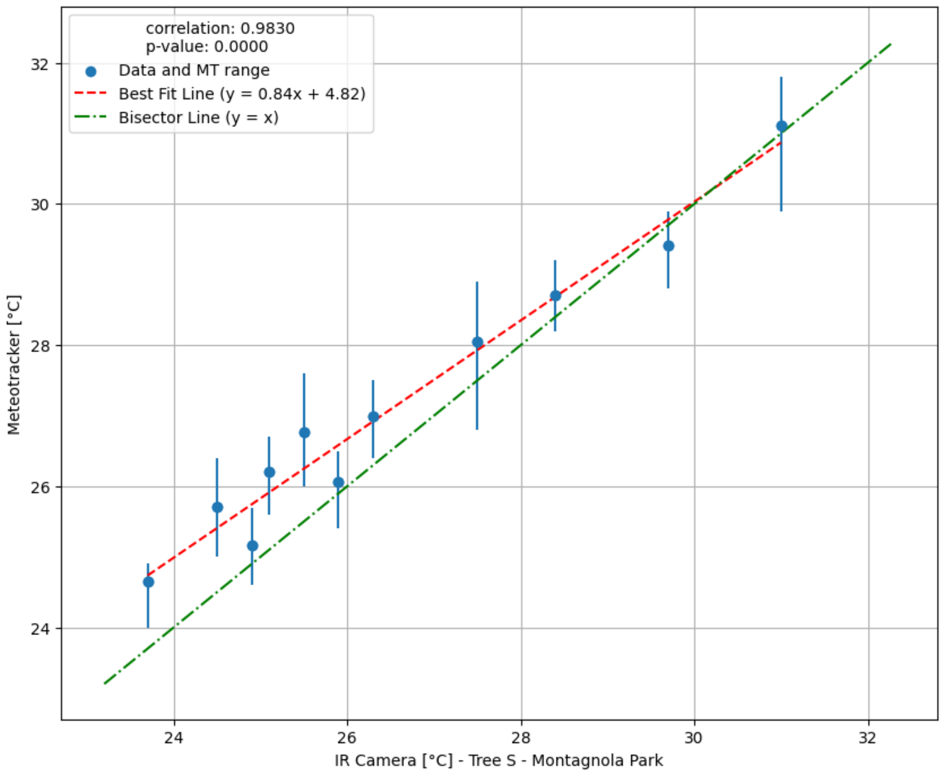

Figure 66 Both tree areas (East and South-facing) exhibit a higher cooling rate compared to that of the air. Furthermore, starting (20:00) and ending (06:00) temperatures are 31 °C and 23 °C for both.

The correlation coefficients are close to unity for all graphs, with p-values of 0.00, indicating an optimal linear relationship between surfaces' IR radiation and air temperatures. Best fit slopes greater than 1 are demonstrative of the fact that the air is cooling faster than the object in question: this is usually the case for all streets and the north-facing façade. The east-facing façade has a coefficient of one, revealing an equal rate of cooling for the air and the façade. All other coefficients are smaller than unity and show a faster cooling for the surfaces than for the air. The results are in agreement and can be explained with the concepts clarified at page 67.

Table 20 Starting (20:00 CEST) and ending (06:00 CEST) temperature for all objects and their differences (°C). South-facing surfaces usually have the highest temperatures, because of their prolonged exposure to the sun, which is especially true for the façades, as they are vertical.

Exposure	**Roofs**			**Roof Mixes**			**Façades**			**Streets**			**Trees**		
	20	**06**	**Δ**	**20**	**06**	**Δ**	**20**	**06**	**Δ**	**20**	**06**	**Δ**	**20**	**06**	**Δ**
East	30	22	8	31	23	8	34	28	6	30	27	3	31	23	8
South	32	22	10	34	24	10	38	29	9	33	28	5	31	23	8
West	32	22	10	32	23	9	36	28	8	30	27	3			
North	29	20	9	31	23	8	34	28	6	33	28	5			

A clearer picture could be painted if these datasets were to be compared with infrared photos taken in the Sant'Orsola district, to analyse and discover how the trends change with different building density and increased vegetation. As clarified before, surfaces like streets and façades fail to cool down because of close by objects absorbing and re-emitting the thermal radiation: if the planar and frontal coefficients are lower, this phenomenon would be damped. At the same time, tree evapotranspiration and impervious surfaces provided by the larger green areas would further influence the trends.

Also, the data could be affected by inaccurate emissivities that were chosen for the settings of the thermal camera or by errors in the MeteoTracker measurements. These matters could be investigated further.

Nonetheless, the results are clear and coherent with the theory.

Conclusively, the climatological review highlighted how the Emilia-Romagna region seems to be undergoing a faster warming than that of Italy or of the world, delineating a scenario of high urgency. Furthermore, the higher temperatures of Bologna were confirmed in all the here conducted climatological analyses, along with the increasing heatwave trends. Moreover, the climatological study demonstrated that Bologna seems to exhibit a persistent Urban Heat Island that largely amplifies local temperatures: the field campaign discovered that such amplifications can reach values of almost 7 °C for urban-rural sites, under summer heatwave and clear sky conditions. Then, the recorded nocturnal 2 °C difference between the densely built Prendiparte area and the Sant'Orsola vegetated and less built area confirms the consequences of the already known thermal interactions between surfaces. Other important results, such as the convergence velocity, the morphological parameters of the two investigated neighbourhood and more, were reported in this chapter.

Conclusion

As the literature review suggests, heatwave events and Urban Heat Islands will likely be intensified and exacerbated by the rising temperatures, posing a major risk for urban populations. Furthermore, the Emilia-Romagna region seems to be undergoing a faster warming than that of Italy or of the world, delineating a scenario of even higher urgency. Fortunately, adaptation and mitigation measures are effective at damping the negative effects of the UHIs, but need to be employed appropriately, as numerous studies confirm. To lay the groundwork for a multi-scale investigation of the UHI in one of the most populated cities of the Padan Valley, a 24-hour intensive field campaign was conducted in Bologna, during a heatwave in the beginning of September. Thermal imagery of the densely built core of the city was acquired and paired with temperature datasets collected via portable sensor devices in two morphologically different neighbourhoods and in the outskirts of the city. The recollected measures were integrated with a climatological review of the city of Bologna in the regional context, demonstrating its hotter temperatures, along with an analysis of heatwave trends, via ISPRA weather station data and Eraclito 91 reanalysis records. In the end, the findings of this thesis are both alarming and clarifying, as Bologna exhibits a persistent Urban Heat Island that largely amplifies local temperatures by values of almost 7 °C for urban-rural sites, under summer heatwave and clear sky conditions. The recorded nocturnal 2 °C difference between the densely built Prendiparte area and the Sant'Orsola vegetated and less built area confirms the consequences of the already known thermal interactions between surfaces. The integration of multi-scale climatological data, from regional reanalysis datasets to street-level thermal imaging, reveals how the urban morphology and materials directly shape the microclimatic behaviour of the city and confirms that surfaces found in the more closed-off positions of the urban canopy (streets) present a lower nocturnal cooling rate, compared to that of roofs, for example, that are able to efficiently radiate the heat away. Still, urban areas entrap more heat because of their low-albedo materials and morphology: nighttime conditions, which should provide thermal relief, instead remain hot in the whole city and particularly so in the central area, putting vulnerable populations at increased risk of heat-related illnesses and mortality. This impact will likely be heightened by the observed long-term climatological trends which show statistically significant increases in minimum temperatures and heatwave intensity and frequency.

As global temperatures continue to rise, and old extremes become the present norm, cities like Bologna will find themselves at the frontline of climate risk impacts: this is why lowering vulnerability is of paramount importance. Mitigation and adaptation strategies, additionally to new urban development that is mindful of the present and future climate are necessary for the welfare of the population. The 2022 death toll in Italy represents an omen for the current and imminent management of the UHI and heatwave question.

Further research on the topic could be conducted by comparing the thermal behaviour of urban surfaces in various neighbourhoods of the city via IR imaging techniques to assess how object temperatures change in zones with different morphological characteristics. This study could be additionally integrated with an evaluation on the emissivity and characteristics of the materials typically employed in Bologna’s urban architecture, along with a verification of efficiency of different and employable mitigative measures.

Appendix

See captions for clarifications on the figures.

Climatology

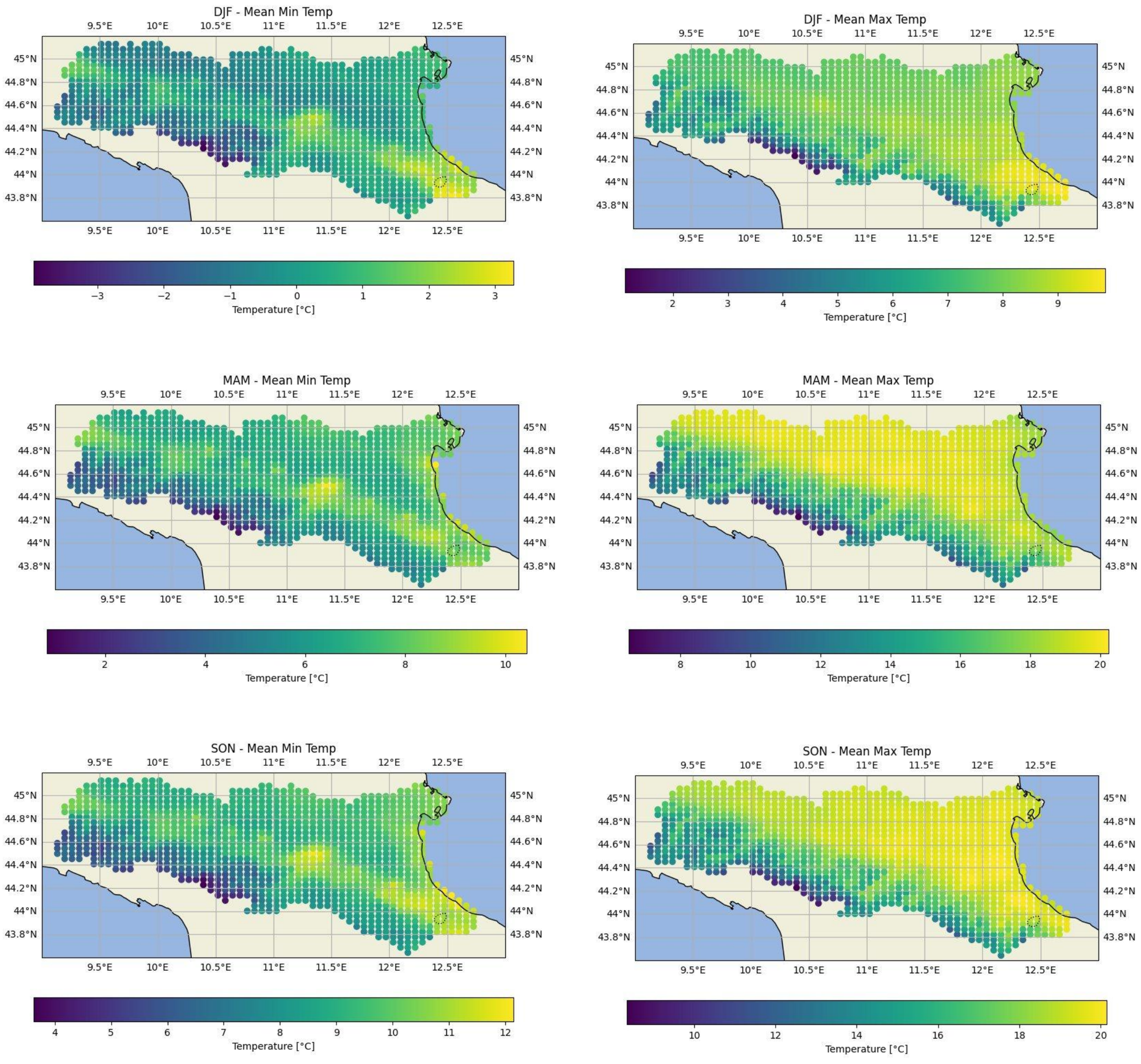

Figure 67 From top to bottom: DJF, MAM, SON average minimum (left) and maximum (right) temperatures for the Emilia-Romagna region, from the Eraclito 91 dataset (1991-2024). Minimum temperatures in particular are a lot higher in bigger cities (UHI).

Tracks

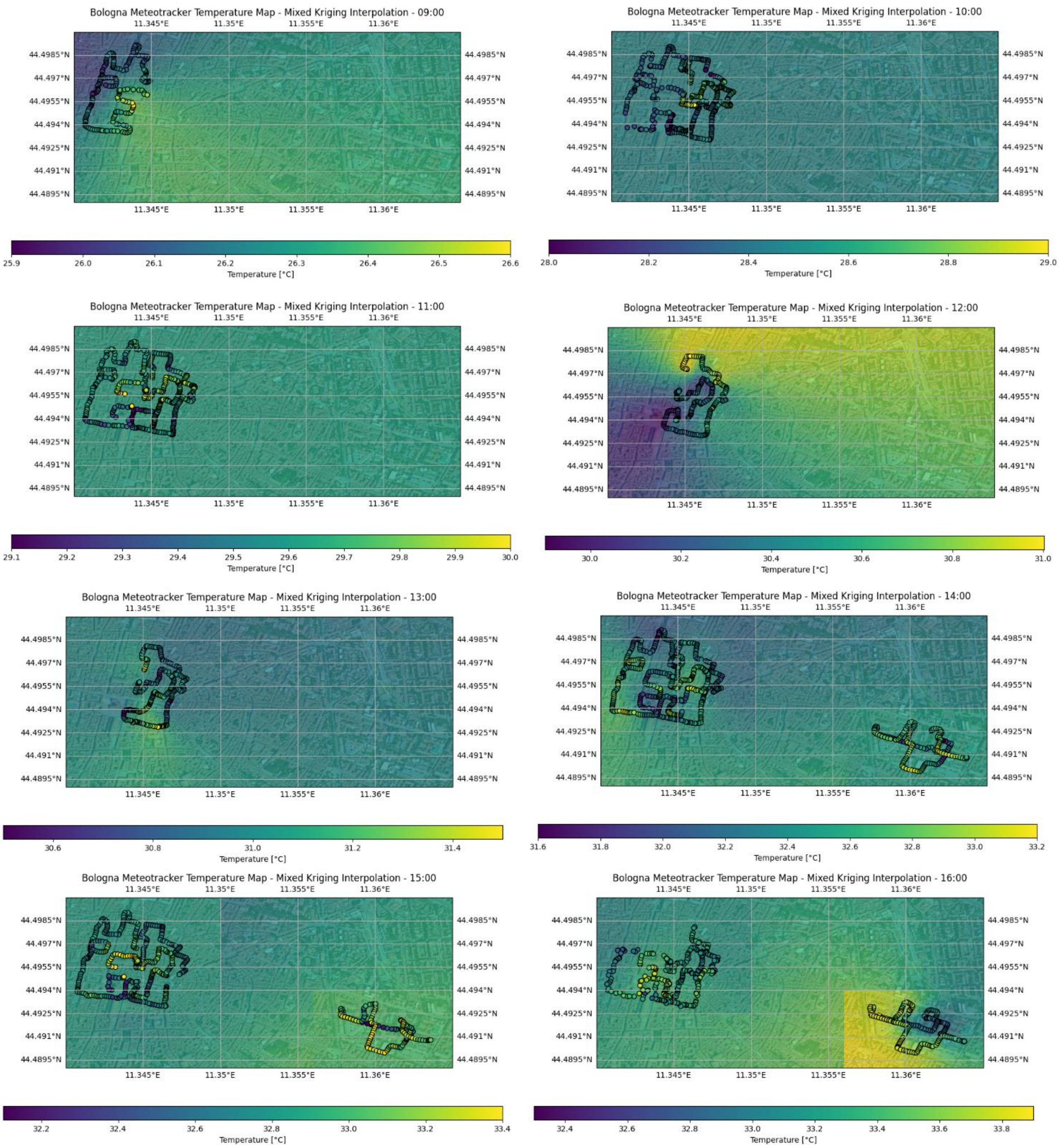

Figure 68 Tracks from TP and SO from 09:00 to 16:00 CEST. There are a few gaps, especially for the SO area. There are no significant differences in temperature between the two areas in the daylight. A few discrepancies can be seen at microscale level because of HVAC systems, shade, traffic or other phenomena.

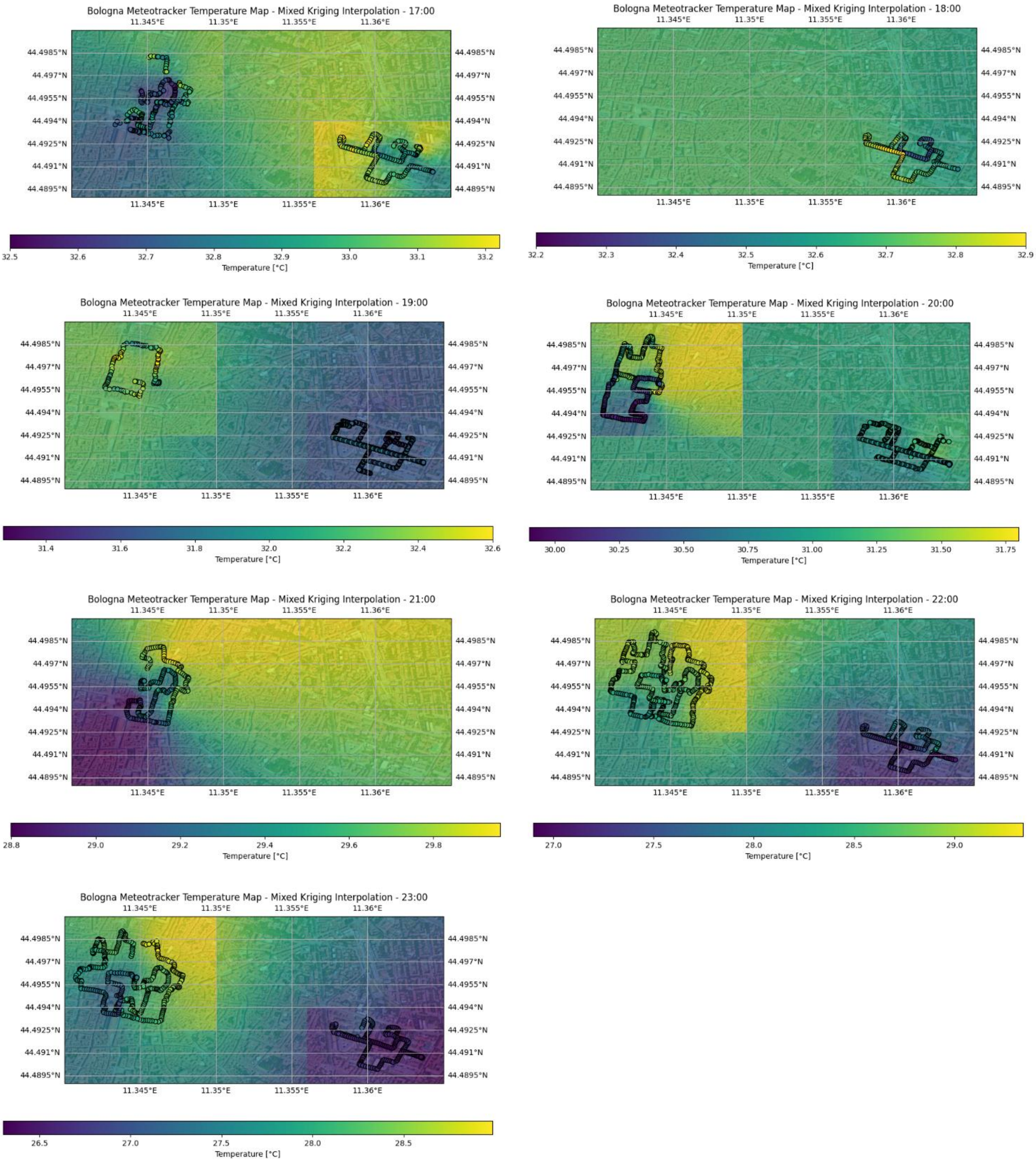

Figure 69 Figure 68 Tracks from TP and SO from 17:00 to 23:00 CEST. From 22:00 CEST, the formation of the UHI can be seen clearly, with differences greater than 2 °C.

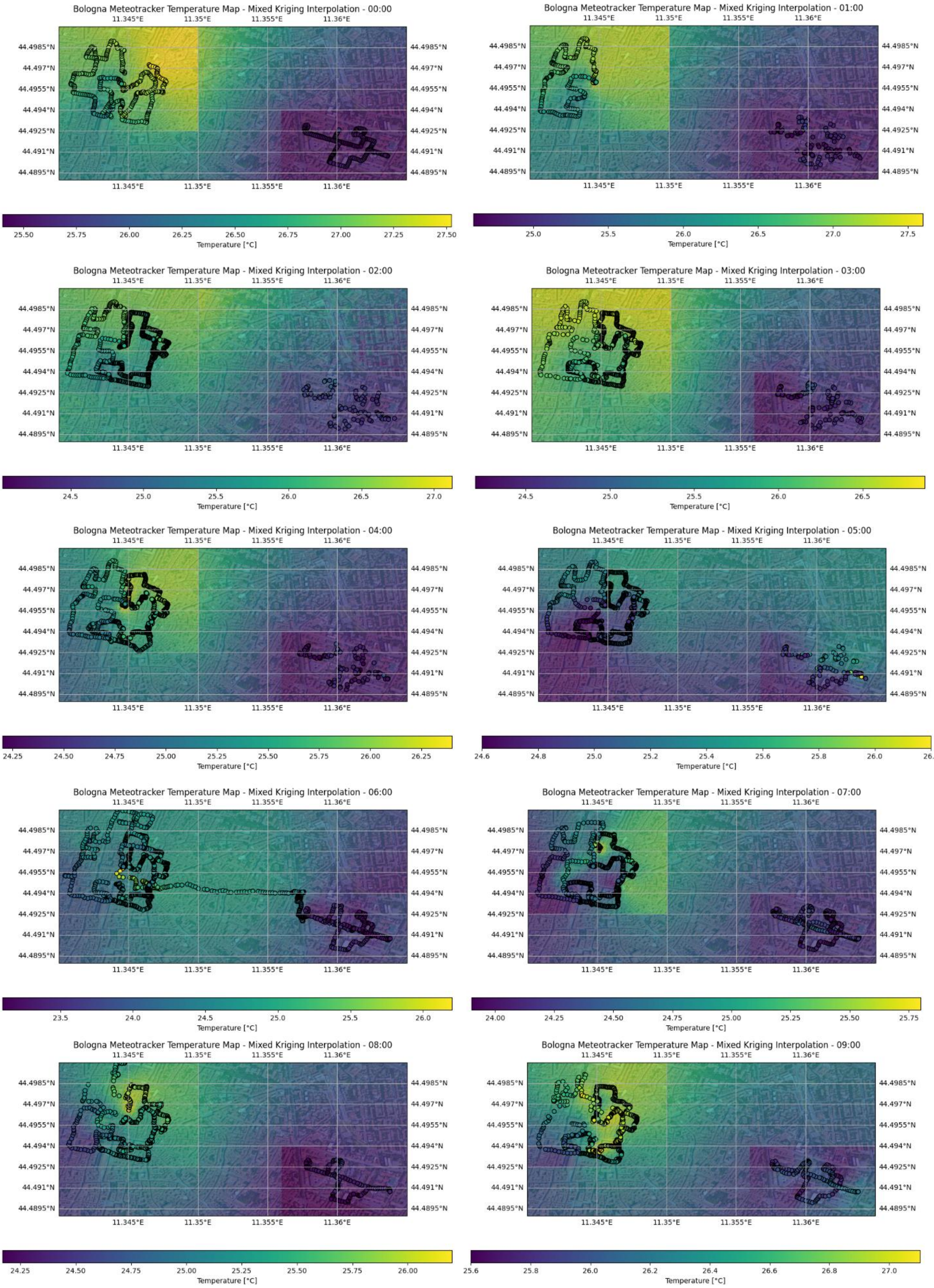

Figure 70 Mostly nocturnal tracks from TP and SO from 00:00 to 09:00 CEST. The UHI can be seen clearly during the night, with differences of around 2 °C. Then, the inter-neighbourhood gradient dissipates with time, as the TP zone cools down and differences start to be come mainly intra-neighbourhood.

Acknowledgements

An enormous thank you to:

Prof. Silvana Di Sabatino, Prof. Francesco Barbano, Dott. Luigi Brogno,

Prof. Carlo Cintolesi, Dott. Francesco De Martin,

Matteo Giovanardi, ‘Succede solo a Bologna’,

Giulia, Letizia,

Alessandro G., Alessandro S., Giada, Giacomo, Giorgia, Lorenzo and everyone else that biked around,

My parents, housemates, friends and all the other people that have supported me,

Momi,

Unibo Offices.

Bibliography

Adil, L., Eckstein, D., Künzel, V., Schäfer, L. (2025). Who suffers most from extreme weather events? Climate Risk Index 2025 Summary. *Germanwatch*

Albini, G., Guerri, G., Munafò, M., & Morabito, M. (2025). Investigation of the Surface Urban Heat Island (SUHI) by two remote sensing-based approaches in Italian regional capitals. *Remote Sensing Applications Society and Environment*, *38*(101567), 101567. doi:10.1016/j.rsase.2025.101567

ARPAE, Guida agli open data meteo-clima

Barbano, F., Brattich, E., Cintolesi, C., Ghafoor Nizamani, A., Di Sabatino, S., Milelli, M., … Parodi, A. (2024). Performance evaluation of MeteoTracker mobile sensor for outdoor applications. *Atmospheric Measurement Techniques*, 17(10), 3255–3278. doi:10.5194/amt-17-3255-2024

Barbano, F., Di Sabatino, S., Stoll, R., & Pardyjak, E. R. (2020). A numerical study of the impact of vegetation on mean and turbulence fields in a European-city neighbourhood. *Building and Environment, 186(107293),* 107293. doi:10.1016/j.buildenv.2020.107293

Calvin, K., Dasgupta, D., Krinner, G., Mukherji, A., Thorne, P. W., Trisos, C., … Ha, M. (2023, July 25). IPCC, 2023: Climate Change 2023: Synthesis Report, summary for Policymakers. Contribution of working groups I, II and III to the Sixth Assessment Report of the Intergovernmental Panel on Climate Change [core writing team, H. lee and J. romero (eds.)]. IPCC, Geneva, Switzerland (P. Arias, M. Bustamante, I. Elgizouli, G. Flato, M. Howden, C. Méndez-Vallejo, … Y. Park, Eds.). *IPCC, 2023: Climate Change 2023: Synthesis Report. Contribution of Working Groups I, II and III to the Sixth Assessment Report of the Intergovernmental Panel on Climate Change [Core Writing Team, H. Lee and J. Romero (Eds.)]. IPCC, Geneva, Switzerland*, pp. 1–34. doi:10.59327/ipcc/ar6-9789291691647.001

Colomer, J., Boubnov, B. M., & Fernando, H. J. S. (1999). Turbulent convection from isolated sources. *Dynamics of Atmospheres and Oceans*, *30*(2–4), 125–148. doi:10.1016/s0377-0265(99)00023-8

Dickinson, R., Henderson-Sellers, A., Kennedy, P., & Wilson, M. (1986). *Biosphere-atmosphere transfer scheme (BATS) for the NCAR community climate model*. doi:10.5065/D6668B58

Di Sabatino, S., Barbano, F., Brattich, E., & Pulvirenti, B. (2020). The multiple-scale nature of Urban Heat Island and its footprint on air quality in real urban environment. *Atmosphere*, 11(11), 1186. doi:10.3390/atmos11111186

Dupont, S., Otte, T. L., & Ching, J. K. S. (2004). Simulation of meteorological fields within and above urban and rural canopies with a mesoscale model. *Boundary - Layer Meteorology*, *113*(1), 111–158. doi:10.1023/b:boun.0000037327.19159.ac

Fernando, H. J. S. (2010). Fluid dynamics of urban atmospheres in complex terrain. *Annual Review of Fluid Mechanics*, *42*(1), 365–389. doi:10.1146/annurev-fluid-121108-145459

Fischer, E. M., & Schär, C. (2010). Consistent geographical patterns of changes in high-impact European heatwaves. *Nature Geoscience*, *3*(6), 398–403. doi:10.1038/ngeo866

FLIR. (2016). User's manual T10xx series

García-León, D., Casanueva, A., Standardi, G., Burgstall, A., Flouris, A. D., & Nybo, L. (2021). Current and projected regional economic impacts of heatwaves in Europe. *Nature Communications*, *12*(1), 5807. doi:10.1038/s41467-021-26050-z

Garrido-Perez, J. M., Vicente-Serrano, S. M., Barriopedro, D., García-Herrera, R., Trigo, R., & Beguería, S. (2024). Examining the outstanding Euro-Mediterranean drought of 2021–2022 and its historical context. *Journal of Hydrology*, *630*(130653), 130653. doi:10.1016/j.jhydrol.2024.130653

Hayes, A. T., Jandaghian, Z., Lacasse, M. A., Gaur, A., Lu, H., Laouadi, A., … Wang, L. (2022). Nature-based solutions (NBSs) to mitigate urban heat island (UHI) effects in Canadian cities. *Buildings*, *12*(7), 925. doi:10.3390/buildings12070925

Heaviside, C., Vardoulakis, S., & Cai, X.-M. (2016). Attribution of mortality to the urban heat island during heatwaves in the West Midlands, UK. *Environmental Health: A Global Access Science Source*, *15 Suppl 1*(S1), 27. doi:10.1186/s12940-016-0100-9

IPCC (2023). Glossary. *Climate Change 2022 – Impacts, Adaptation and Vulnerability*, pp. 2897–2930. doi:10.1017/9781009325844.029

Kottek, M., Grieser, J., Beck, C., Rudolf, B., & Rubel, F. (2006). World Map of the Köppen-Geiger climate classification updated. *Meteorologische Zeitschrift*, *15*(3), 259–263. doi:10.1127/0941-2948/2006/0130

Liu, Y., Chu, C., Zhang, R., Chen, S., Xu, C., Zhao, D., … Cao, Z. (2024). Impacts of high-albedo urban surfaces on outdoor thermal environment across morphological contexts: A case of Tianjin, China. *Sustainable Cities and Society*, *100*(105038), 105038. doi:10.1016/j.scs.2023.105038

Oke, T. R. (1973). City size and the urban heat island. *Atmospheric Environment*, *7*(8), 769–779. doi:10.1016/0004-6981(73)90140-6

Oke, T. R. (1982). The energetic basis of the urban heat island. *Quarterly Journal of the Royal Meteorological Society. Royal Meteorological Society (Great Britain)*, *108*(455), 1–24. doi:10.1002/qj.49710845502

O’Malley, C., Piroozfar, P., Farr, E. R. P., & Pomponi, F. (2015). Urban Heat Island (UHI) mitigating strategies: A case-based comparative analysis. *Sustainable Cities and Society*, *19*, 222–235. doi:10.1016/j.scs.2015.05.009

Perkins, S. E. and L. V. Alexander (2012). On the measurement of heatwaves. *J.Clim.,* 26, 4500–451

Possega, M., Aragão, L., Ruggieri, P., Santo, M. A., & Di Sabatino, S. (2022). Observational evidence of intensified nocturnal urban heat island during heatwaves in European cities. *Environmental Research Letters*, *17*(12), 124013. doi:10.1088/1748-9326/aca3ba

Qiu, G.-Y., Li, H.-Y., Zhang, Q.-T., Chen, W., Liang, X.-J., & Li, X.-Z. (2013). Effects of evapotranspiration on mitigation of urban temperature by vegetation and urban agriculture. *Journal of Integrative Agriculture*, *12*(8), 1307–1315. doi:10.1016/s2095-3119(13)60543-2

Román A, O., Prieto C, M. J., Mancilla F, P., Astudillo O, P., Dussaubat A, A. M., Miguel W, C., & Lara M, J. (2009). Association between air pollution and cardiovascular risk. *Revista medica de Chile*, *137*(9), 1217–1224. doi:/S0034-98872009000900013

Russo, S., Dosio, A., Graversen, R. G., Sillmann, J., Carrao, H., Dunbar, M. B., … Vogt, J. V. (2014). Magnitude of extreme heat waves in present climate and their projection in a warming world. *Journal of Geophysical Research Atmospheres*, *119*(22), 12,500-12,512. doi:10.1002/2014jd022098

Tan, J., Zheng, Y., Tang, X., Guo, C., Li, L., Song, G., … Li, F. (2010). The urban heat island and its impact on heat waves and human health in Shanghai. *International Journal of Biometeorology*, *54*(1), 75–84. doi:10.1007/s00484-009-0256-x

Ulpiani, G. (2021). On the linkage between urban heat island and urban pollution island: Three-decade literature review towards a conceptual framework. *The Science of the Total Environment*, *751*(141727), 141727. doi:10.1016/j.scitotenv.2020.141727

United Nations (2018). The World’s Cities in 2018 – Data Booklet

Zhou, X., & Chen, H. (2018). Impact of urbanization-related land use land cover changes and urban morphology changes on the urban heat island phenomenon. *The Science of the Total Environment*, *635*, 1467–1476. doi:10.1016/j.scitotenv.2018.04.091

Sitography

ARPAE Arpae Emilia-Romagna

ARPAE Eraclito91 - Dataset climatico dal 1991 - Dataset - Dati Arpae

ARPAE Index of /opendata/erg5v2/timeseries

ARPAE Proiezioni climatiche in Emilia-Romagna — Arpae Emilia-Romagna

ARPAE Rete di monitoraggio idrometeorologica — Arpae Emilia-Romagna

Comune di Bologna Diapositiva 1

Copernicus, 2023 2022 saw record temperatures in Europe and across the world | Copernicus

Copernicus, 2023 Europe's contrasting summer | Copernicus

D3xter dext3r

Github simc-opendata-examples/erg5/README.md at master · ARPA-SIMC/simc-opendata-examples · GitHub

Google Earth https://www.google.it/intl/it/earth/index.html

IEA Italy Climate Resilience Policy Indicator – Analysis - IEA

ISPRA My OpenLayers Map

ISTAT, 2022 Aggiornamento della base dati di mortalità totale giornaliera comunale | Gennaio-Giugno e Luglio 2022 – Istat

ISTAT, 2025 Bilancio demografico mensile

MET Éireann, 2023 Summer Centre - Met Éireann - The Irish Meteorological Service

MeteoTracker MeteoTracker – Patented technology for professional weather measurements

PTM PTM - Piano Territoriale Metropolitano - Home Page

Regione Emilia-Romagna https://geoportale.regione.emilia-romagna.it/

WMO Climate change and heatwaves